

THE FLORIDA STATE UNIVERSITY

COLLEGE OF ARTS AND SCIENCES

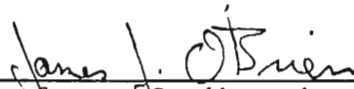
MECHANISMS OF STRATOSPHERIC OZONE TRANSPORT

by

RICHARD BENTON ROOD

A Dissertation submitted to the
Department of Meteorology
in partial fulfillment of the
requirements for the degree of
Doctor of Philosophy

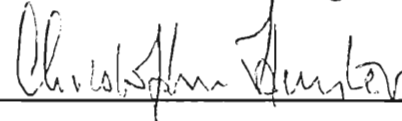
Approved:

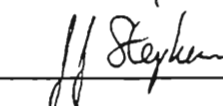


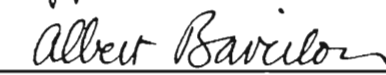
Professor Co-directing Dissertation



Professor Co-directing Dissertation











December, 1982

Abstract

Two β -plane planetary wave models are used to study ozone transport in the stratosphere. In the first model, ozone transport is calculated for steady, dissipative planetary waves using the Eulerian, Lagrangian-mean, and residual circulations. A Lagrangian model of parcel dynamics is used to interpret planetary wave-photochemistry interaction. In chemically active regions the mean field ozone changes are found to be significant only where there are large gradients in chemical sources and sinks along particle trajectories. The largest changes in the mean field are found in the lower stratosphere and are due to the Lagrangian-mean advection.

In the second model, ozone transport is calculated for the combined diabatic and time dependent planetary wave circulations. Both circulations are instrumental in the formation of the polar spring ozone maximum. The diabatic circulation transports ozone into the lower stratosphere, and planetary waves transport large amounts of ozone northward during sudden and final warmings. Using the transport mechanisms revealed in these models, a scenario is deduced to explain observed large scale ozone transport phenomena.

Acknowledgements

This work was performed at the Naval Research Laboratory under Office of Naval Research contracts N000-81-C-2038 and N00173-80-C-0181.

I am most grateful to Dr. Mark Schoeberl who has generously given much needed guidance and direction to me, and without whom this research would not have been possible. I am also grateful to Dr. James J. O'Brien for serving as my Co-advisor and to Drs. J. Stephens, A. Barcilon, C. Hunter, and N. LaSeur for serving on my committee. I must also thank Dr. M. A. Rennick for her support and efforts prior to the undertaking of my doctoral research.

I am most appreciative to my wife Janna for her patience and her ability to proofread, and promise her that estuarial herbs and Hawaii are in the future somewhere.

I am greatly indebted to Maggie York who has done much out of kindness to insure that this dissertation is successfully completed. I am also thankful to G. Beattie, V. Grishkot, P. Thume, and J. Carroll for their logistical support, and more importantly for helping me with the word processor.

Finally, I would like to remember and express my gratitude to Professor Richard A. Craig, with whom I began my graduate research, and in whom I observed some of the most admirable traits a scientist can possess. I hope I learned something from him.

Contents

Abstract.....	ii
Acknowledgements.....	iii
Contents.....	iv
List of Figures.....	viii

Chapter 1: INTRODUCTION TO THE OZONE TRANSPORT PROBLEM

1.1. Introduction.....	1
1.2. Diffusion Models.....	2
1.3. General circulation models.....	5
1.4. Lagrangian-mean models.....	7
1.5. Objectives.....	10

Chapter 2: MODEL DESCRIPTIONS

AND THE OBSERVED OZONE DISTRIBUTION

2.1. Introduction.....	12
2.2. Chemistry model.....	19
2.3. Dynamic models.....	23
2.3a. Steady state model.....	23
2.3b. Time dependent β -plane model	28
2.4. Observations of ozone.....	31
2.4a. Time dependent β -plane model	31
2.4. Observations of ozone.....	31

Chapter 3: TRANSPORT BY STEADY STATE PLANETARY WAVES

3.1. Introduction.....46

3.2. Constituent dynamics.....46

3.3. Results.....53

 3.3a. Dynamic quantities.....53

 3.3b. Eulerian transport.....62

 3.3c. Lagrangian-mean transport.....67

 3.3d. The "stirring" term.....71

 3.3e. Lagrangian model.....74

 3.3f. The effect of eddy
 transport on the mean field.....83

3.4. Conclusions.....89

Chapter 4: TRANSPORT BY TRANSIENT PLANETARY WAVES
AND THE DIABATIC CIRCULATION

4.1. Introduction.....92

4.2. Dynamics.....92

 4.2a. 600 m topography.....93

 4.2b. 900 m topography.....99

 4.2c. The diabatic circulation.....100

 4.2d. Initialization.....101

4.3. Transport by the diabatic circulation.....105

4.4. Planetary wave transport.....113

 4.4a. Conservative transport.....113

 4.4b. Chemical transport.....117

 4.4a. Conservative transport.....113

 4.4b. Chemical transport.....117

Chapter 4 (continued)

4.5. Transport by both waves and the diabatic circulation.....	122
4.6. Discussion.....	131
4.6a. Diabatic circulation.....	133
4.6b. Planetary waves.....	133
4.7. Summary.....	154

Chapter 5: SUMMARY AND A POSSIBLE OZONE TRANSPORT SCENARIO

5.1. Introduction.....	156
5.1. Low latitude ozone.....	157
5.1a. The diabatic circulation and the initial ozone distribution.....	157
5.1b. Geometric effects.....	158
5.1c. Photochemistry.....	160
5.1d. Planetary waves.....	165
5.2. Vertical structure.....	165
5.2a. Small scale dynamics.....	165
5.2b. Photochemistry.....	166
5.3. Unstable waves.....	167
5.4. Summary and discussion.....	168
5.4a. Steady state waves.....	168
5.4b. Time dependent waves.....	173
5.4c. A possible transport scenario.....	182
5.4c. A possible transport scenario.....	182

Appendix A: NOMENCLATURE AND CONVENTIONS.....	187
Appendix B: NUMERICAL PROPERTIES OF THE ADVECTION-DIFFUSION EQUATION.....	189
References.....	197
Vita	207

List of Figures

Figure 2.1. A comparison of the analytic and numerical solution of the advection-diffusion equation using different numerical schemes.....16

- a. Forward in time, second order in space (same as Clancy (1981), Fig. 2)
- b. Forward in time, fourth order in space
- c. Centered in time, fourth order in space

(+ on the numerical solution)

Figure 2.2. Schematic representation of the atmosphere divided into photochemical, transitional, and conservative regions based on the ratio of the dynamical to the photochemical time scale.....22

Figure 2.3. a. Mean zonal wind profile for the steady state model.....26

- b. Magnitude of the steady state geopotential.....26

Figure 2.4. Initial mean zonal wind profile for the time dependent β -plane model.27

Figure 2.5. Latitude-height cross section of ozone for March/April in partial pressure and ozone/air number mixing ratio (from Dütsch, 1974).34

Figure 2.6. 6 year average time-height cross section of ozone partial pressure at Arosa, Switzerland (from Dütsch, 1974).35

(FROM DÜTSCH, 1974).35

Figure 2.7.	Vertical distribution of ozone from 3 soundings in late winter and early spring (μmb) (from Dütsch, 1974).	36
	a. Arctic type b. Polar type c. Subtropical type	
	Temperature on left in $^{\circ}\text{C}$.	
Figure 2.8.	10 year average latitude-time cross section of total ozone in Dobson Units (DU) (from London <u>et al.</u> , 1976).	41
Figure 2.9.	Latitude-time cross section of total ozone data from Nimbus 4 BUUV (DU) (from Hilsenrath <u>et al.</u> , 1979).	42
Figure 2.10.	Mean total ozone north of 40° (from Zullig, 1973).	43
Figure 2.11.	Reproduction of Figure 2.8 north of 30° from mid-December through April.	44
Figure 3.1.	Zonal mean ozone distribution for the steady state model (ppm).	55
Figure 3.2.	Eulerian zonal mean velocities (cm sec^{-1}).	56
	a. \bar{v} b. \bar{w}	
Figure 3.3.	Stokes drifts (cm sec^{-1}).	57
	a. v^S b. w^S	
Figure 3.4.	Lagrangian-mean velocities (cm sec^{-1}).	60
	a. v^L b. w^L	
	a. v^L b. w^L	

Figure 3.5.	Residual velocities (cm sec ⁻¹).....	61
	a. v^*	
	b. w^*	
Figure 3.6.	Eulerian fluxes of ozone (ppm m sec ⁻¹).....	65
	a. horizontal flux	
	b. vertical flux	
Figure 3.7.	Mean ozone tendency, $\partial\bar{\mu}/\partial t$, as calculated with the Eulerian formulation (ppm sec ⁻¹).....	66
Figure 3.8.	Mean ozone tendency caused by advection (ppm sec ⁻¹).....	69
	a. Lagrangian-mean velocity	
	b. residual velocity	
Figure 3.9.	Total mean ozone tendency as calculated with the Lagrangian formulation (ppm sec ⁻¹)...	70
Figure 3.10.	Mean ozone tendency caused by "stirring" (ppm sec ⁻¹).....	70
Figure 3.11.	Projection of displacement fields η, ζ on the y, z plane (km).	78
Figure 3.12.	Parcel orbiting through a region of discontinuous photochemistry $\partial\bar{\mu}/\partial t > 0$	78
Figure 3.13.	Solution, at large t, of perturbation ozone density for an elliptically orbiting parcel..	82
	a. constant photochemistry	
	b. photochemistry at the bottom of the transition layer	
Figure 3.14.	90 day zonal mean ozone change, with the mean chemistry included, at the latitude of the maximum ozone increase in Fig 3.7 (ppm).....	86
Figure 3.14.	90 day zonal mean ozone change, with the mean chemistry included, at the latitude of the maximum ozone increase in Fig 3.7 (ppm).....	86

Figure 3.15.	90 day zonal mean ozone change, with the mean chemistry included, at the northern and southern extremes, as determined by Lagrangian-mean advection (LGM) and residual velocity advections (+) (ppm).....	87
	a. Southern	
	b. Northern	
Figure 4.1.	Zonal mean wind for 600 m topography at the channel center (m sec^{-1}).....	95
Figure 4.2.	Geopotential amplitude for 600 m topography at the channel center (gpm).....	95
Figure 4.3.	Zonal mean wind for 900 m topography at the channel center (m sec^{-1}).....	98
Figure 4.4.	Geopotential amplitude for 900 m topography at the channel center (gpm).....	98
Figure 4.5.	Diabatic circulation at the winter solstice (cm sec^{-1}).....	103
	a. meridional component	
	b. vertical component	
Figure 4.6.	Initial ozone profile (ppm).....	104
Figure 4.7.	Change in ozone at the center of the channel (60°) for transport by the diabatic circulation alone (ppm).....	107
Figure 4.8.	Same as Fig. 4.7 but at 74°	107
Figure 4.9.	Latitude-time cross section of total ozone as calculated with the diabatic circulation (DU).....	108
	diabatic circulation (DU).....	108

Figure 4.10.	Change in ozone at 74° with horizontally varying chemistry (ppm).....	112
	a. cosine of latitude dependence	
	b. $\lambda=0$ north of 67°	
Figure 4.11.	Change in ozone for 600 m topography at 46° with no chemistry (ppm).....	115
	(bold solid line is the critical line)	
Figure 4.12.	Same as Fig. 4.11 but at 74°	115
Figure 4.13.	Same as Fig. 4.12 but for 900 m topography..	116
Figure 4.14.	Change in ozone for 600 m topography at 46° with chemistry (ppm).....	120
	(bold solid line is the critical line)	
Figure 4.15.	Same as Fig. 4.14 but at 74°	120
Figure 4.16.	Same as Fig. 4.15 but for 900 m topography..	121
	(bold dashed line is the critical line at the center of the channel)	
Figure 4.17.	Change in ozone for the combined planetary wave (900 m) and diabatic circulations at 46° with chemistry (ppm).....	124
Figure 4.18.	Same as Fig. 4.17 but at 60°	125
Figure 4.19.	Same as Fig. 4.17 but at 74°	126
Figure 4.20.	Time-latitude cross section of total ozone as calculated with the combined planetary wave-diabatic circulation (DU).....	130
	wave-diabatic circulation (DU).....	130

Figure 4.21.	Stream functions for a horizontal critical line (from Matsuno and Nakamura, 1979).	
	a. Eulerian mean.....	136
	b. Lagrangian-mean.....	137
Figure 4.22.	Eulerian mean flux at day 25 (ppm m sec^{-1})..	142
	a. horizontal	
	b. vertical	
Figure 4.23.	Horizontal eddy flux at day 25 conservative transport (ppm m sec^{-1}).....	143
	(bold solid line is the critical line)	
Figure 4.24.	a. Same as Fig. 4.23 but at day 31.....	144
	b. Wave transience at day 31.....	145
	c. \bar{q}_y at day 31.....	145
	(chain-dot = 0, dash < 0, solid > 0)	
Figure 4.25.	Eddy horizontal flux at day 47 for conservative transport during the rise of the critical line (ppm m sec^{-1}).....	151
	(bold solid line is the critical line)	
Figure 4.26.	Eliassen-Palm (EP) flux divergence during the rise of the critical line.....	152
	(negative values correspond to westerly acceleration)	
	solid lines > 0	
	dashed lines < 0	
	chain-dot =0	
Figure 4.27.	Horizontal eddy flux on day 31 for chemical transport (ppm m sec^{-1}).....	153
	(bold solid line is the critical line)	
Figure 5.1.	Comparison of spherical and β -plane geometry.....	162
Figure 5.1.	Comparison of spherical and β -plane geometry.....	162

Figure 5.2.	Latitudinal dependence of the lower boundary of the photochemically controlled region (circles) and the upper boundary of the dynamically controlled region (squares), for November and December (from Gille <u>et al.</u> , 1980).....	163
Figure 5.3.	Meridional cross section of the zonal mean wind velocity (m sec^{-1}).....	164
	a. 17 February 1979	
	b. 19 February	
	c. 20 February	
	d. 21 February	
	e. 23 February	
	f. 27 February	
	(from Palmer, 1981)	
Figure 5.4.	Simulated zonal mean total ozone (DU) (from Mahlman <u>et al.</u> , 1980).....	172
Figure 5.5.	Change in ozone at 74° for 200 m topography (ppm).....	177
Figure 5.6.	Horizontal eddy flux of ozone (ppm m sec^{-1})	
	a. measured by Gille <u>et al.</u> (1980).....	178
	b. for 200 m topography.....	179
Figure 5.7.	Schematic summary of transport mechanisms.....	180
	a. steady state planetary waves	
	b. diabatic circulation and transient waves	
Figure B.1.	Growth rate of the numerical solution for forward time differences as a function of diffusion. For $G > 0$, the solution is unstable.....	195
	($\Delta x = 100 \text{ km}$, $\Delta t = 10 \text{ hours}$, $u = .6 \text{ m sec}^{-1}$)	

Figure B.2. Integration of Clancy's (1981) oceanic case with $\Delta t = 10$ hours. Same as Figure 2.1c but with the time step increased an order of magnitude.



Chapter 1

INTRODUCTION TO THE OZONE TRANSPORT PROBLEM

1.1 Introduction

Due to the complex nature of ozone photochemistry and atmospheric dynamics it has been difficult to discern the mechanisms most important for the maintenance of the ozone distribution. To simultaneously model both the photochemistry and the dynamics is a prodigious task as each system involves a variety of temporal and spatial scales. One goal of atmospheric scientists is to understand transport dynamics so that they may be simplified and then meaningful predictions of ozone perturbations by pollutants can be generated for a considerably reduced computational cost.

The oxygen photochemistry (Chapman, 1930; Craig, 1965) predicts that the maximum amount of ozone should be observed in the tropical stratosphere and the minimum amount observed in the polar stratosphere. However, even as early as 1930 it was known that the maximum amount of ozone occurs at extratropical latitudes (Dobson, 1930), and it thus was postulated that atmospheric transport redistributes ozone from its tropical source regions to polar latitudes.

latitudes.

Simple mean cell circulations were proposed by Brewer (1949)

and Dobson (1956) which were capable of transporting ozone from tropical to polar regions. Planetary wave mechanisms were also suggested that were capable of producing poleward, downward transport (Newell, 1961, 1963). As more data became available and dynamical theory developed, it became obvious that the transport of minor constituents was a complex interaction of planetary waves and the mean circulation (Mahlman, 1969). An excellent review of the history of stratospheric circulation and transport studies is given in Hsu (1980).

Since the classic study of Craig (1950), the photochemical models of ozone have become progressively more complex. The remeasurement of rate coefficients by Benson and Axworthy (1957) indicated that oxygen-only photochemical models would predict more ozone than is observed (Hunt, 1966). Catalytic destruction cycles involving hydrogen oxides, nitrogen oxides, and halogen oxides have been added to the photochemistry models. With the addition of these reactions it became obvious that anthropogenic pollutants might cause serious degradation of the ozone layer (WMO, 1981). Complete photochemical models now require the use of over 100 chemical reactions (Johnson and Podolske, 1978). Use of the complete set of photochemical equations requires that the dynamics be simplified in order to make the problem tractable. The most common parameterization has been to treat atmospheric transport as if it were diffusive.

parameterization has been to treat atmospheric transport as if it were diffusive.

1.2 Diffusion models

The dynamics in photochemistry models have been parameterized with both one-dimensional (1-D) and two-dimensional (2-D) schemes. The 1-D models represent transport by vertical diffusion from high altitude source regions to the lower stratosphere where ozone is observed to accumulate (McConnell and McElroy, 1973). Hunten (1975) pointed out that vertical diffusion models are useful because of the tendency of the atmosphere to be horizontally stratified. Upward motions are always associated with compensating downward motions; therefore, the atmosphere "looks like just another big eddy" (Hunten, 1975). Strobel (1981), however, has shown that 1-D diffusion models are only strictly valid when the horizontal gradient of the constituent is small, a condition not valid for ozone.

Two-dimensional models attempt to model the atmosphere more realistically by approximating both vertical and latitudinal transport (Hidalgo and Crutzen, 1977; Harwood and Pyle, 1977; Miller et al., 1981). In 2-D models a mean advective field is usually prescribed and wave motions are modeled by a diffusion scheme. Such diffusion parameterizations are often based on the empirical theory of Reed and German (1965) which has been shown to be inconsistent with the hydrodynamics of planetary wave transport (Matsuno, 1980).

Hidalgo and Crutzen (1977) and Harwood and Pyle (1977) use an Eulerian mean formulation where ozone is advected with a zonal mean velocity and the zonal mean effects of the planetary waves are modeled by diffusion. In another 2-D model Miller et al. (1981) use the concepts of the Lagrangian-mean circulation, as discussed by

Dunkerton (1978), to derive a Lagrangian-mean circulation for the stratosphere. Miller et al. use this Lagrangian-mean field instead of the Eulerian velocity for the mean field advection.

The problems of applying diffusion models to atmospheric dynamics has been discussed by Mahlman (1975), Tuck (1979), and Pyle and Rogers (1980a). These authors have pointed out the inadequacies of diffusion parameterizations when trying to model countergradient transport, the spatial variation of chemical sources and sinks, and the diffusion of different chemical species. These processes are important for ozone in some parts of the atmosphere and should be properly represented in ozone models.

Matsuno (1980), Clark and Rogers (1978), Dunkerton (1980), and Plumb (1979) have shown that the nature of planetary waves is advective rather than diffusive for an inert tracer. This means that the diffusion tensor should be antisymmetric rather than symmetric as is generally assumed. Matsuno (1980), Strobel (1981), and Holton (1981) show that there are also diagonal components in the diffusion tensor which are associated with chemical source terms and wave growth and decay.

The manner in which diffusion parameterizations have been applied to the atmosphere is a source of uncertainty in the results of chemical models. Pyle and Rogers (1980a), however, argue that a dynamically consistent reformulation of the diffusion coefficients might allow for the continued use of diffusion models. Strobel (1981) might allow for the continued use of diffusion models. Strobel (1981) has formulated such a consistent theory for linear waves with complex frequencies. This theory demonstrates the strong coupling

between the magnitude of the diffusion coefficients and photochemistry. Because of this strong coupling, a simple diffusion model can adequately predict ozone dynamics only under special circumstances.

Even with all the shortcomings, diffusion can improve the results of chemical models. A recent study by Pyle and Rogers (1980b) shows that the addition of diffusion generates more realistic ozone distributions than those produced by the diabatic circulation alone. Since it is impossible to fully model both photochemistry and dynamics such parameterizations are desirable and necessary. In the next section attempts to study ozone with an accurate representation of the dynamics and a simplified chemistry will be discussed.

1.3 General circulation models

Several general circulation models have been used to study ozone transport and the interaction of radiation, dynamics, and photochemistry (Clark, 1970; Cunnold et al., 1975; Schlesinger and Mintz, 1979; and Mahlman et al., 1980, and the references therein). These models emphasize an accurate representation of the dynamics, but the chemistry is modeled in a simplified manner. General circulation studies have met with some success in modeling the large scale features of the ozone distribution, but no general circulation model has ever reproduced all of the large scale features of the ozone distribution, but no general circulation model has ever reproduced all of the large scale features of the ozone distribution.

For example, the quasigeostrophic model of Clark (1970)

established the usefulness of the Chapman photochemistry in modeling ozone and demonstrated that the stratospheric circulation was able to perturb the radiative equilibrium ozone distribution to a distribution that approximated observations. In particular, planetary waves were found to transport large amounts of ozone from equatorial source regions to high latitudes. By increasing the horizontal gradient of temperature, Clark was able to generate high latitude warmings; however, these model warmings do not accurately represent the observed characteristics of stratospheric warmings. Therefore, while the dynamics in this model do indeed cause an increase in ozone at high latitudes, the mechanisms that lead to this increase are in doubt due to the inability of the model to accurately represent observed dynamical features.

Using the same dynamical equations of Clark (1970), Cunnold et al. (1975) generated more accurate zonal mean circulations than Clark; however, the model did not generate stratospheric warmings. In their formulation of the ozone continuity equation Cunnold et al. used a large vertical eddy diffusion coefficient, based on diffusivities of 1-D chemistry models, which dominated the vertical transport in the model. Although Cunnold et al. did calculate a polar spring ozone maximum, the accumulation of ozone at high latitudes was underestimated.

Mahlman et al. (1980) used a 3-D primitive equation model to perform two ozone transport experiments. In the first experiment

perform two ozone transport experiments. In the first experiment the ozone was specified at 10 mb (the upper boundary) and was not allowed to deviate from this climatological value. In the second

experiment, ozone was calculated at 10 mb using a simple oxygen, hydrogen, nitrogen photochemistry. Mahlman et al. predicted the vertical structure in the lower stratosphere quite accurately using either of the specified photochemistries. This indicates that the ozone distribution in the lower conservative region of the stratosphere is to a large degree independent of the details of the photochemistry.

The most serious discrepancy encountered by Mahlman et al. was in the calculation of the total ozone field. Their spring maximum was too large, occurred too far south, and too late in the spring. The model of Mahlman et al. (1980) did not produce midwinter stratospheric warmings and, indeed, none of the general circulation models accurately represent warming events. It was suggested in Mahlman et al. (1980) that the transport during a stratospheric warming might be important in improving their results.

General circulation studies are so complex that transport mechanisms are difficult to isolate and describe. The dynamics are a combination of diabatically forced circulations and wave regimes, and it is difficult to pinpoint the dominant transport mechanisms. Therefore, the use of simple models to study the transport associated with specific dynamic mechanisms might be useful not only for application to chemical models but for interpreting general circulation model results.

circulation model results.

1.4 Lagrangian-mean models

In general the constituent and dynamics fields in atmospheric

studies are formulated as a mean field and a deviation field. The mean fields are generally formed by taking averages around a latitude circle in what is called the Eulerian formulation. An alternative to the Eulerian zonal mean and deviation method is the Lagrangian-mean method (Andrews and McIntyre, 1978; McIntyre, 1980), in which averages are taken over particular fluid tubes. As the averaging operator is defined, the Lagrangian-mean velocity is the center of mass velocity of a particular ensemble of fluid particles and is zero when the conditions of the noninteraction theorem (Boyd, 1976; Andrews and McIntyre, 1978, Dunkerton, 1980) are met.

With the above attributes it may seem natural to study tracer transport in the Lagrangian-mean system. However, it turns out the Lagrangian-mean transform is complicated and is easily formulated only for the most simple flows (McIntyre, 1980). Furthermore, dispersion of the particles about their center of mass may render the location of the center of mass of little use in the actual location of the tracer (Hsu, 1980). McIntyre (1980) has suggested that some sort of continuous reinitialization of the Lagrangian-mean model might solve this problem, but no practical scheme is currently available.

Much of the work concerning the application of the Lagrangian-mean to the transport of tracers in the stratosphere is based on the concepts of Dunkerton (1978). Dunkerton shows that for steady, non-dissipating planetary waves, the Lagrangian-mean circulation of the stratosphere is to first order the zonal mean circulation first estimated by Murgatroyd and Singleton (1961). This circulation is

specifically the radiatively forced circulation (diabatic circulation).

Planetary waves are dissipative and not steady and have a significant effect on tracer transport; therefore, the diabatic circulation is not sufficient to describe all the large scale transport processes. Schoeberl (1981a) has calculated the Lagrangian-mean circulation associated with steady, dissipative planetary waves. Schoeberl found that planetary waves transport ozone from southern to northern regions, and that strong downward transport can be obtained with "realistic" mean zonal wind profiles. It is found that in the lower stratosphere the Lagrangian-mean flow associated with planetary waves is dominate over the diabatic circulation.

The 2-D model of Miller et al. (1981) used a modified version of Dunkerton's diabatic circulation and a diffusion tensor based on the coefficients of Luther (1974) and Hunten (1975). Since the Lagrangian-mean circulation as calculated by Dunkerton (1978) does not include the effects of dissipative planetary waves, the use of the Luther and Hunten diffusion coefficients does not accurately represent planetary wave effects. The large scale transport by waves in this model are advective, and any diffusion parameterization must include an antisymmetric component.

In another approach to the diffusion problem Holton (1981) and Strobel (1981) use the residual circulation defined by Andrews and ~~in another approach to the diffusion problem Holton (1981) and~~ Strobel (1981) use the residual circulation defined by Andrews and McIntyre (1976) to calculate tracer transport. Holton's model incorporates both planetary wave and diabatic effects. A diffusion

model is then used to calculate the small scale correction to the advection by the residual circulation. This formulation involves an antisymmetric tensor that represents an advective correction to the residual circulation which is assumed to be negligible. If this antisymmetric component is indeed small then the diffusive part of the model should truly represent subplanetary wave effects.

1.5 Objectives

The global scale transport of ozone can be divided into two circulation regimes: transport by the diabatic circulation and transport by large scale waves. Each of these transport regimes is important and both must be modeled in a complete study. There are, of course, important smaller scale processes that significantly affect the ozone distribution. These small scale processes are particularly important in the lower stratosphere and in the troposphere. No attempt will be made here to study these small scale processes.

In this dissertation steady state and time dependent planetary wave models are used to investigate ozone transport by the diabatic circulation and the planetary waves. The steady state model is formulated in both the Eulerian and Lagrangian-mean systems and results from the two formulations compared. The Lagrangian-mean circulation is also compared to the residual circulation. Using the Lagrangian-mean displacement fields a Lagrangian parcel model is developed to study the interaction of photochemistry and dynamics. The simplicity of the steady state model makes it easier to use than

the time dependent model to understand the fundamental transport mechanisms; however, the steady state model has the disadvantage that potentially important transient effects are neglected.

In the time dependent model quasigeostrophic waves are calculated on a midlatitude β -plane. This model is the same as used in Schoeberl (1982a, 1982b) to study vacillation and wave saturation. A diabatic circulation based on the flow calculated by Dunkerton (1978) is superimposed on the planetary wave circulation. With this model it is possible to identify the transport characteristics of the planetary waves and the diabatic circulation and, therefore, measure their relative importance.

The use of these simple models aids in the understanding of the specific mechanisms involved in the interaction of photochemistry and dynamics. With this understanding it is possible to make a rational approach to the development of dynamic simplifications appropriate for chemical models.

In Chapter 2 the dynamic and transport models are described with particular attention given to the transport scheme. In Chapter 3 the transport by steady, dissipative waves is covered and the Eulerian, Lagrangian-mean, and residual circulations are compared. The transport by the diabatic circulation, the planetary wave circulation, and the two circulations combined is presented for the time dependent β -plane model in Chapter 4. Finally, the results of the various models will be discussed and interpreted in Chapter 5.

the various models will be discussed and interpreted in Chapter 5.

Chapter 2

MODEL DESCRIPTIONS AND THE OBSERVED OZONE DISTRIBUTION

2.1 Transport model

A general transport model has been developed that is capable of interfacing with a variety of dynamic models or a specified time dependent data set. The transport model runs in an off-line fashion; that is, the constituent distribution does not affect the dynamics. Since ozone is radiatively active, with the use of an off-line model it has been tacitly assumed that the change in radiative forcing associated with the changes in the ozone field is small. This assumption is valid as most of the transport in this model takes place during winter when insolation is small, and in the infrared, ozone cooling is much smaller than carbon dioxide cooling (Apruzese et al., 1982). Mahlman and Moxim (1978) discuss in detail the differences between on-line and off-line models.

For the transport model, the constituent continuity equation (Eq. 3.1) is written in discrete form using fourth order centered finite differences in the meridional and vertical directions. The longitudinal dependence is represented by zonal harmonics, and the time derivatives are estimated with second order centered differences. The spatial differences are written in the leapfrog. The spatial differences are written in the

general form

$$\frac{\partial \mu}{\partial y} = C_1 \frac{(\mu_{i+1} - \mu_{i-1})}{\Delta y} + C_2 \frac{(\mu_{i+2} - \mu_{i-2})}{\Delta y} \quad (2.1)$$

where $C_1 = 2/3$ and $C_2 = -1/12$ for fourth order accuracy (Ames, 1977; Haltiner and Williams, 1980). Further details of the numerical scheme are given in Appendix B.

Mahlman and Sinclair (1977) review in some detail the difficulties of modeling fluid advection. They tested several transport algorithms using a one-dimensional model with a steady, uniform flow and cyclic boundary conditions. The most serious deficiency encountered by Mahlman and Sinclair was the generation of nonphysical negative mixing ratios which had to be removed. This removal process is called "filling" (Mahlman and Moxim, 1978). Filling is a subjective process that usually involves borrowing mass from surrounding grid points in a mass conserving fashion so that negative mixing ratios are increased to zero.

Mahlman and Sinclair found that the pseudo-spectral method produced the best results when a large number of waves and a short time step were used. However, the pseudo-spectral scheme requires a large amount of computer time and memory. Of the other schemes tested the fourth order derivative scheme worked well and is computationally efficient (see also Kreiss and Olinger, 1972).

Clancy (1981) has suggested that the advection-diffusion equation can be efficiently integrated for a wide range of parameters using second order spatial differences and a forward time

scheme. A comparison of the current model with Clancy's scheme illustrates the computational gain of the fourth order differences.

Following Clancy, the advection-diffusion equation,

$$\frac{\partial S}{\partial t} = -u \frac{\partial S}{\partial x} + D \frac{\partial^2 S}{\partial x^2}$$

is integrated with $\Delta t = 3600$ sec, $\Delta x = 10^5$ m, $u = .6$ m sec⁻¹, and $D = 10^3$ m² sec⁻¹. The initial condition is

$$S = S_0 \sin(kx) \quad (t = 0)$$

and the boundary conditions are

$$S = -S_0 \exp(-k^2 Dt) \sin(kx - ukt)$$

for $x = 0$ and 10^9 m, where $k = 2\pi(10^8 \text{ m})^{-1}$. The results after 30 days using second order spatial differences and forward time differences are shown in Fig. 2.1a (same as Clancy Fig. 2). In Fig. 2.1b forward time differences are still used, but the second order differences are replaced with the fourth order estimates. The phase error in Fig. 2.1b has been reduced to nearly zero, but as in Fig. 2.1a the amplitude is overestimated.

Figure 2.1. A comparison of the analytic and numerical solution of the advection-diffusion equation using different numerical schemes.

- a. Forward in time, second order in space
(same as Clancy (1981), Fig. 2)
- b. Forward in time, fourth order in space
- c. Centered in time, fourth order in space

(+ on the numerical solution)

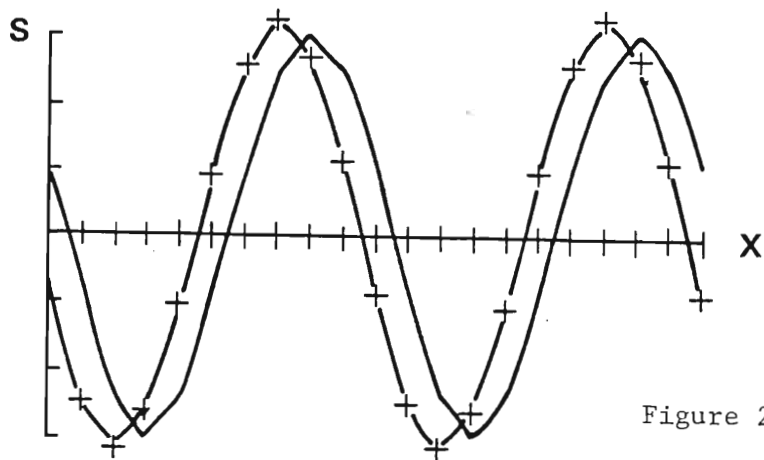


Figure 2.1a

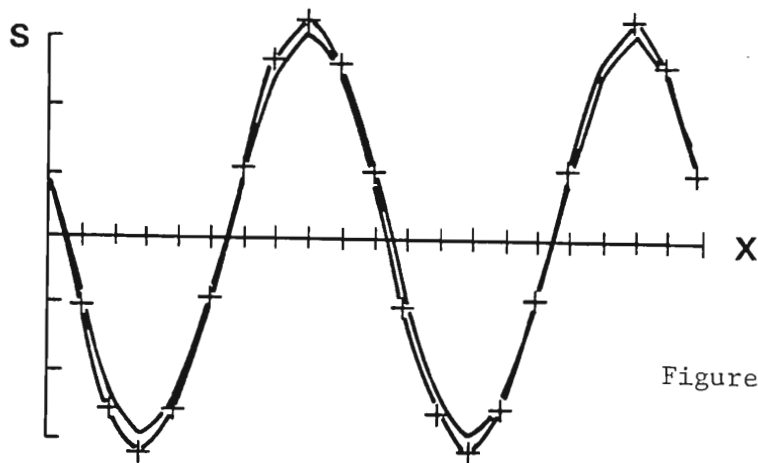


Figure 2.1b

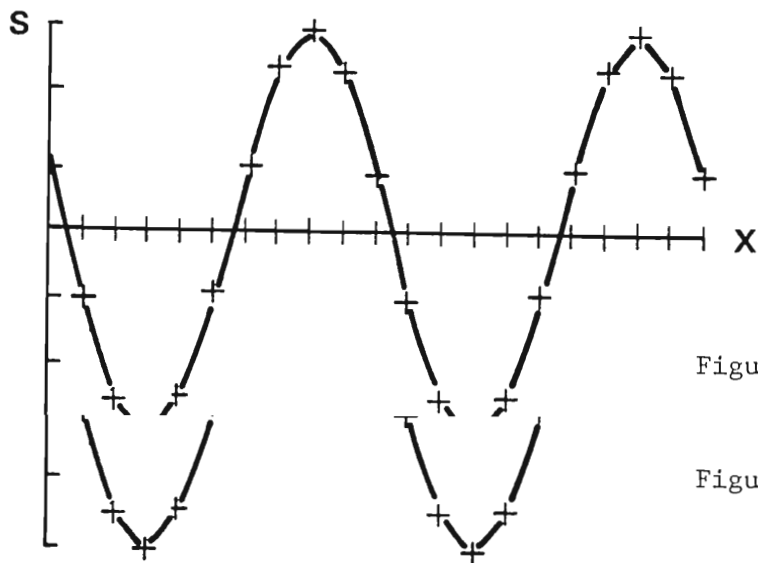


Figure 2.1c

Figure 2.1c

In Fig 2.1c the same problem has been redone using centered time differences and fourth order spatial differences. Both the phase error and the amplitude error have been reduced to the point that the numerical solution and the analytic solution are virtually indistinguishable. The use of forward time differences, as in Fig. 2.1a and 2.1b, leads to an unstable solution when the diffusion is zero (Haltiner and Williams, 1980, p. 130). The incorporation of diffusion by Clancy serves to stabilize his scheme. A more detailed analysis of this problem is presented in Appendix B.

Using second order differences without diffusion to model ozone transport leads to unrealistic results because $2\Delta x$ waves generated in regions of large gradients propagate throughout the domain and dominate the computed transport. Only with the incorporation of very large diffusion can this effect be countered for long integrations. The inferiority of second order transport models is well illustrated in Mahlman and Sinclair (1977).

Besides filling, there are other nonphysical processes that must often be incorporated into transport models in order to obtain reasonable numerical results. Diffusion is commonly introduced to represent subscale effects (Mahlman and Moxim, 1978). As indicated above, diffusion generally increases the numerical stability of a finite difference scheme and reduces the occurrence of negative mixing ratios.

At the boundary some technique must be used in order to close

At the boundary some technique must be used in order to close the finite difference scheme. In this model either the ozone density or flux is specified at the boundary, and the derivative at

the first interior point is represented by second order centered differences ($C_1 = 1/2$, $C_2 = 0$ in Eq. 2.1). With this closure system the boundary points and the first two interior points are directly affected by the prescription of the boundary.

The closure method chosen generally affects the ability of the model to conserve mass due to the uncompensated difference terms at each boundary. In a problem where there is no flux through the boundary and no source or sink terms, it is possible to calculate the mass change caused by these uncompensating terms and then distribute an appropriate mass correction over the model domain. In a problem with boundary fluxes and sources, mass correction becomes more complex.

Closure at the boundaries has another effect which particularly manifests itself in the ozone problem. Since the mixing ratio estimates at or near the boundaries are less accurate estimates than at the interior points, transport into the polar region, a region of special interest, will be inaccurate.

The philosophy taken in this study is to incorporate as little subjectivity as possible, so that important transport mechanisms will be revealed. Neither diffusion nor mass correction have been incorporated into this model, and it has not been necessary to incorporate filling.

The omission of diffusion means that the lower regions of the stratosphere and troposphere are expected to be poorly modeled. In particular there is no mechanism for tropospheric-stratospheric interaction and there are no subplanetary scale dynamics to produce

small scale mixing effects. As a result, there is sometimes a tendency for ozone to build up to unrealistic levels in the lower stratosphere. In certain instances an ozone "shock front" develops and the finite difference estimates of the derivatives become very poor, ultimately leading to the failure of the model in all regions. Strong ozone fronts do not develop with the dynamics used here.

The ability of the model to conserve mass has been studied using an inert tracer. The model does not conserve mass exactly and the entirety of the mass correction can be attributed to noncompensating finite difference terms. The mass discrepancy remains small for the integration times considered here. When ozone chemistry is included the total ozone in the model domain never differs unrealistically from the initial total ozone. For these reasons it was judged that the incorporation of any mass correcting techniques would contaminate the model results at least as badly as the uncorrected mass. Therefore, the results presented here have no mass correction added.

2.2 Chemistry model

The chemistry used in this study is extremely simple, namely:

$$Q = -\lambda\mu \quad (\lambda > 0) \quad (2.2)$$

$$Q = -\lambda\mu \quad (\lambda > 0) \quad (2.2)$$

where Q is the photochemical source term (see Eq. 3.1), λ is the photochemical relaxation rate, and μ is the constituent mixing

ratio. This formulation requires that the perturbations relax back to zero, while changes in the mean field relax to the mean equilibrium. The rate of relaxation is inversely proportional to λ , which is assumed to be a function of height only. The λ values are based on those of Hartmann and Garcia (1979).

The chemical reactions that the λ values are based on are the oxygen-only reactions (Chapman reactions) with a modified ozone destruction rate to represent catalytic destruction. Ozone chemistry is temperature dependent; however, the temperature dependence is weak (Hartmann and Garcia, 1979; Garcia and Hartmann, 1980) and will be neglected here.

It is convenient to divide the atmosphere into three regions in order to discuss ozone transport (Fig. 2.2). The lower region is the region in which ozone is assumed to be a conservative tracer ($\lambda \ll k\bar{u}$). In the upper region ozone photochemistry is so fast ($\lambda \gg k\bar{u}$) that the transport is unimportant. The middle region is defined by the ratio $.1 < \lambda/\bar{u}k < 10$ and is called the transition region (Hartmann and Garcia, 1979). The interaction of the photochemistry with the dynamics is expected to be greatest in the transition region.

Figure 2.2. Schematic representation of the atmosphere divided into photochemical, transitional, and conservative regions based on the ratio of the dynamical to the photochemical time scale.

HEIGHT (km)

80

40

20

0

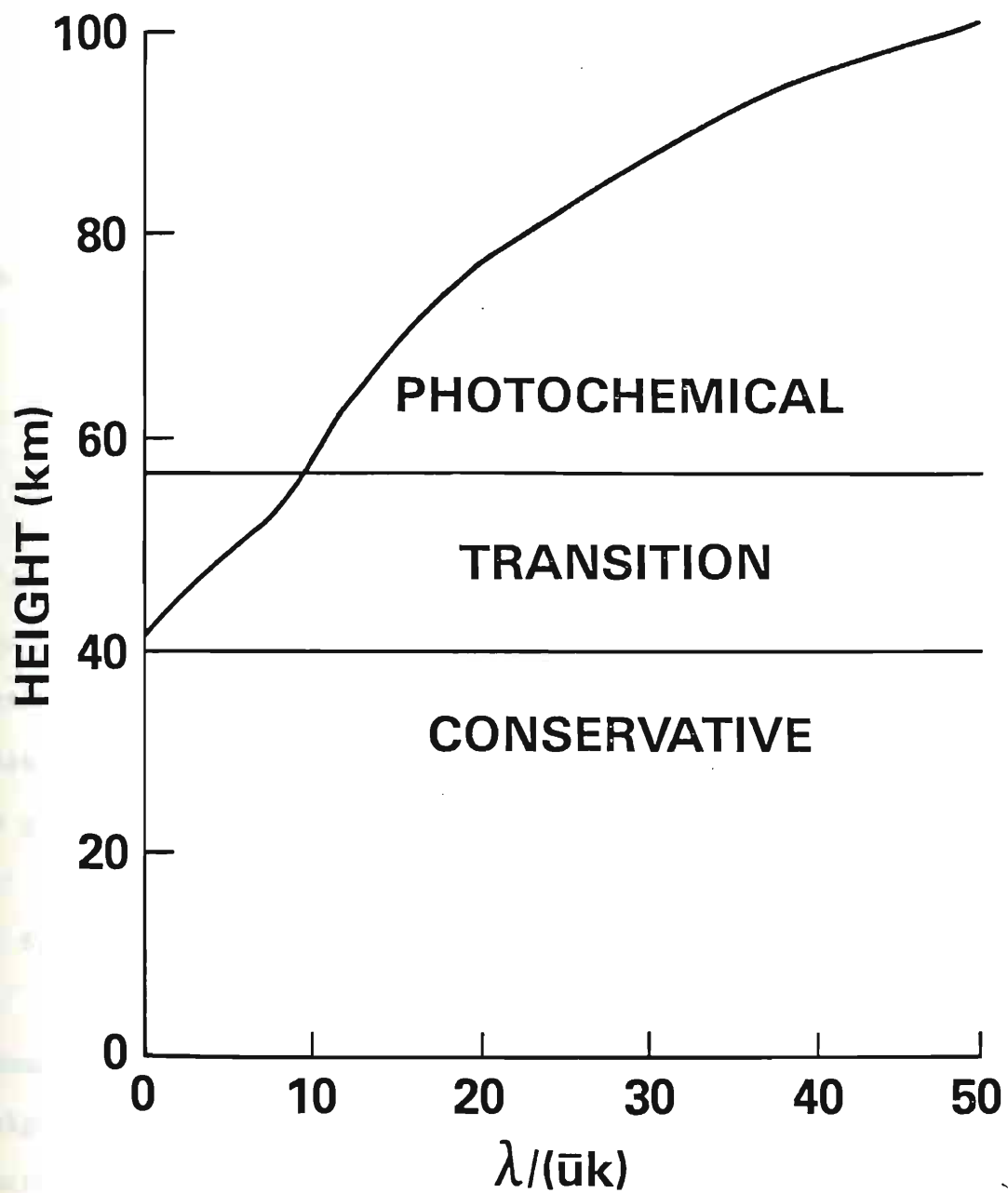


Figure 2.2

Figure 2.2

2.3 Dynamic models

The planetary waves are represented in all the dynamic models by the quasigeostrophic potential vorticity equation. The governing equation is

$$\left(\frac{\partial}{\partial t} + a + \bar{u} \frac{\partial}{\partial x} \right) q' + \frac{1}{\bar{f}} \frac{\partial \bar{q}}{\partial y} \frac{\partial \phi'}{\partial x} = F' \quad (2.3)$$

where q' is defined as in Holton (1975). The mean flow equation is

$$\frac{\partial \bar{q}}{\partial t} = - \frac{\partial (\bar{q}' v')}{\partial y} - a(\bar{q} - \bar{q}_0) + \bar{F} \quad (2.4)$$

\bar{q} is the wave induced change in the background potential vorticity \bar{q}_0 . Damping is modeled as Newtonian cooling and Rayleigh friction, which are assumed to be equal, and is represented by a . F is diabatic forcing other than Newtonian cooling. Other nomenclature is given in the Appendix A.

a. Steady state model

In the steady state model $\frac{\partial}{\partial t}$ is assumed to be zero and β -plane geometry is used. The damping is a slowly varying function of height except in the uppermost regions where it is assumed to increase at an exponential rate. This region of increase provides a sponge layer to reduce reflections from the upper boundary and is increase at an exponential rate. This region of increase provides a sponge layer to reduce reflections from the upper boundary and is well above the region where ozone transport is being studied. The time scale of the damping below the sponge layer is approximately 10

days, which is representative of the physical processes in the middle or upper stratosphere (Schoeberl and Strobel, 1978; Dickinson, 1973). The diabatic forcing, F , is assumed to be zero; therefore, only the steady state planetary wave transport is modeled.

Equations (2.3) and (2.4) are solved for a wavenumber one perturbation with forcing analogous to a mean zonal wind of 10 m sec^{-1} flowing over a 1 km mountain. The mean zonal wind profile and the geopotential amplitude are shown in Fig. 2.3. The mean zonal wind is presumed to approximate the polar night jet. The geopotential reaches a maximum amplitude of about 1 km in the mesosphere and does not exceed the steady state saturation limit (Schoeberl, 1982a). The magnitude of the geopotential is in rough agreement with observation (van Loon et al., 1973). The eddy geopotential field is used to calculate the wave forced mean meridional and vertical velocity.

It is assumed in the steady state model that wave effects on the mean flow are not so large that the wave field needs to be recomputed with the perturbed mean flow. This restricts the validity of the steady state model to small amplitude waves and is consistent with the transport approximations to be made later (Section 3.2). This model is the Eulerian analogue to the Lagrangian-mean model of Schoeberl (1981a).

Lagrangian-mean model of Schoeberl (1981a).

Figure 2.3. a. Mean zonal wind profile
for the steady state model.
b. Magnitude of the steady state geopotential.

Figure 2.4. Initial mean zonal wind profile
for the time dependent β -plane model.

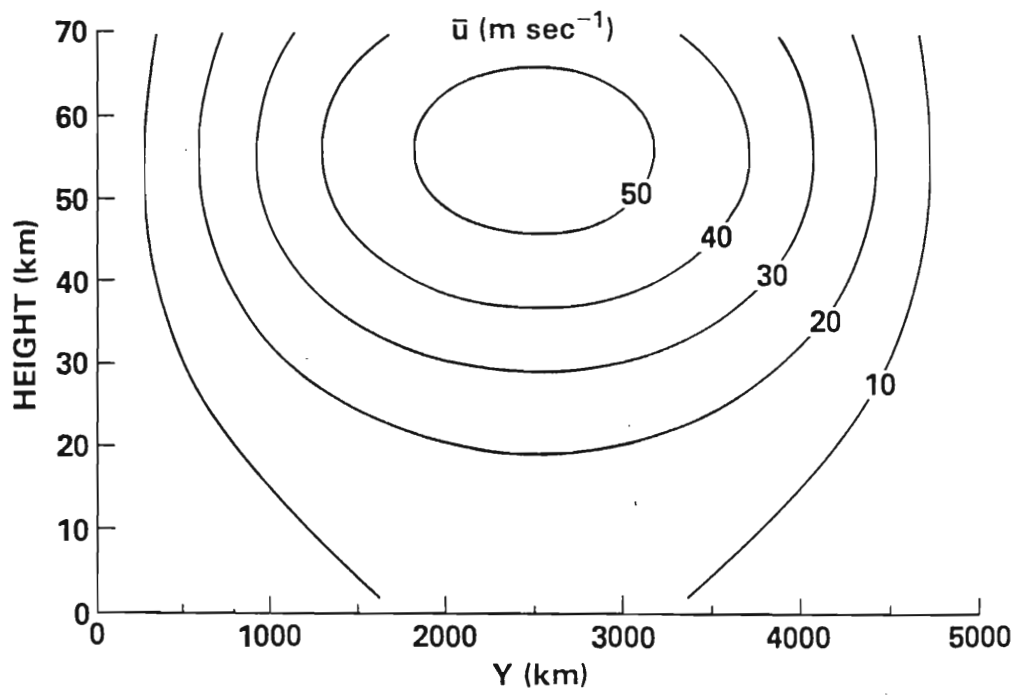


Figure 2.3a

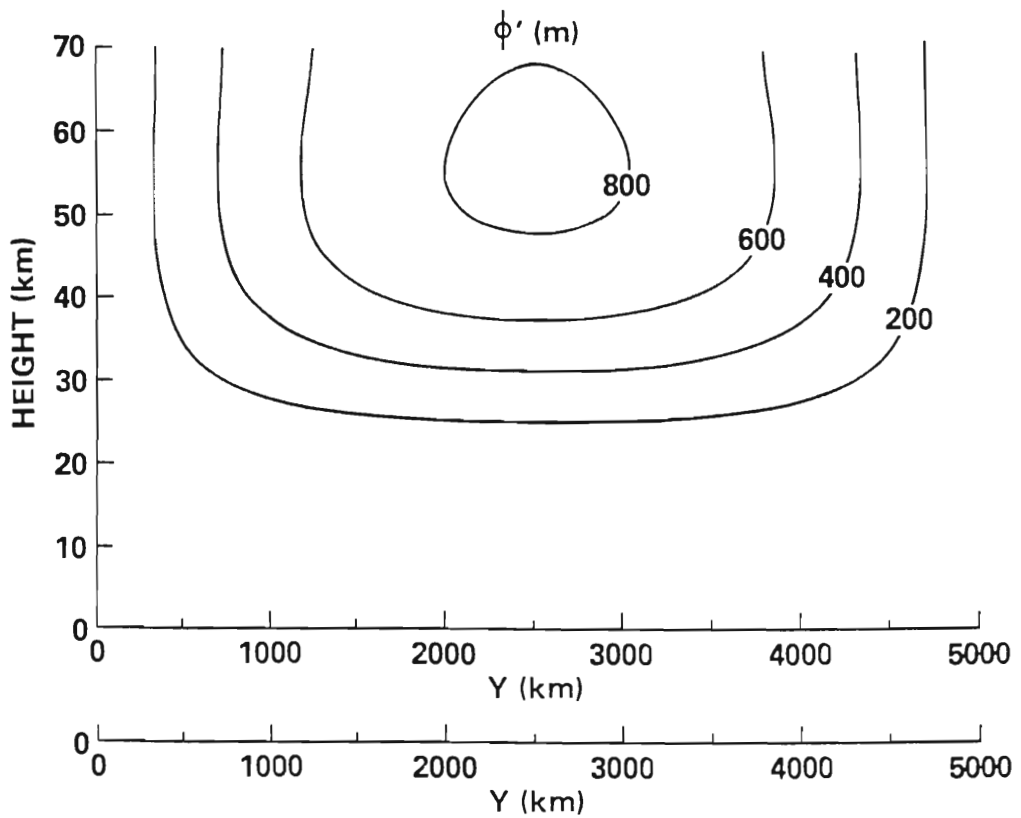


Figure 2.3b

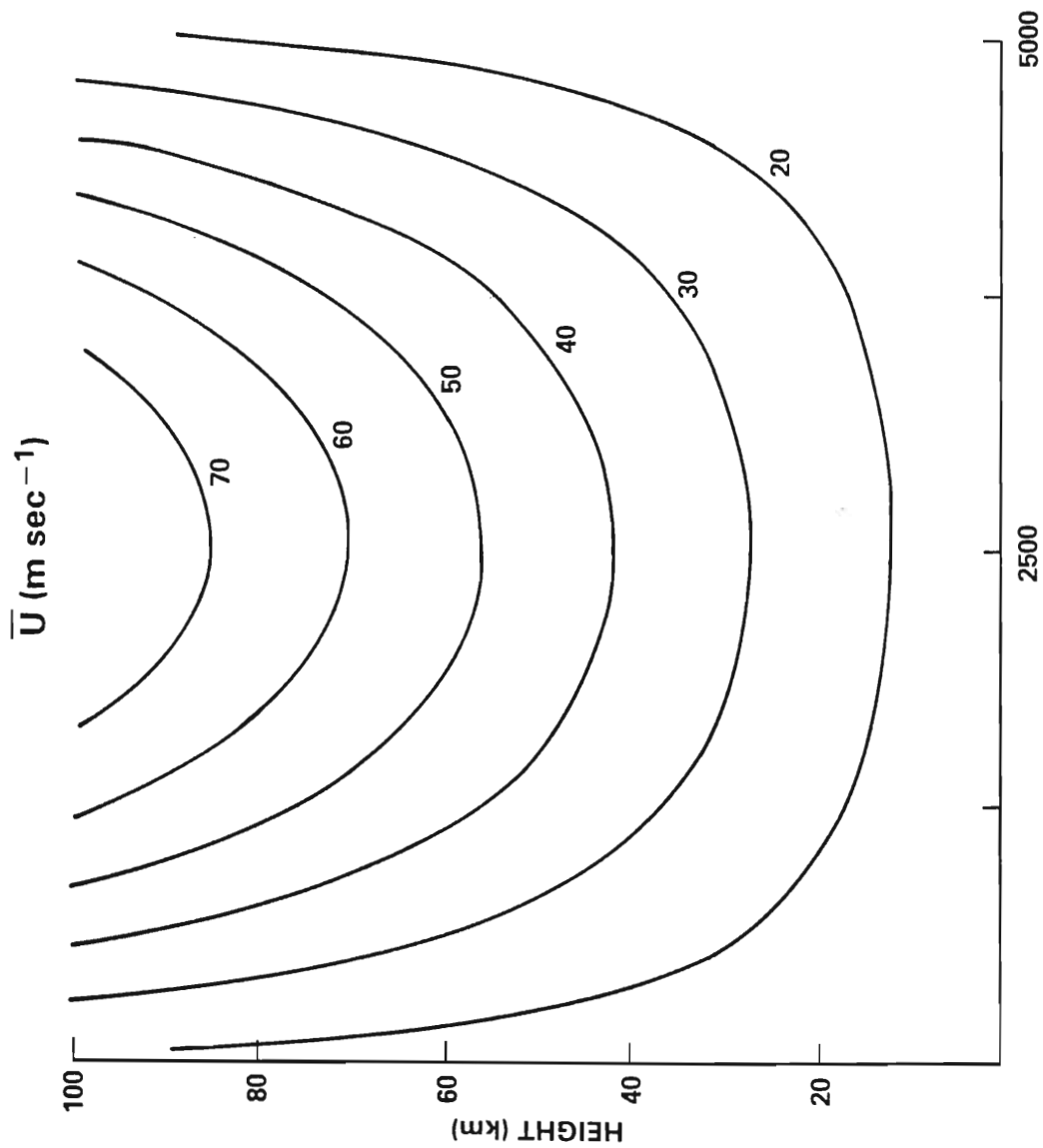


Figure 2.4

Y (km)

b. Time dependent β -plane model

In the time dependent β -plane model the diabatic forcing, F in Eqs. (2.3) and (2.4), is assumed to be zero, and the Newtonian cooling and Rayleigh friction are similar to that of the steady state model. Diabatic effects are modeled by adapting a circulation from Dunkerton (1978) and Murgatroyd and Singleton (1961) and superimposing this circulation on the calculated planetary wave circulation.

The waves are forced by zonal flow over a mountain. The basic state mean zonal wind profile is shown in Fig. 2.4. This model is quasilinear in that after every time step the wave perturbed mean field is calculated; the waves are then recalculated using the updated mean fields. The mountain height is a model parameter and the behavior of the model varies depending on the mountain height. The planetary wave model is described in Schoeberl (1982b).

For small mountains equilibrium is reached in which westerlies are present everywhere. For mountains in an intermediate range the model produces at least one stratospheric warming and then is observed to reach a steady state with a permanent layer of easterlies. For large topography the model produces a series of warmings, i.e. it vacillates. For the transport experiments two mountain heights will be used: 600 m and 900 m. Both of these mountain heights are in the intermediate range where there is a warming and the eventual onset of a permanent layer of easterlies. mountain heights are in the intermediate range where there is a warming and the eventual onset of a permanent layer of easterlies.

The β -plane transport model is centered at 60° N and has a horizontal extent of 5000 km. This corresponds to a latitudinal

extent from 37.5° to 82.5° . The domain extends from the ground to 100 km. There are 20 grid points in the horizontal and 40 grid points in the vertical and a perimeter of points around the grid at which the boundary values are prescribed.

At the top and bottom of the model the constituent flux is set equal to zero. This boundary condition is accurate at the top since the ozone is in photochemical equilibrium. At the northern and southern boundaries the flux associated with the planetary waves is assumed to be zero. At the southern boundary, where ozone is observed to have relatively little annual variation, the flux by the diabatic circulation is calculated assuming that ozone is constant. The flux associated with the diabatic circulation at the northern boundary is assumed to be zero.

The closure of the finite difference scheme directly involves the prescribed boundary point and the first interior point. The second and third interior point are directly associated with the first interior point at each time step. Because of this possible direct contamination by the closure system, results will be presented at horizontal grid points 4 (46°) and 17 (74°) as representative of the northern and southern regions of the model. Table 2.1 lists the grid points, the corresponding distance from the southern boundary of the β -channel, and the latitude for the time dependent model.

dependent model.

Table 2.1
Horizontal Distance Scales for the Time
Dependent β -plane Model

Grid Point	Y (km)	Latitude $^{\circ}$
1	235	39.6
2	476	41.8
3	714	43.9
4	952	46.1
5	1190	48.2
6	1428	50.4
7	1667	52.5
8	1905	54.6
9	2143	56.8
10	2381	58.9
11	2619	61.1
12	2857	63.2
13	3095	65.4
14	3333	67.5
15	3571	69.6
16	3810	71.8
17	4048	73.9
18	4285	76.1
19	4523	78.2
20	4761	80.4

2.4 Observations of ozone

In order to evaluate the success of the transport model it is necessary to compare the calculated results to the observed ozone distribution. In this section a brief review of the observed behavior of ozone will be given. Some mention should be made concerning the units used in reporting the observations. The transport calculations will be done using the mixing ratio (ppm) as the basic unit of measure. Many of the observations have been made in other units such as ozone partial pressure or absolute density. Due to the variation of atmospheric density, the ozone distribution appears quite different in the various units. Kreuger and Minzner (1976) present conversion factors in their Table 2. Much of the general review of the ozone distribution is taken from Craig (1965) and Dütsch (1974).

The ozone distribution in the Southern Hemisphere is less well known and considerably different from that in the Northern Hemisphere. The distribution in the Southern Hemisphere will not be discussed here since the dynamics are more appropriate for the Northern Hemisphere. There will be some comment made about transport mechanisms in the Southern Hemisphere based on model results in Chapter 5.

At extratropical latitudes the ozone density reaches a maximum in the lower stratosphere between 15 and 30 km. The mixing ratio maximum occurs at somewhat higher altitudes between 35 and 45 km. In the lower stratosphere between 15 and 30 km. The mixing ratio maximum occurs at somewhat higher altitudes between 35 and 45 km. Above and below the ozone maximum the average state shows a monotonic decrease of ozone concentration; though, at any time an

ozone sounding might show considerable vertical structure due to small scale transport. There is ozone of stratospheric origin in the troposphere, but the amounts are quite small; and there is no attempt made here to model tropospheric ozone.

The absolute maximum amounts of ozone in the Northern Hemisphere occur at polar latitudes in the lower stratosphere during late winter and early spring. This is in complete disagreement with photochemical theory which predicts maximum amounts in the tropics at high altitudes in the middle and upper stratosphere. Figure 2.5 shows a March/April pole to pole cross section of ozone in both ozone density and ozone/air number mixing ratio. The predominant maximum seen at high latitudes in the density field is not clearly seen in the mixing ratio field since this maximum occurs in a region of relatively high atmospheric density. Two important features to note in the mixing ratio field are the positive horizontal gradient at high latitudes in the lowest part of the stratosphere and the negative horizontal gradient at high latitudes in the middle and upper stratosphere (Dütsch, 1974).

In the photochemical region the variation of ozone is quite small. In the lower stratosphere, however, the variation is large on both daily and seasonal time scales. Much of the daily variation is due to the infusion of synoptic size weather systems into the stratosphere and will not be modeled here. The seasonal variation is due to the diabatic circulation and planetary wave transport and stratosphere and will not be modeled here. The seasonal variation is due to the diabatic circulation and planetary wave transport and will be investigated in this dissertation.

Figure 2.5. Latitude-height cross section of ozone for March/April in partial pressure and ozone/air number mixing ratio (from Dütsch, 1974).

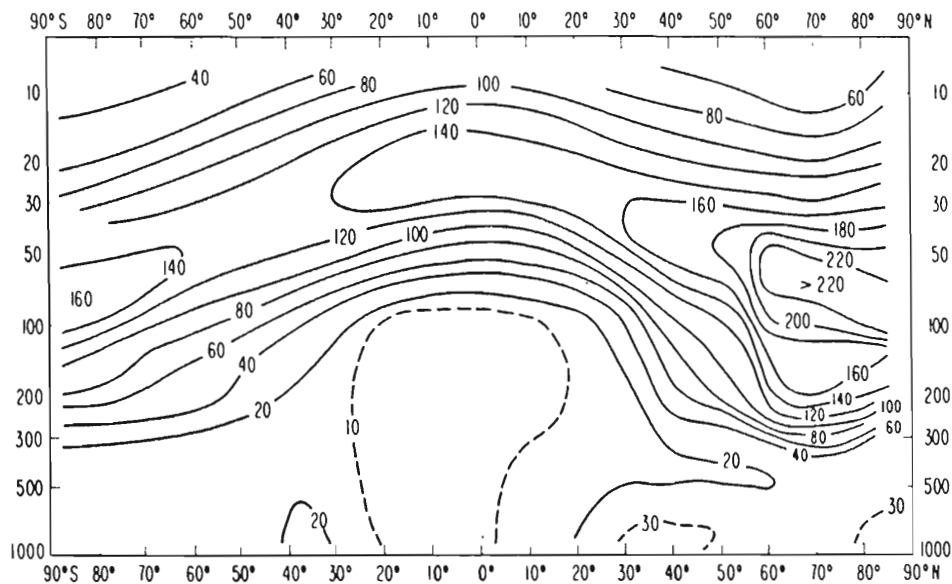
Figure 2.6. 6 year average time-height cross section of ozone partial pressure at Arosa, Switzerland (from Dütsch, 1974).

Figure 2.7 Vertical distribution of ozone from 3 soundings in late winter and early spring (μmb) (from Dütsch, 1974).

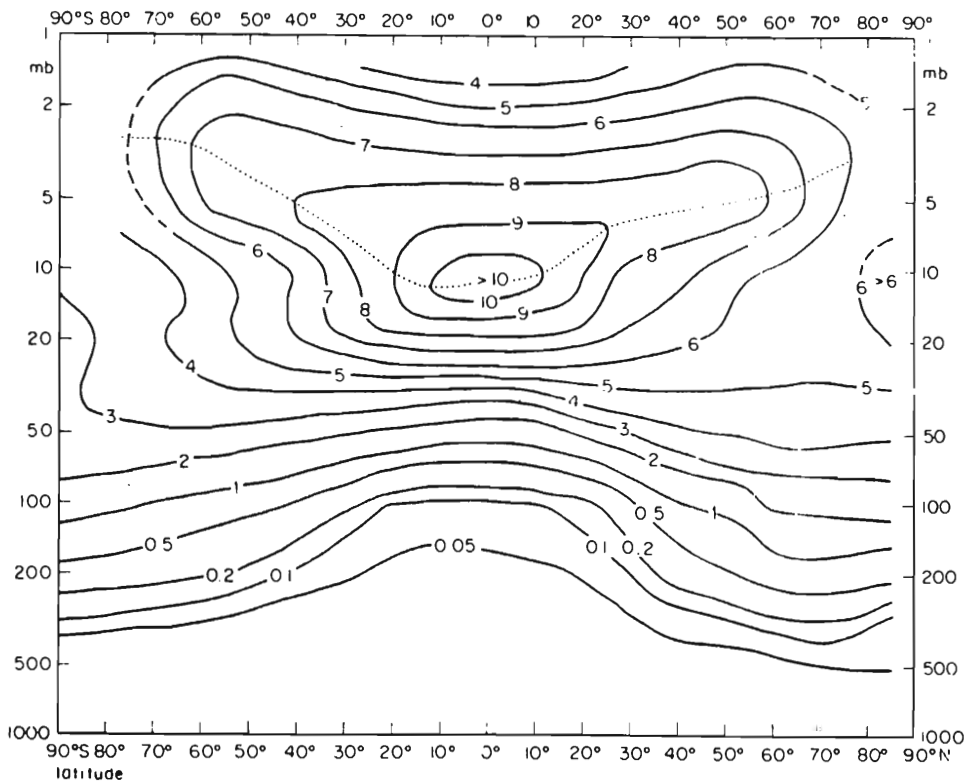
- a. Arctic type
- b. Polar type
- c. Subtropical type

Temperature on left in $^{\circ}\text{C}$.

Temperature on left in $^{\circ}\text{C}$.



Partial Pressure



Mixing Ratio



Mixing Ratio

Figure 2.5

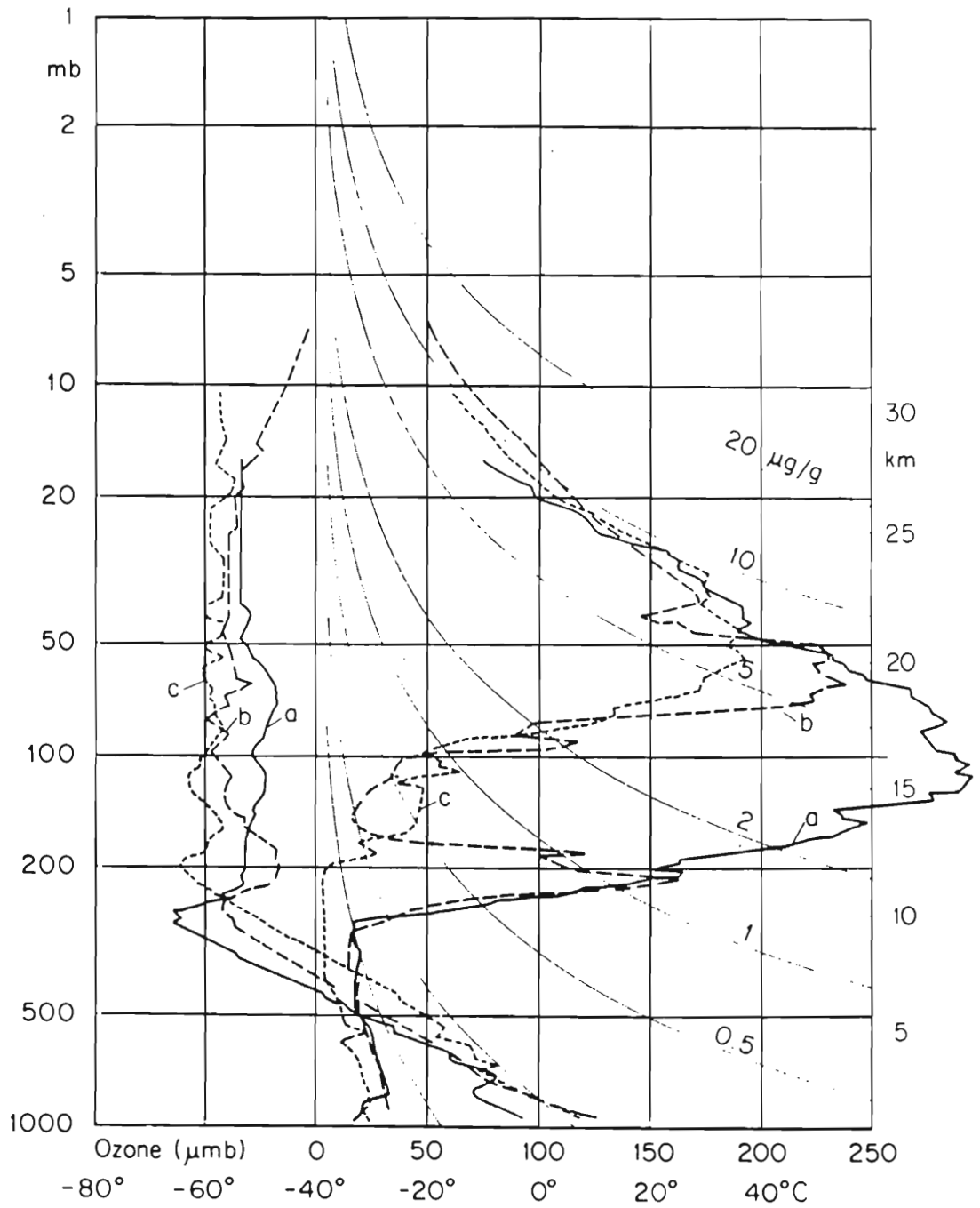


Figure 2.7

Figure 2.7

Figure 2.6 shows a time cross section of vertical ozone over Arosa, Switzerland. The most important feature to note is the strong increase between 30 and 50 mb (21-25 km) which begins in December and reaches a maximum in late winter. By the first of April there is a definite decreasing trend. Since this maximum appears in the conservative portion of the stratosphere, it can be deduced that transport is responsible for the ozone buildup. Another notable feature is the minimum concentration that occurs at the level of the tropopause.

In Figure 2.7 is shown the vertical distribution from three soundings in late winter and early spring. In the polar type sounding (b) there is a pronounced secondary density maximum in the lowest part of the stratosphere and a primary maximum around 21 km. In the Arctic type (a) there is just one broad maximum centered at 100 mb. In the subtropical type profile (c) there is only one large maximum, and there is relatively little ozone in the lower stratosphere.

Retrieval of vertical profiles in general requires the inversion of remote sensing observations which involve strongly overlapping contribution functions. Consequently, there are significant inaccuracies in the determination of the vertical profile. Ozonesondes have been used to directly determine the vertical structure, but these observations are limited in both space and time. Total ozone has been studied longer and is known with vertical structure, but these observations are limited in both space and time. Total ozone has been studied longer and is known with greater accuracy than the vertical structure; therefore, total ozone will be used in many of the comparisons of the model results to

observation. Using total ozone for comparison has the disadvantage that model errors might be masked during the integration to form the total amounts.

Many of the features of the behavior of total ozone have been known since the early days of ozone observations. Using a network of only six instruments, Dobson (1930) deduced that both total ozone and the temporal variation of total ozone increased with increasing latitude. Perhaps the most extensive documentation of analyzed total ozone observations is the atlas of London et al. (1976) which contains ten years of data from 1957-1967. The average latitude-time cross section of total ozone in Dobson Units (DU) is shown in Fig. 2.8 and is not greatly different in the Northern Hemisphere from the cross section published by Götz (1951). This figure shows a rapid buildup of ozone at middle and high latitudes during winter. The maximum is reached at polar latitudes around the first of March. During early winter the maximum amount of ozone is found to between 60° and 70° N. There is a lack of data north of 80° so that the results in the extreme north are of dubious quality.

The regularity of the total ozone field is demonstrated in Fig. 2.9 taken from Hilsenrath et al. (1979). These data from the NIMBUS 4 BUW experiment show some fluctuation in the annual variation of total ozone, but the large scale features remain quite constant during the time series.

Figure 2.10 from Zullig (1973) helps to demonstrate the extent of the interannual variation in the total ozone field.

Figure 2.10 from Zullig (1973) helps to demonstrate the extent of the interannual variation in the total ozone field. In this figure the average amount of total ozone in the Northern Hemisphere

north of 40° for three winters is shown. Even with the large amount of averaging involved in the formation of these graphs, there is an obvious temporal wave evident in the data. In the two winters during which warmings occur (1962/63, 1967/68), the maximum amount of ozone is approximately 6% larger, and the increase is more sudden, than in the winter during which no major warming occurs. While Zullig's observations are a rather limited amount of data on which to base transport theories, it is safe to conclude that major stratospheric warmings have a strong influence on the ozone distribution.

Figure 2.8. 10 year average latitude-time cross section of total ozone in Dobson Units (DU) (from London et al., 1976).

Figure 2.9. Latitude-time cross section of total ozone data from Nimbus 4 BUUV (DU) (from Hilsenrath et al., 1979).

Figure 2.10. Mean total ozone north of 40° (from Zullig, 1973).

Figure 2.11 Reproduction of Figure 2.8 north of 30° from mid-December through April.

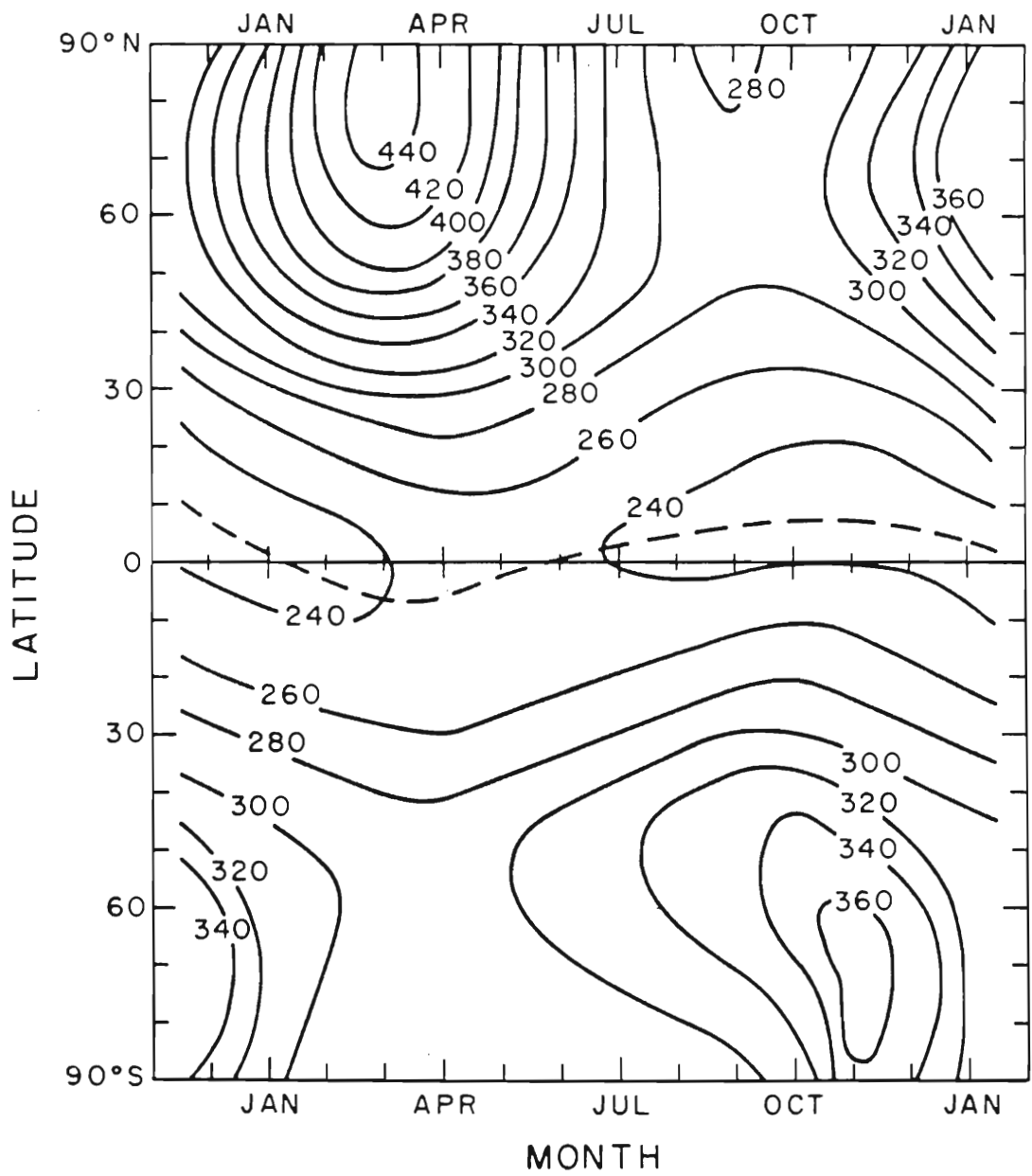


Figure 2.8

Figure 2.8

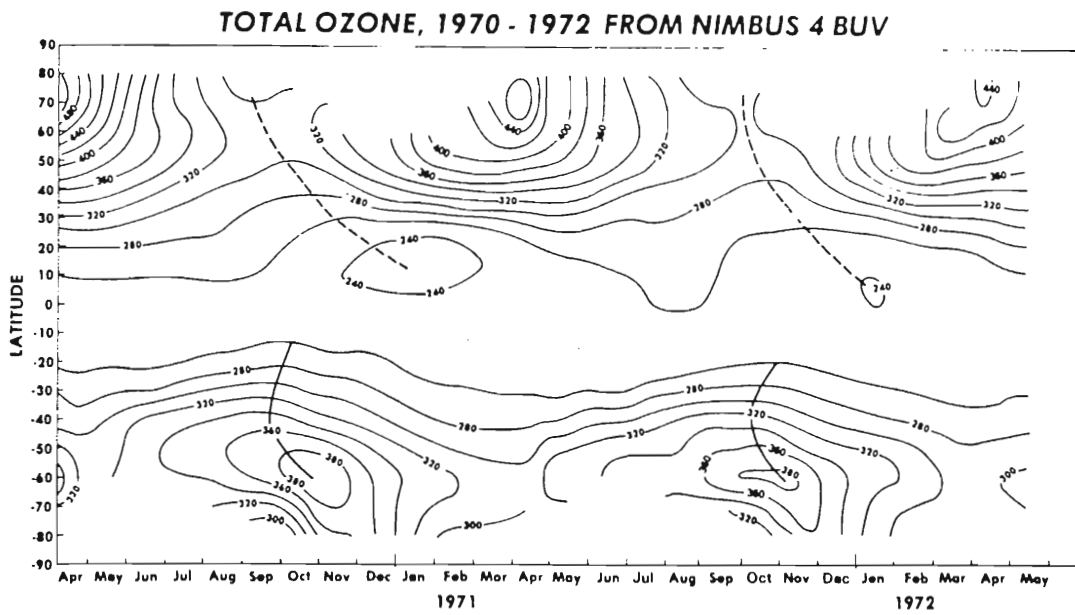


Figure 2.9

MEAN TOTAL OZONE NORTH OF 40°

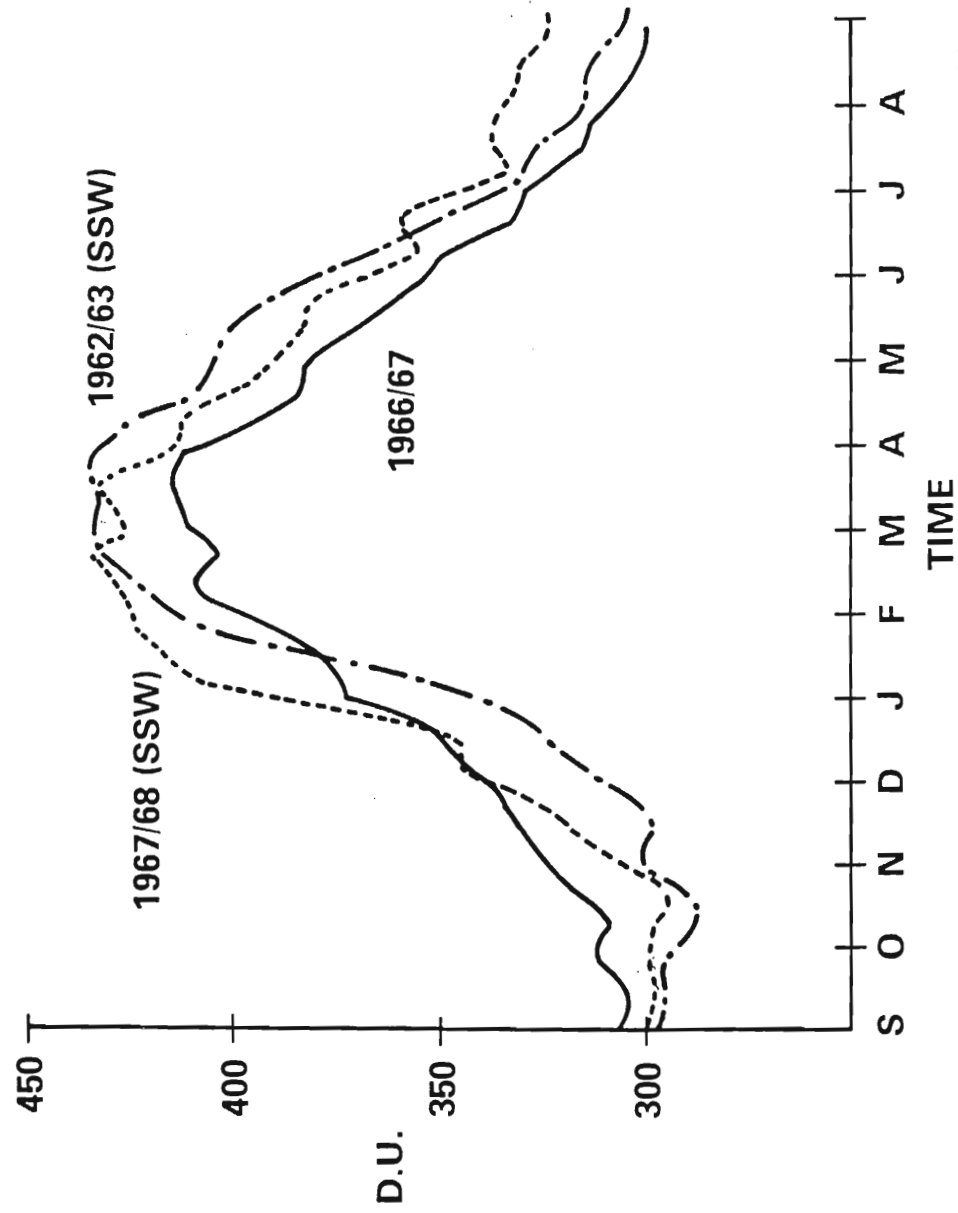


Figure 2.10

TOTAL OZONE (D.U.)

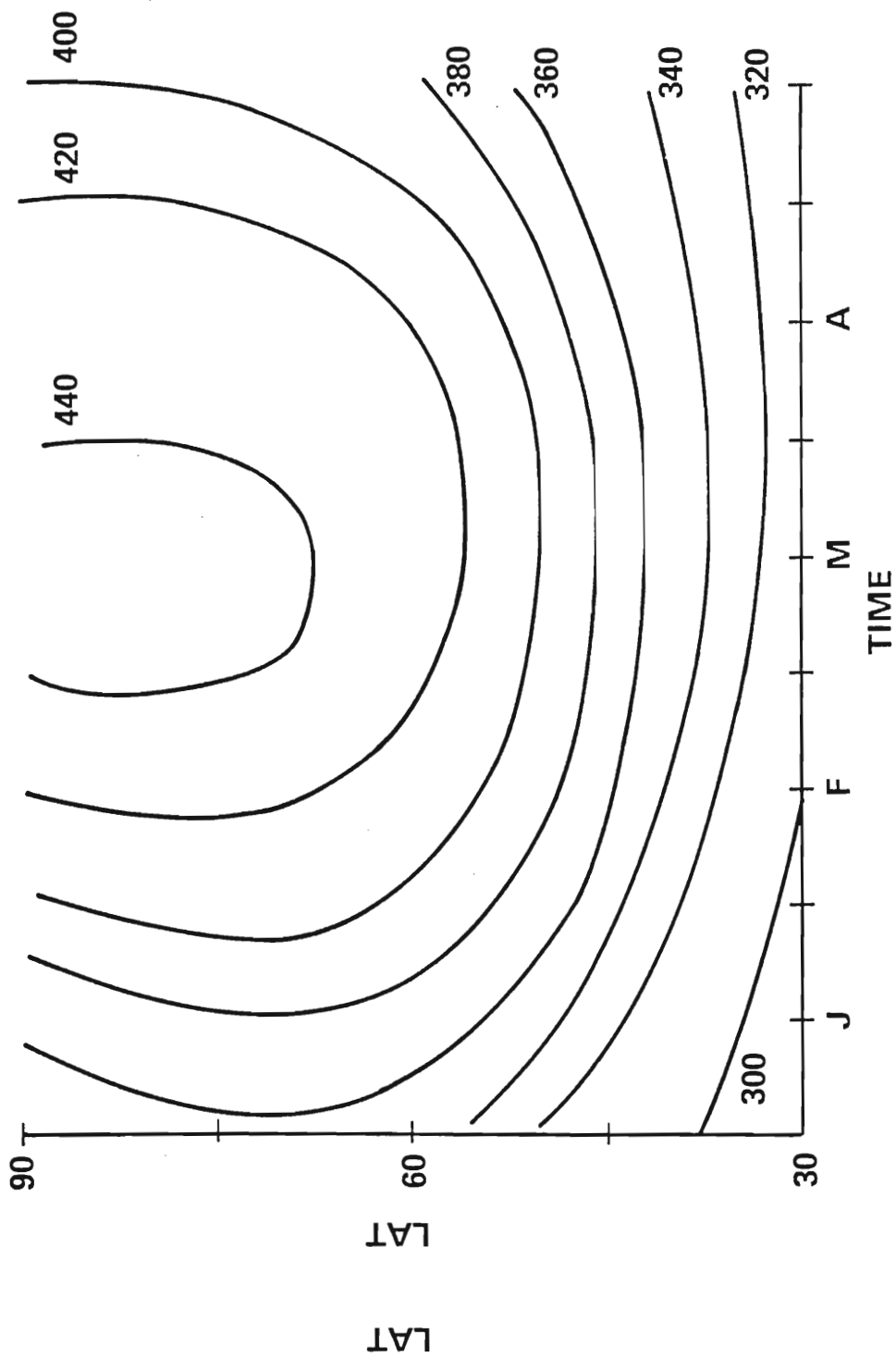


Figure 2.11

The basic features of the ozone variability that will be studied here are the total ozone amount at extratropical latitudes and the transport of ozone into the lower stratosphere during winter. Total ozone increases at all latitudes during winter with the magnitude of the increase being largest near the pole. During early winter the maximum is in subpolar latitudes. Much of this increase in total ozone is associated with the injection of large amounts of ozone between 21 and 25 km. There is little change in the ozone above 40 km and the observed changes in this region can be explained photochemically. The total ozone reaches a maximum in early March at polar latitudes and decreases uniformly until it reaches a minimum in the fall.

The time dependent β -plane transport model will be used to run simulations from mid-December until April. In order to facilitate comparisons to observations a reproduction of the appropriate portion of the average total ozone field given by London et al. (1976) is presented in Fig. 2.11.

Chapter 3

TRANSPORT BY STEADY STATE PLANETARY WAVES

3.1 Introduction

In this chapter steady state transport by stationary planetary waves on a β -plane is presented. In Section 3.2 the continuity equation is developed for small amplitude waves in both the Eulerian and Lagrangian-mean formulations, and the relation between the residual circulation and the Lagrangian-mean velocity is derived. In Section 3.3 model results are presented and a Lagrangian model based on particle trajectories is given. The results are discussed and summarized in Section 3.4.

3.2 Constituent dynamics

The ozone continuity equation is formulated in both the Eulerian and Lagrangian-mean systems. In general, the constituent continuity equation is

$$\frac{D\mu}{Dt} = Q \quad (3.1)$$

$$\overline{\frac{D\mu}{Dt}} = \overline{Q} \quad (3.1)$$

where Q represents the source term. By decomposing the fields into

zonal averages and deviations and linearizing, the Eulerian formulation is obtained:

$$\frac{\partial \bar{\mu}}{\partial t} + \bar{u}_i \frac{\partial \bar{\mu}}{\partial x_i} + \overline{u_i' \frac{\partial \mu'}{\partial x_i}} = \bar{Q} \quad (3.2)$$

and

$$\frac{\partial \mu'}{\partial t} + u_i' \frac{\partial \bar{\mu}}{\partial x_i} + \bar{u}_i \frac{\partial \mu'}{\partial x_i} = Q' \quad (3.3)$$

where repeated indices indicate summation. It is pertinent to note that the zonal mean equation contains eddy flux terms which represent the effects of wave transport. The tendency for the eddy transport to be counteracted by the advection by the mean flow has been discussed extensively, and represents a major difficulty of atmospheric transport problems (Dunkerton, 1980; Mahlman and Moxim, 1978).

Using the Lagrangian-mean formulation (Andrews and McIntyre, 1978) it is possible to redefine the averaging operator such that wave forcing does not appear in the mean equation. Using this concept the mean continuity equation is written as

$$\left(\frac{\partial}{\partial t} + u_i^L \frac{\partial}{\partial x_i} \right) u^L = Q^L \quad (3.4)$$

In this system the time rate of change of the Lagrangian-mean ozone

In this system the time rate of change of the Lagrangian-mean ozone distribution is equal to the advection by the Lagrangian-mean velocity plus a source term.

The difference between the Lagrangian-mean and the Eulerian zonal mean is defined as the Stokes correction

$$\mu^s \equiv \mu^L - \bar{\mu}$$

Relating the Lagrangian-mean transform to the Eulerian zonal mean by the premise that the unperturbed fluid would be described by the Eulerian flow, it is possible to define the Stokes correction to second order as

$$\mu^s = \overline{\xi_i \frac{\partial \mu^L}{\partial x_i}} + \frac{1}{2} \overline{\xi_i \xi_j} \frac{\partial^2 \bar{\mu}}{\partial x_i \partial x_j} \quad (3.5)$$

where $\xi_i = (\xi_1, \xi_2, \xi_3) = (\xi, \eta, \zeta)$ are the displacements from the equilibrium position of the fluid.

The displacement fields are related to the Eulerian perturbation velocity fields by the following equation (Matsuno and Nakamura, 1979):

$$\left(\frac{\partial}{\partial t} + \bar{u} \frac{\partial}{\partial x} \right) \xi_i = u_i^L + \xi_j \frac{\partial}{\partial x_j} \bar{u}_i + \dots \quad (3.6)$$

The mean meridional circulation is forced by the waves and is assumed to be second order in wave amplitude ($O(a^2)$). Therefore, the changes in the mean ozone field are $O(a^2)$ and the terms assumed to be second order in wave amplitude ($O(a^2)$). Therefore, the changes in the mean ozone field are $O(a^2)$ and the terms involving \bar{v} , \bar{w} in (3.3) and (3.6) can be ignored. The perturbation equation can now be written to $O(a^2)$ as

$$\frac{\partial \mu'}{\partial t} + \bar{u} \frac{\partial \mu'}{\partial x} + v' \frac{\partial \bar{\mu}_0}{\partial y} + w' \frac{\partial \bar{\mu}_0}{\partial z} = -\lambda \mu' \quad (3.7)$$

Using the mass continuity equation, (3.2) may be written as

$$\frac{\partial \bar{\mu}}{\partial t} + \frac{\partial}{\partial y} (\bar{v} \bar{\mu}_0 + \overline{v' \mu'}) + \frac{1}{\rho} \frac{\partial}{\partial z} \rho (\bar{w} \bar{\mu}_0 + \overline{w' \mu'}) = -\lambda \bar{\mu} \quad (3.8)$$

where $\bar{\mu}$ now represents changes in the mean field from the equilibrium value $\bar{\mu}_0$.

The relation between the perturbation velocity fields and the displacement fields (Eq. 3.6) can be rewritten for steady waves as

$$ik\bar{u}\xi = u' + \eta \frac{\partial \bar{u}}{\partial y} + \zeta \frac{\partial \bar{u}}{\partial z}$$

$$ik\bar{u}\eta = v' \quad , \quad ik\bar{u}\zeta = w'$$

These are the equations used to calculate the Lagrangian-mean displacements.

Under the assumptions above, the following relationships between the Eulerian and the Lagrangian-mean quantities can be written for steady waves:

written for steady waves: ^{1.} -

$$\frac{\partial \mu}{\partial t}^L = \frac{\partial \bar{\mu}}{\partial t} + O(a^4) \quad (3.9a)$$

$$\bar{v}^S = \overline{\xi_i \frac{\partial v^r}{\partial x_i}} + O(a^4) \quad (3.9b)$$

$$\bar{w}^S = \overline{\xi_i \frac{\partial w^r}{\partial x_i}} + O(a^4) \quad (3.9c)$$

$$\bar{Q}^L = \bar{Q} + \overline{\xi_i \frac{\partial Q^r}{\partial x_i}} \quad (3.9d)$$

Therefore (3.4) can be written to the same accuracy as (3.8) as

$$\frac{\partial \bar{\mu}}{\partial t} = -u_i^L \frac{\partial \bar{\mu}_0}{\partial x_i} - \overline{\xi_i \frac{\partial \lambda \mu^r}{\partial x_i}} - \lambda \bar{\mu} \quad (3.10)$$

The first term on the right hand side of (3.10) will be referred to as the advective term; the second term is the "stirring" term; and the third term is the mean chemistry. The stirring term represents the effects of the planetary waves moving ozone parcels through a region of varying photochemistry. This term will be discussed in detail later. Equations (3.7), (3.8), and (3.10) are the ozone continuity equations used in this study.

A number of authors have suggested that the Lagrangian-mean velocity may be a suitable quantity to approximate the large scale transport of ozone in chemical models (Dunkerton, 1978; Miller et al., 1981; McIntyre, 1980). However, since the Lagrangian-mean transport of ozone in chemical models (Dunkerton, 1978; Miller et al., 1981; McIntyre, 1980). However, since the Lagrangian-mean velocity can be difficult to calculate, it has also been suggested that the residual circulation defined by Andrews and McIntyre (1976)

might be an adequate approximation for the Lagrangian-mean velocity (Holton, 1981). Strobel (1981) has derived a general linearized 2-D transport model using the residual circulation for waves with complex frequencies. The relation between the residual velocity and the Lagrangian-mean velocity for steady, dissipating planetary waves is outlined below.

The eddy mass continuity equation can be written in terms of the parcel displacement fields as

$$\frac{\partial \xi}{\partial x} + \frac{\partial \eta}{\partial y} + \frac{1}{\rho} \frac{\partial \rho \zeta}{\partial z} = 0 \quad (3.11)$$

Using (3.11) and the definition of the Stokes corrections it is possible to write

$$\mathbf{v}^L = \bar{\mathbf{v}} + \frac{1}{\rho} \frac{\partial}{\partial z} \overline{\rho \mathbf{v}^* \zeta} \quad (3.12)$$

and

$$w^L = \bar{w} - \frac{\partial}{\partial y} \overline{v^* \zeta} \quad (3.13)$$

The residual circulation for the current problem is

$$\mathbf{v}^* = \bar{\mathbf{v}} - \frac{1}{\rho N^2} \frac{\partial}{\partial z} \rho \overline{\mathbf{v}^* \phi_z^*} \quad (3.14)$$

$$v^* = \bar{v} - \frac{1}{\rho N^2} \frac{\partial}{\partial z} \rho \overline{v^* \phi_z^*} \quad (3.14)$$

and

$$w^* = \bar{w} + \frac{1}{N^2} \frac{\partial}{\partial y} \overline{v' \phi'_z} \quad (3.15)$$

Using the eddy thermodynamic equation

$$(a + \bar{u}ik) \phi'_z - f v' \frac{\partial \bar{u}}{\partial z} + \bar{u}ik N^2 \zeta = 0$$

and multiplying by v' and averaging, it can be shown that

$$\overline{v' \phi'_z} = - \frac{N^2 ik \bar{u} \overline{v' \zeta} - f \bar{v}'^2 \frac{\partial \bar{u}}{\partial z}}{(a + ik \bar{u})} \quad (3.16)$$

Using (3.16) and comparing (3.12) and (3.13) with (3.14) and (3.15) it is clear that the Lagrangian-mean velocity and the residual velocity are equal only when $a = 0$. When $a = 0$, however, both the Lagrangian-mean and the residual circulation are zero and the transport by the waves and the mean flow exactly counterbalance each other. Since a is an order of magnitude or more smaller than $k\bar{u}$ below the sponge layer in this model, the Lagrangian-mean and residual circulations should be similar. When transience or external heating and cooling processes are allowed, the relationship between the two circulations becomes more complex. In Holton's (1981) parameterization, the difference between the Lagrangian-mean and residual circulations is contained in the antisymmetric part of the diffusion tensor and is assumed to be negligible. and residual circulations is contained in the antisymmetric part of the diffusion tensor and is assumed to be negligible.

In the next section the Eulerian velocities, the Lagrangian-mean quantities, and the residual circulation will be presented for

steady, dissipative planetary waves. Zonal mean ozone changes can then be calculated and the various transport methods can be compared.

3.3 Results

The zonal mean ozone distribution used in the steady state model is shown in Fig. 3.1. This distribution is based on the October/November values given by Dütsch (1969) and is similar to the distribution used by Hartmann and Garcia (1979).

a. Dynamic quantities

The \bar{v} and \bar{w} fields are shown in Fig. 3.2. These fields, as expected, show rising motion in the northern regions of the β -channel and sinking motion in the southern regions. The meridional velocity is from north to south. This flow is forced by the northward eddy heat transport of the planetary waves.

The Stokes drifts as calculated with (3.9b) and (3.9c) are shown in Fig. 3.3. These drifts can be viewed as the effective velocity fields associated with the wave. The Stokes drifts are directed in an opposite sense to the Eulerian mean velocity and are of approximately the same magnitude. This demonstrates the tendency for the wave fields to counterbalance the mean fields.

Figure 3.1. Zonal mean ozone distribution
for the steady state model (ppm).

Figure 3.2. Eulerian zonal mean velocities (cm sec⁻¹).

a. \bar{v}

b. \bar{w}

Figure 3.3. Stokes drifts (cm sec⁻¹).

a. v^S

b. w^S

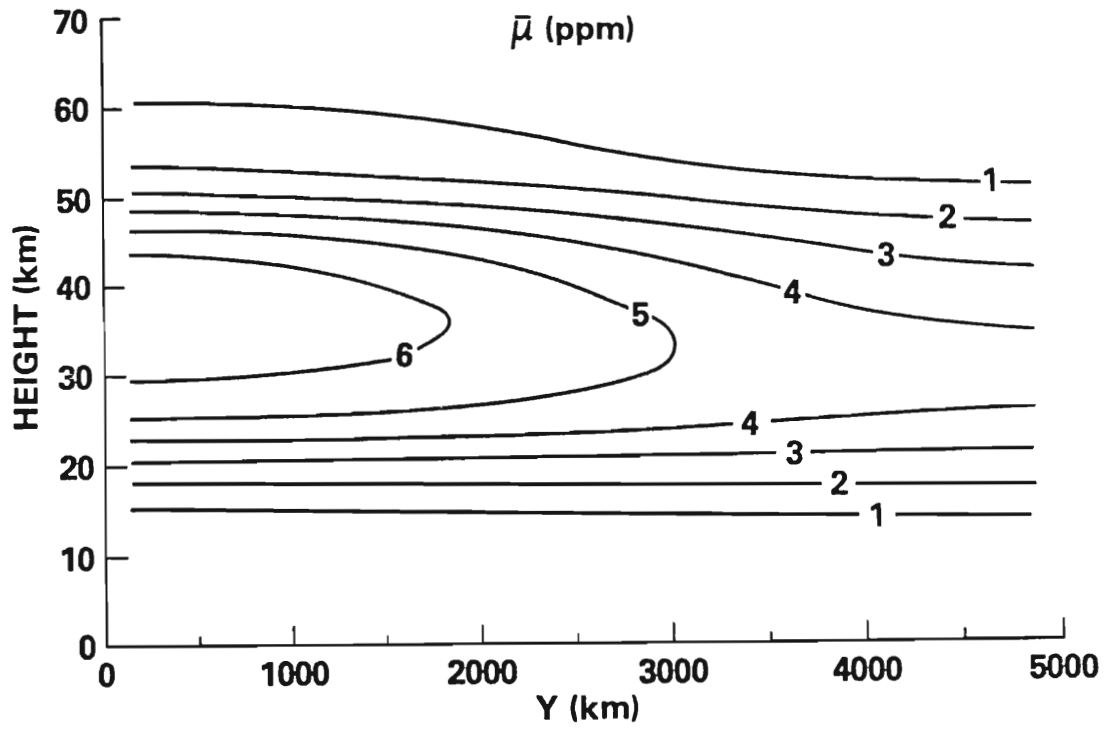


Figure 3.1

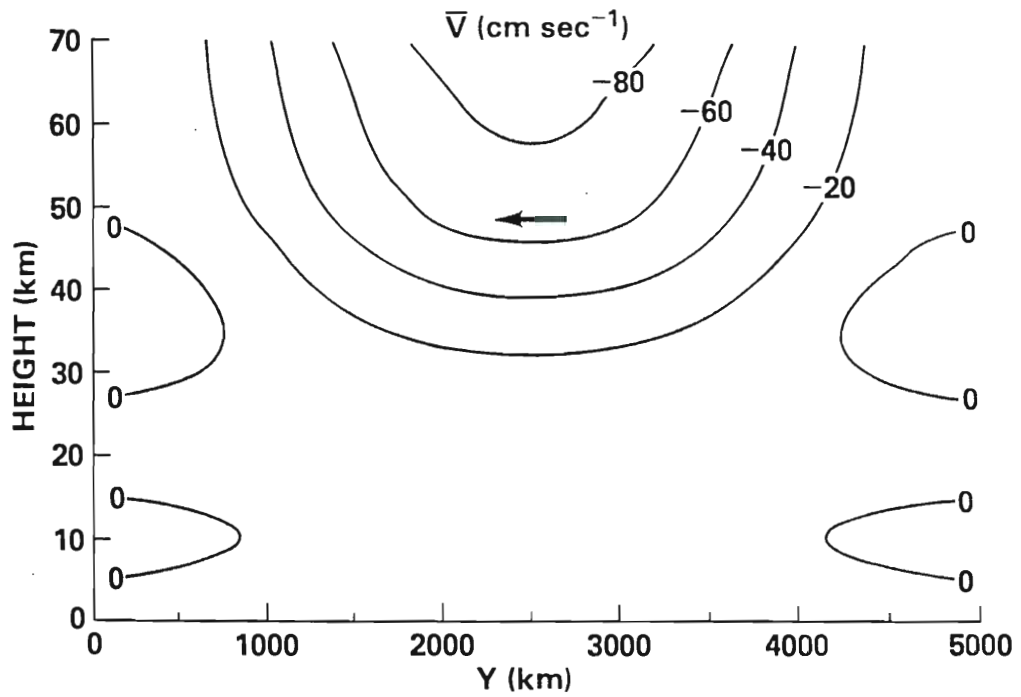


Figure 3.2a

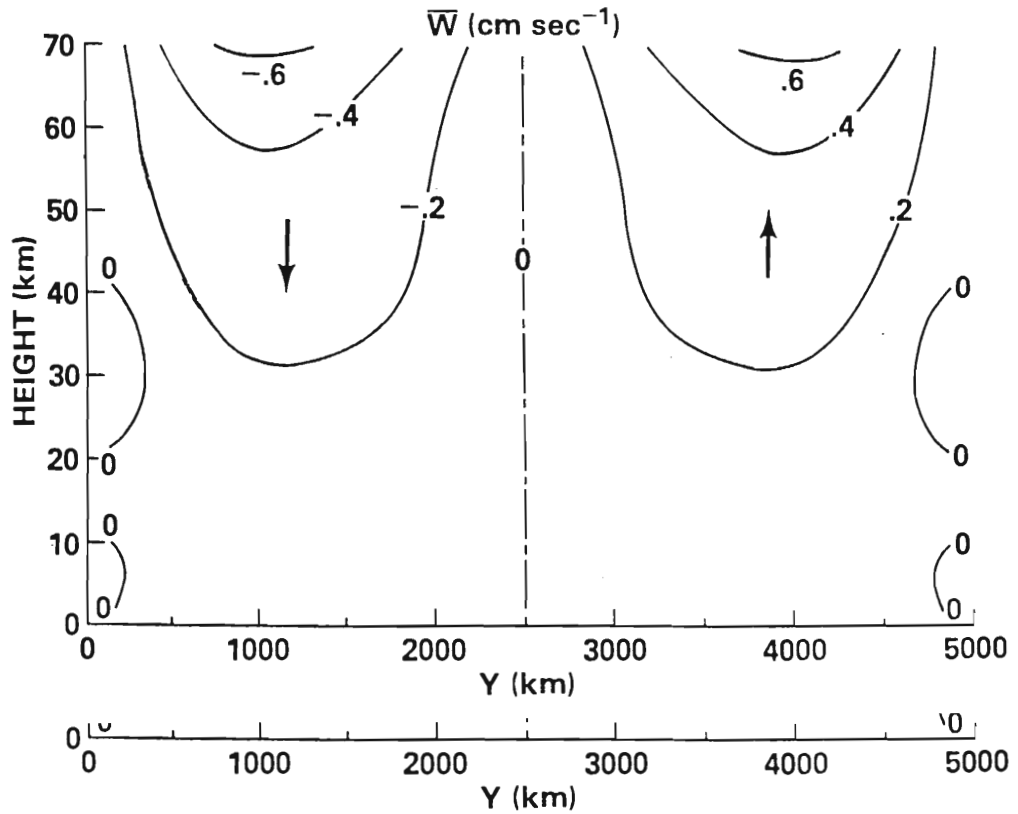


Figure 3.2b

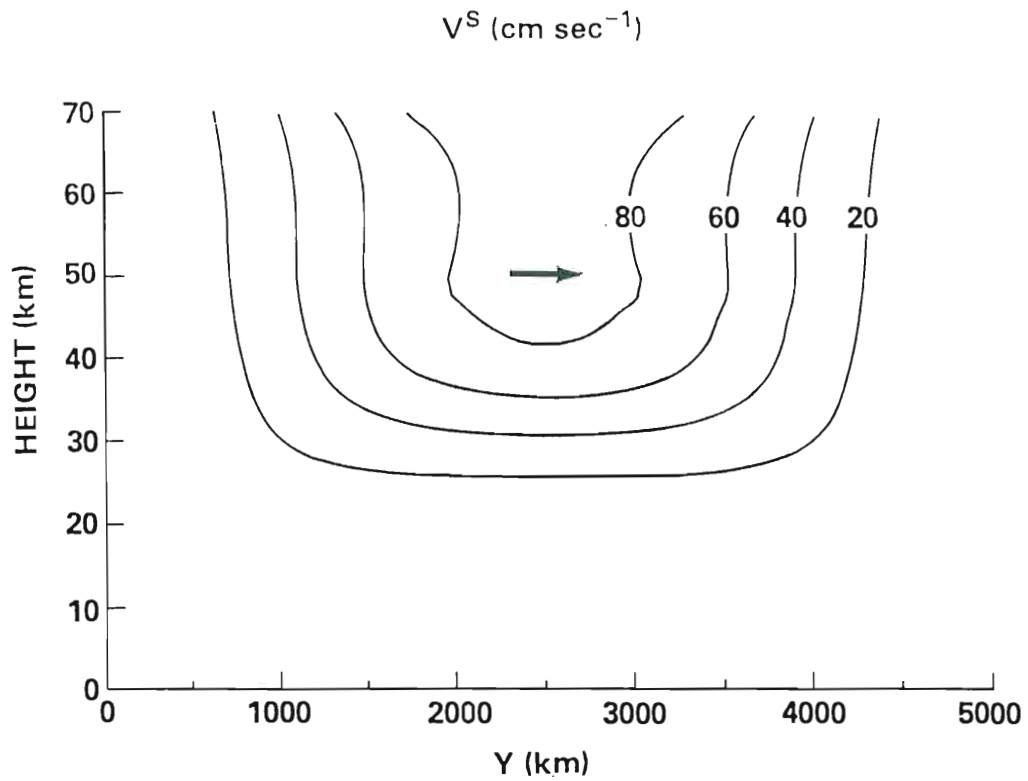


Figure 3.3a

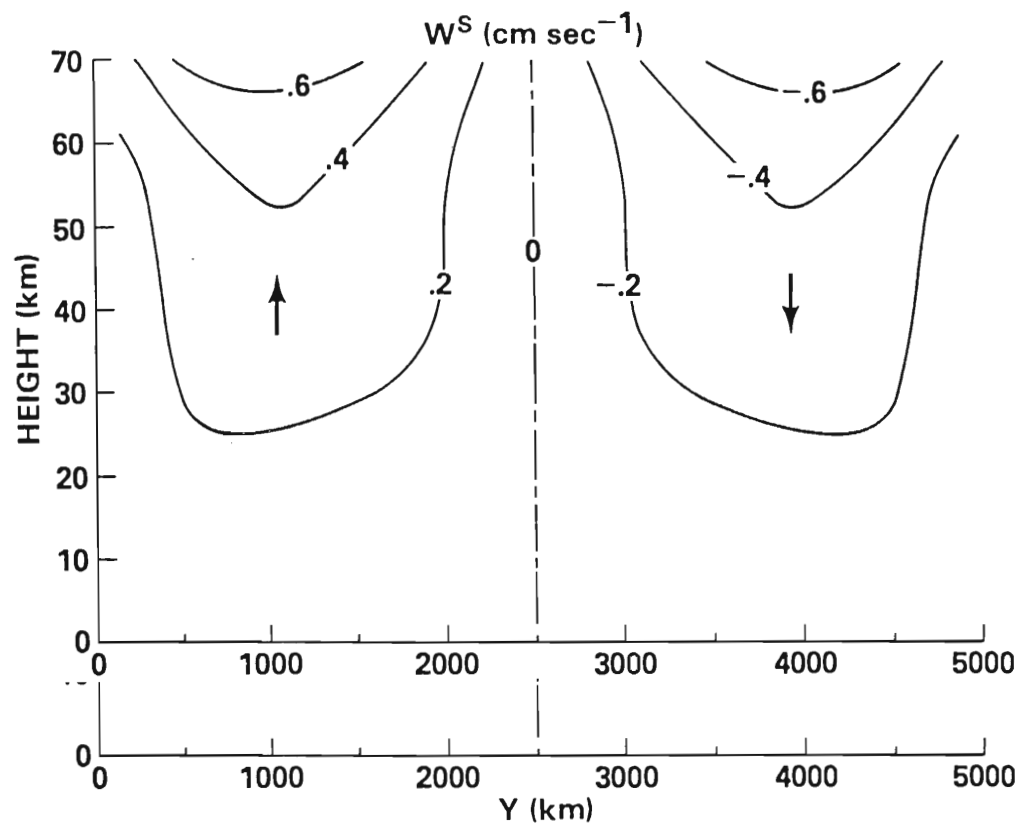


Figure 3.3b

The Lagrangian-mean velocity fields, which are the sums of the Eulerian zonal mean and the Stokes drifts, are shown in Fig. 3.4. The sense of the circulation is rising motion in the southern regions and sinking motion in the polar regions. This motion is the same as indicated by Schoeberl (1981a). Furthermore, this motion would tend to enhance the diabatic circulation as calculated by Dunkerton (1978). The Lagrangian-mean velocity is of much smaller magnitude than either the Stokes drifts or the Eulerian mean velocities.

The residual circulation is shown in Fig. 3.5. It is geometrically similar to the Lagrangian-mean velocity but the meridional component is approximately 30% larger than the Lagrangian-mean meridional velocity. The largest differences between the two circulations occur in the region where $\partial \bar{u} / \partial z$ is largest. Similar increases are calculated in the vertical residual velocity field.

Figure 3.4. Lagrangian-mean velocities (cm sec^{-1}).

a. v^L

b. w^L

Figure 3.5. Residual velocities (cm sec^{-1}).

a. v^*

b. w^*

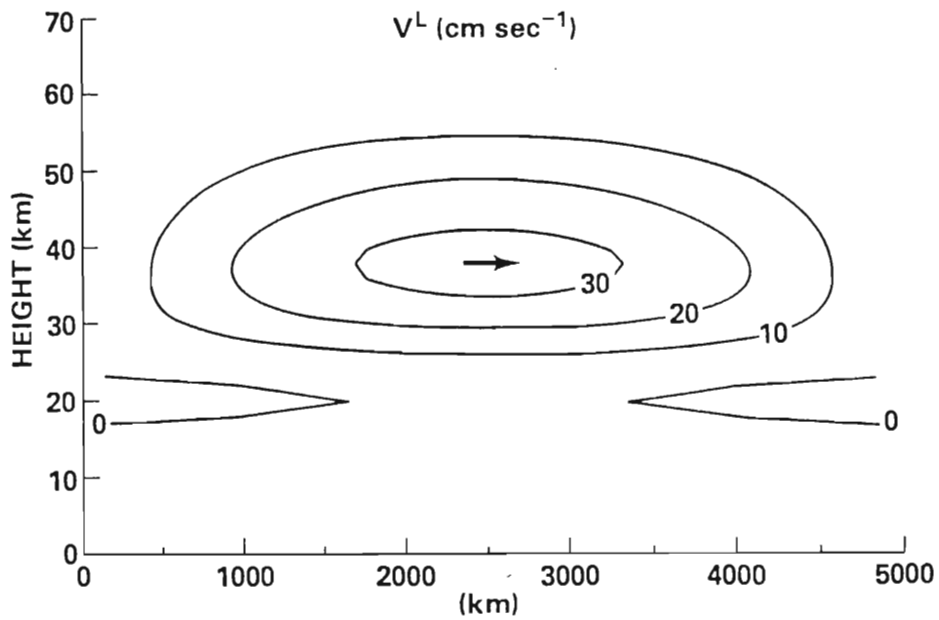


Figure 3.4a

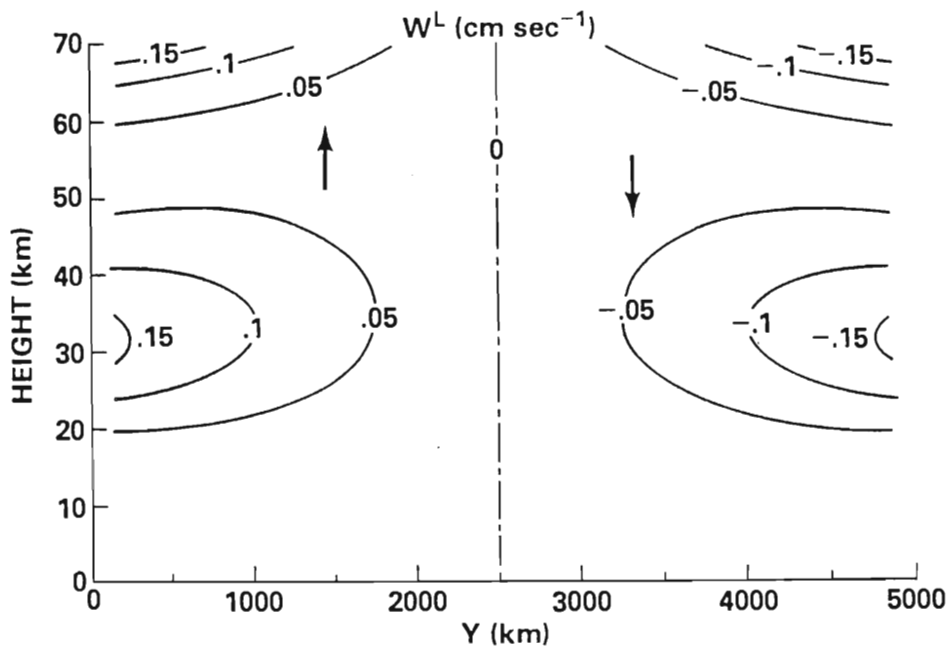


Figure 3.4b

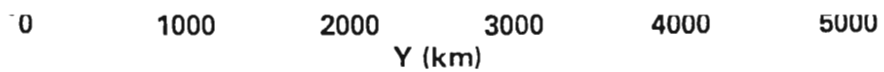


Figure 3.4b

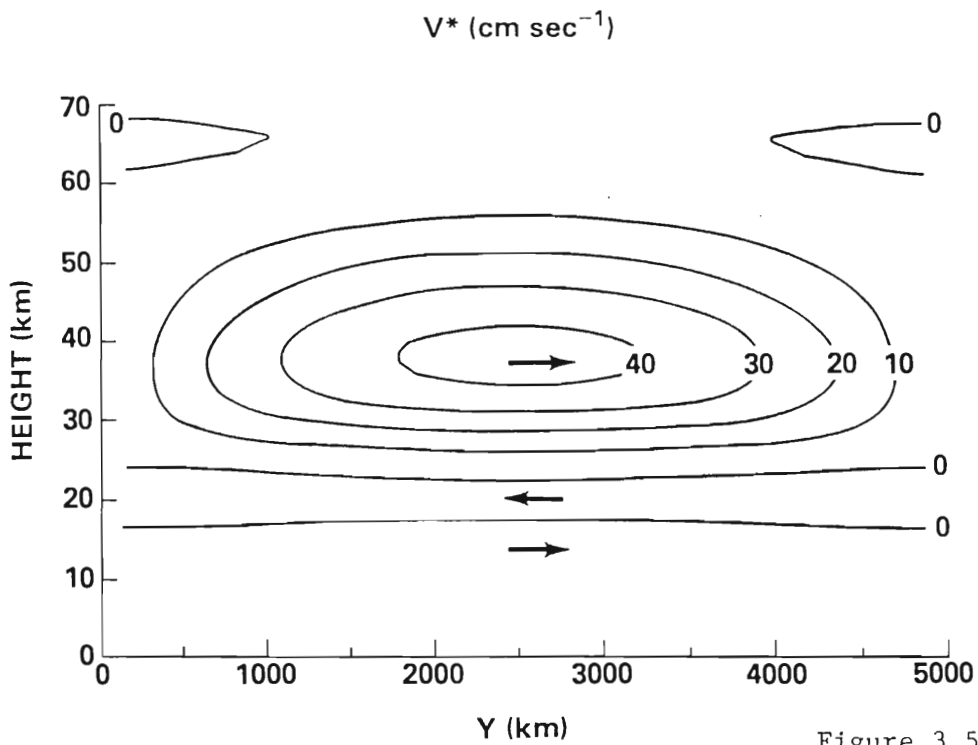


Figure 3.5a

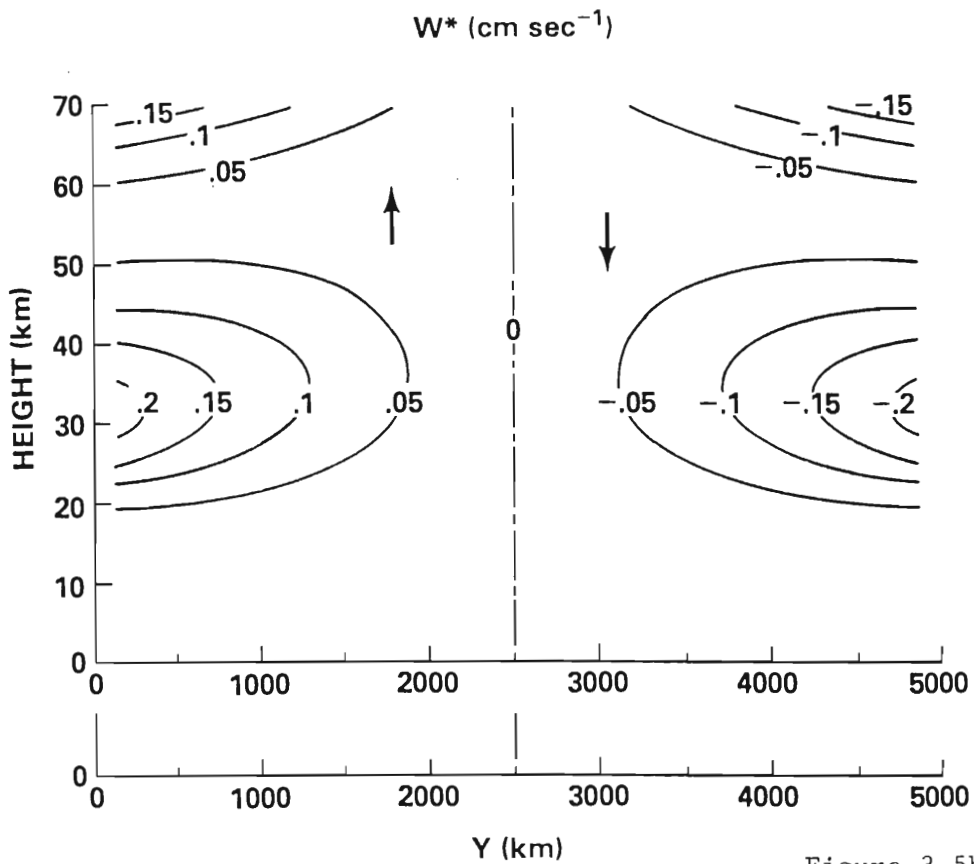


Figure 3.5b

b. Eulerian transport

The continuity equations (3.7), (3.8), and (3.10) are solved using the appropriate dynamic quantities. Since the mean chemistry appears in the same form in both (3.8) and (3.10) it is ignored in order that it might not obscure the differences between the two formulations. The effects of the mean chemistry term will be considered separately.

The horizontal ($\overline{v\mu} + \overline{v'\mu'}$) and vertical ($\overline{w\mu} + \overline{w'\mu'}$) fluxes as calculated by the Eulerian method are shown in Fig. 3.6. The vertical flux is upward in the northern region of the model and downward in the southern region. The vertical flux is confined primarily to the conservative region and reflects the Eulerian-mean vertical velocity field.

The horizontal flux field is quite complicated showing two regions of northward transport separated by a region of southward transport. Once again the flux is largest in the conservative region. The lower region of northward flux is dominated by eddy flux as described by Clark and Rogers (1978). The region of southward flux is dominated by the mean meridional velocity. The upper region of northward transport is once again dominated by the eddy flux. In the upper most regions of the model both the horizontal and vertical fluxes are very small due to rapid photochemical relaxation.

The rate of change of the mean ozone field is calculated as the photochemical relaxation.

The rate of change of the mean ozone field is calculated as the divergence of the fluxes. This field is shown in Fig. 3.7. There is an increase of ozone in the northern section and a decrease in

the southern section. Despite the fluxes being largest in the conservative region, the mean field change is concentrated almost entirely in the transition region in agreement with the results of Hartmann and Garcia (1979).

Figure 3.6. Eulerian fluxes of ozone (ppm m sec^{-1}).

a. horizontal flux

b. vertical flux

Figure 3.7. Mean ozone tendency, $\frac{\partial \bar{\mu}}{\partial t}$, as calculated with the Eulerian formulation (ppm sec^{-1}).

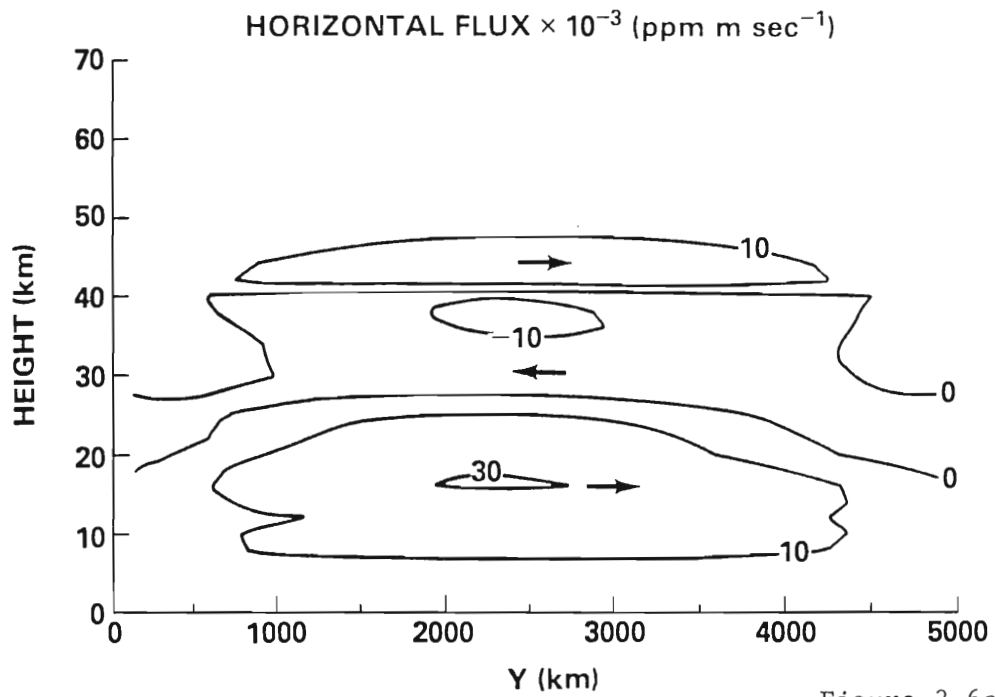


Figure 3.6a

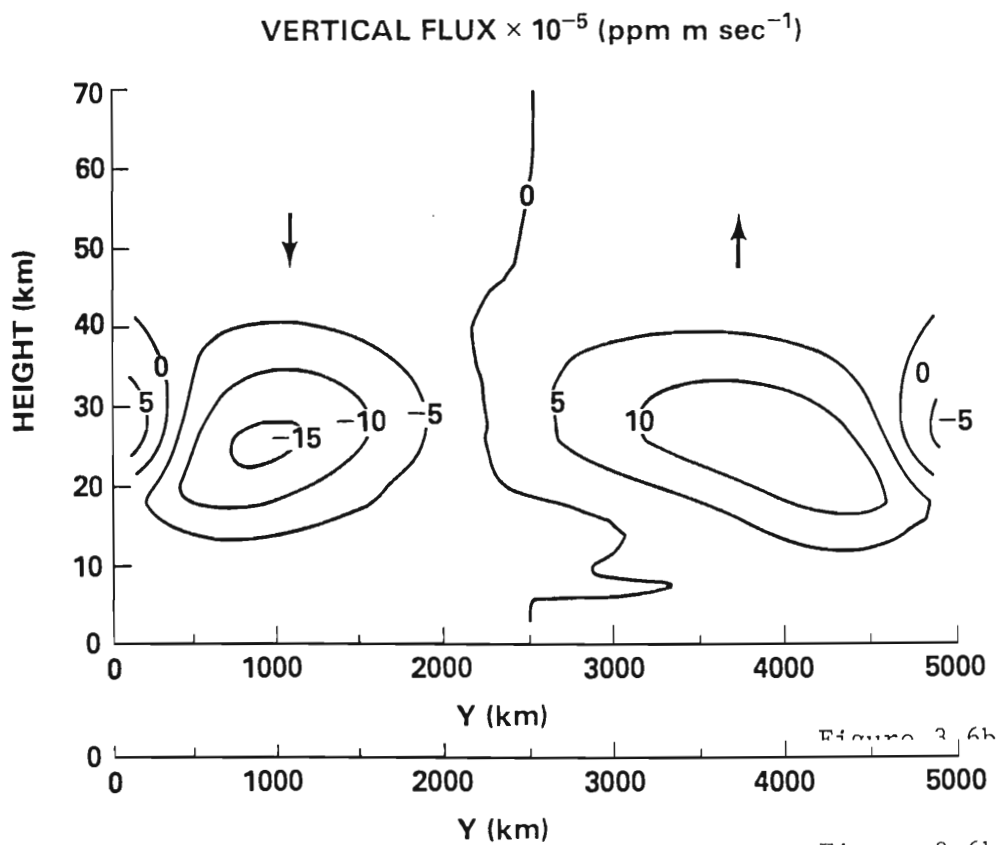


Figure 3.6b

Figure 3.6b

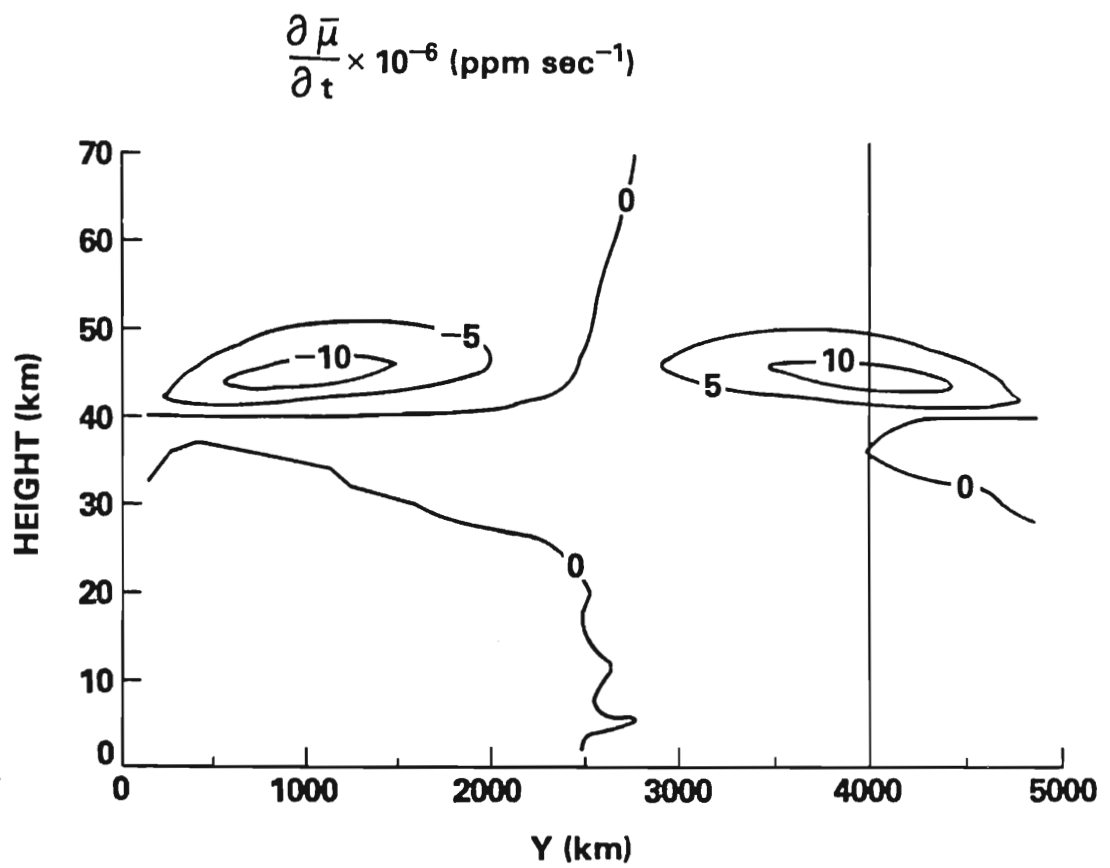


Figure 3.7

c. Lagrangian-mean transport

The Lagrangian-mean results are shown in Figures 3.8-3.10. The advective term as defined in Eq. (3.10) is shown in Fig. 3.8. In the extreme polar region there is a decrease of ozone above the ozone maximum and a buildup of ozone in the lower stratosphere. In the southern regions there is a decrease in the lower stratosphere and an increase in the upper stratosphere. These changes are primarily due to the vertical advection. There is a strong transport of ozone northward by the meridional Lagrangian-mean velocity in the midlatitudes. The Lagrangian-mean velocity associated with planetary waves advects ozone poleward and downward.

The advective term calculated using the residual circulation shows increases and decreases in the mean ozone field in the same regions as the Lagrangian-mean calculations. In all regions the magnitude of advection by the residual circulation is larger. Differences as large as 30% are calculated reflecting the increased magnitude of the residual circulation.

Comparison of Figures 3.10 and 3.7 show that the mean field changes are the same when calculated by the Eulerian or Lagrangian-mean methods. Substituting the residual velocity for the Lagrangian-mean velocity causes no significant changes in the calculation of the mean field changes.

Figure 3.8. Mean ozone tendency
caused by advection (ppm sec^{-1}).

a. Lagrangian-mean velocity

b. residual velocity

Figure 3.9. Total mean ozone tendency as calculated
with the Lagrangian formulation (ppm sec^{-1}).

Figure 3.10. Mean ozone tendency
caused by "stirring" (ppm sec^{-1}).

LAGRANGIAN-MEAN ADVECTION $\times 10^{-8}$ (ppm sec $^{-1}$)

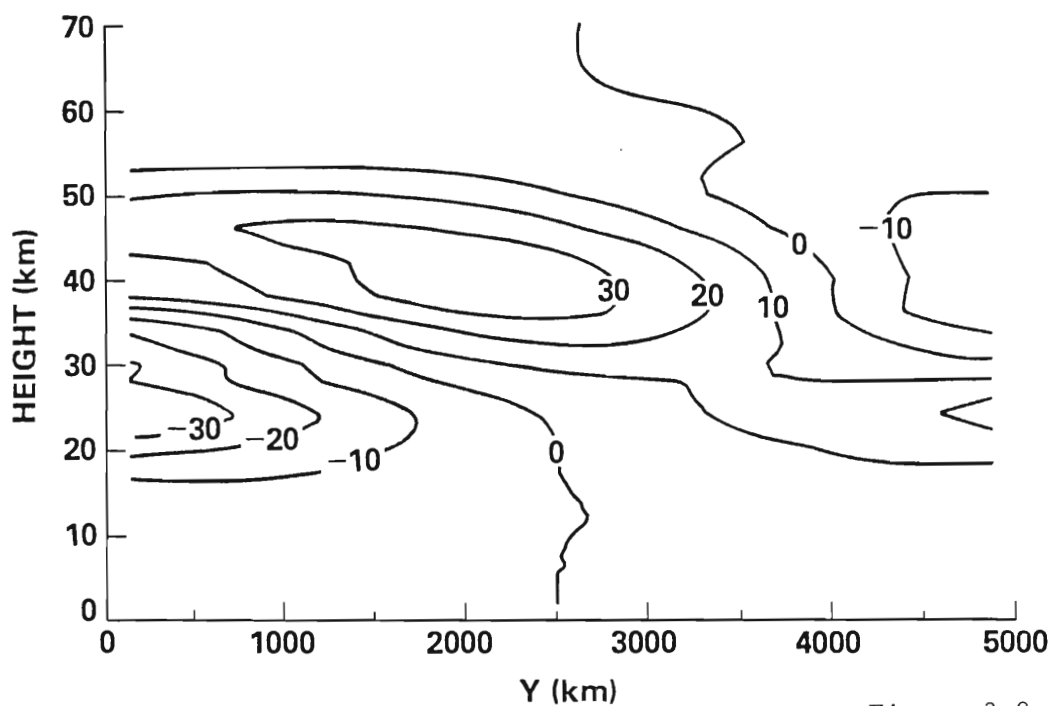


Figure 3.8a

RESIDUAL ADVECTION $\times 10^{-8}$ (ppm sec $^{-1}$)

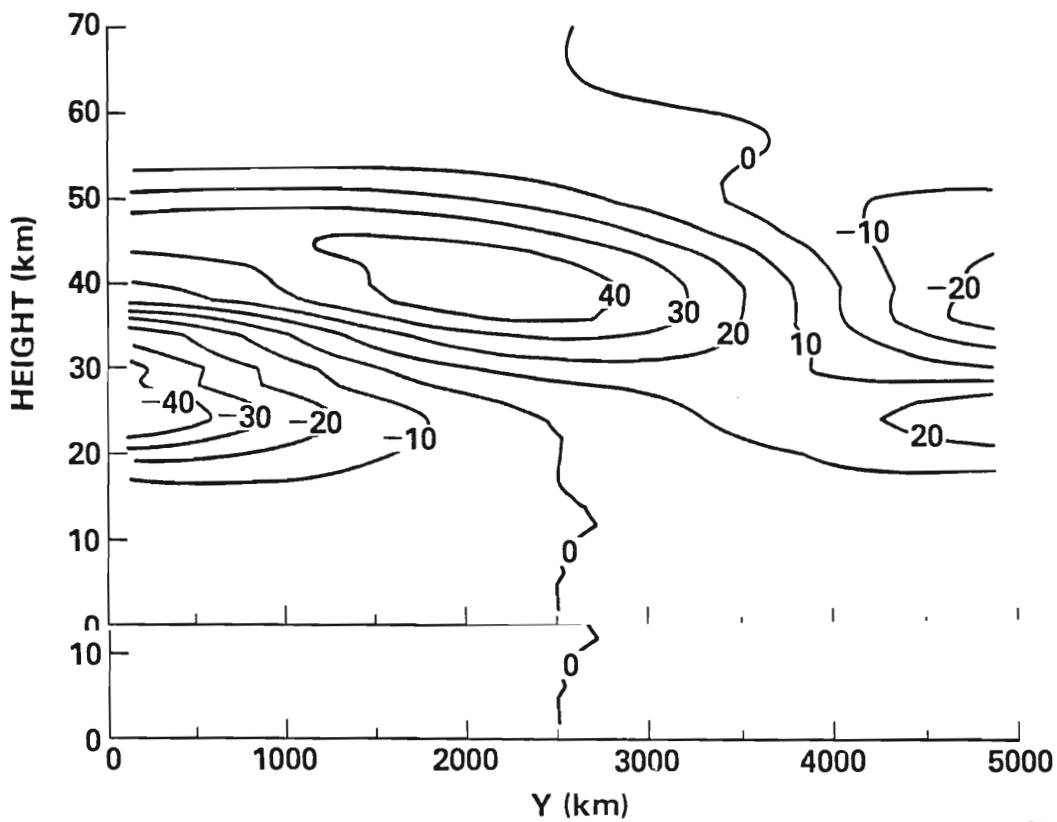


Figure 3.8b

STIRRING TERM $\times 10^{-6}$ (ppm sec $^{-1}$)

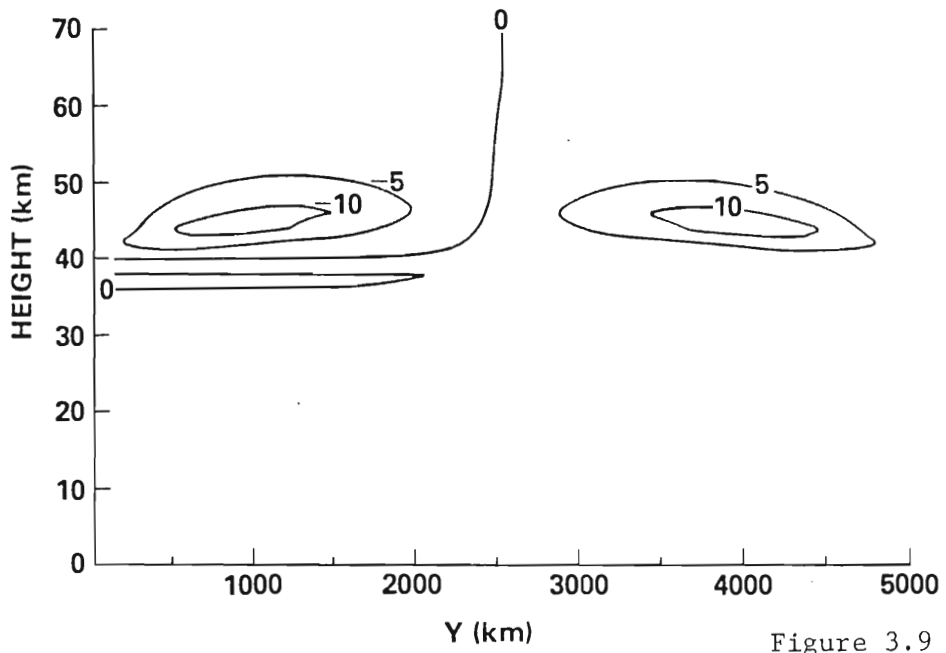


Figure 3.9

$\frac{\partial \bar{\mu}}{\partial t} \times 10^{-6}$ (ppm sec $^{-1}$)

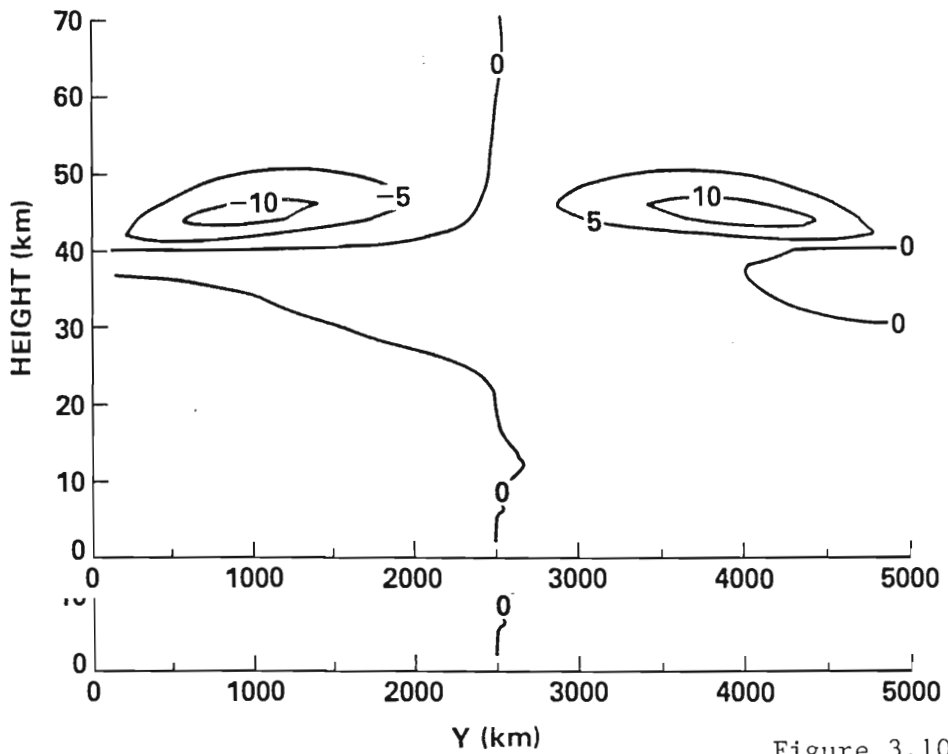


Figure 3.10

d. The "stirring" term

The magnitude of the stirring term is shown in Fig. 3.9. This field quite accurately represents the ozone time rate of change shown in Fig. 3.10. The advection by the Lagrangian-mean velocity is less than 1% of the stirring term in regions where ozone is photochemically active. The stirring term is identically zero when the photochemistry is zero.

In order to understand the physical meaning of the stirring term and its analogy to the Eulerian problem, it is helpful to compare the stirring term to the eddy flux. Assuming that the wave is steady and stationary (3.7) becomes

$$\mu' = - \frac{\lambda - ik\bar{u}}{\lambda^2 + (k\bar{u})^2} u'_i \frac{\partial \bar{\mu}_o}{\partial x_i} \quad (3.17)$$

The change in the zonal mean ozone field due to the divergence of the eddy flux (DEF) is

$$\begin{aligned} \text{DEF} &= - \frac{1}{\rho} \frac{\partial}{\partial x_j} \rho \overline{u'_j \mu'} \\ &= \frac{1}{\rho} \frac{\partial}{\partial x_j} \rho \left\{ \frac{\lambda}{\lambda^2 + (k\bar{u})^2} \overline{\text{Re}(u'_j) \text{Re}(u'_i)} \frac{\partial \bar{\mu}_o}{\partial x_i} + \frac{k\bar{u}}{\lambda^2 + (k\bar{u})^2} \overline{\text{Re}(u'_j) \text{Im}(u'_i)} \frac{\partial \bar{\mu}_o}{\partial x_i} \right\} \end{aligned} \quad (3.18)$$

$$(3.18)$$

The stirring term (ST) is

$$\begin{aligned}
 \text{ST} &= - \overline{\xi_j \frac{\partial \lambda \mu'}{\partial x_j}} = - \frac{1}{\rho} \frac{\partial}{\partial x_j} \overline{\rho \lambda \xi_j \mu'} \\
 &= \frac{1}{\rho} \frac{\partial}{\partial x_j} \frac{\rho \lambda}{k\bar{u}} \left\{ \frac{\lambda}{\lambda^2 + (k\bar{u})^2} \overline{\text{Im}(u'_j) \text{Re}(u'_i)} \frac{\partial \bar{\mu}_o}{\partial x_i} + \frac{k\bar{u}}{\lambda^2 + (k\bar{u})^2} \overline{\text{Re}(u'_j) \text{Re}(u'_i)} \frac{\partial \bar{\mu}_o}{\partial x_i} \right\}
 \end{aligned}
 \tag{3.19}$$

ST is functionally very similar to DEF. In order to investigate the precise similarities it is useful to consider the limits of λ relative to the dynamic frequency $k\bar{u}$.

For $\lambda/k\bar{u} < 1$,

$$\frac{1}{\lambda^2 + (k\bar{u})^2} \approx \frac{1}{(k\bar{u})^2} \left(1 - \frac{\lambda^2}{(k\bar{u})^2} \right)
 \tag{3.20}$$

Using (3.20), (3.18) and (3.19) can be rewritten to lowest order as:

$$\text{DEF} = \frac{1}{\rho} \frac{\partial}{\partial x_j} \rho \left\{ \frac{\lambda}{(k\bar{u})^2} \overline{\text{Re}(u'_j) \text{Re}(u'_i)} \frac{\partial \bar{\mu}_o}{\partial x_i} + \frac{1}{(k\bar{u})} \overline{\text{Re}(u'_j) \text{Im}(u'_i)} \frac{\partial \bar{\mu}_o}{\partial x_i} \right\}
 \tag{3.21}$$

(3.21)

and

$$ST = \frac{1}{\rho} \frac{\partial}{\partial x_j} \frac{\rho \lambda}{(k\bar{u})^2} \overline{\text{Re}(u'_j)\text{Re}(u'_i)} \frac{\partial \bar{\mu}_o}{\partial x_i} \quad (3.22)$$

Thus for small λ the divergence of the eddy flux can be divided into a purely chemical and purely conservative part. The conservative part, the second term on the RHS of (3.21) is the conservative flux described by Clark and Rogers (1978). The chemical part of DEF is identical to ST; therefore, for small λ it can be explicitly shown that the stirring term represents the chemical contribution of the divergence of the eddy flux.

For large λ DEF approaches zero, while ST approaches some finite value. In fact, as λ becomes large ST loses its explicit chemistry dependence and becomes

$$ST = u_i^s \frac{\partial \bar{\mu}_o}{\partial x_i} \quad (3.23)$$

At this limit both the Eulerian mean, (3.8), and Lagrangian-mean, (3.10) continuity equations become

$$\frac{\partial \bar{\mu}}{\partial t} = - \bar{u}_i \frac{\partial \bar{\mu}_o}{\partial x_i} - \lambda \bar{\mu} \quad (3.24)$$

Eq. (3.24) indicates that, when the photochemistry is strong, the wave effects become small so that the mean field changes are governed by the mean chemistry and the advection by the Eulerian-wave effects become small so that the mean field changes are governed by the mean chemistry and the advection by the Eulerian-mean velocity.

e. Lagrangian model

While the analysis above reveals the relationship of the stirring term to the divergence of the eddy flux, the physical nature of the stirring term remains obscured in the mathematics. Hartmann (1981) showed how pure oscillatory motion of a fluid parcel could produce changes in the mean ozone density in a fluid tube. A similar Lagrangian approach can be used here to investigate the effects of the planetary wave and to further coalesce the Lagrangian-mean and Eulerian viewpoints.

The Lagrangian model is based on the particle trajectories as determined by the Lagrangian-mean displacement fields. Using (2.3) and assuming that \bar{u} is constant and F' is zero, it can be shown that for harmonic disturbances the horizontal displacement field, η , and the vertical displacement field, ζ are given by

$$\eta = \eta_0 \cos(\alpha z + kx) \quad (3.25)$$

and

$$\zeta = \zeta_0 \cos(\alpha z + kx) + \zeta_1 \sin(\alpha z + kx) \quad (3.26)$$

where α is the vertical wavenumber. The coefficients, η_0 , ζ_0 , and ζ_1 are functions of height, meridional distance, and the dynamic parameters. For a particular value of y and z , the projection of η and ζ on the y, z plane is an ellipse (Fig. 3.11). These parameters. For a particular value of y and z , the projection of η and ζ on the y, z plane is an ellipse (Fig. 3.11). These displacement fields are similar to those calculated by Matsuno (1980) and Danielsen (1981).

The displacement fields provide a model of the parcel motion associated with a planetary wave. The planetary wave displaces a particular parcel from its equilibrium position and causes the parcel to move in a helical trajectory around the globe. The Lagrangian-mean velocity is the velocity at which the axis of the helix moves. For the small amplitude, steady state waves of this model the vertical extent of the ellipse is on the order of 1-3 km and the horizontal extent is on the order of hundreds of kilometers.

First consider a parcel in the absence of chemistry. The equilibrium density of the parcel, μ_p , is $\bar{\mu}_0(0,0)$. If the parcel is displaced to (η, ζ) , then the perturbation density μ' is equal to the parcel density minus the background density. If the displacements are small, then

$$\mu' = -\eta \frac{\partial \bar{\mu}_0}{\partial y} - \zeta \frac{\partial \bar{\mu}_0}{\partial z}$$

Assuming that $\bar{\mu}_0$ is a function of z only and that it increases with height, then positive ozone perturbations are generally associated with northward motion and negative ozone perturbations are associated with southward motion (see Fig. 3.11). This is equivalent to northward eddy flux of ozone. Hence this is the Lagrangian description of the conservative flux as defined by Clark and Rogers (1978). This conservative flux is largely cancelled by the wave induced mean circulation.

and Rogers (1978). This conservative flux is largely cancelled by the wave induced mean circulation.

In the case when ζ_1 in (3.26) is zero, which corresponds to an evanescent wave, the trajectories then become lines instead of

ellipses. Then the perturbations are equally correlated with both northward and southward velocity and the conservative eddy flux is identically zero.

Figure 3.11. Projection of displacement fields η, ζ on the y, z plane (km).

Figure 3.12. Parcel orbiting through a region of discontinuous photochemistry $\frac{\partial \bar{\mu}}{\partial z} > 0$.

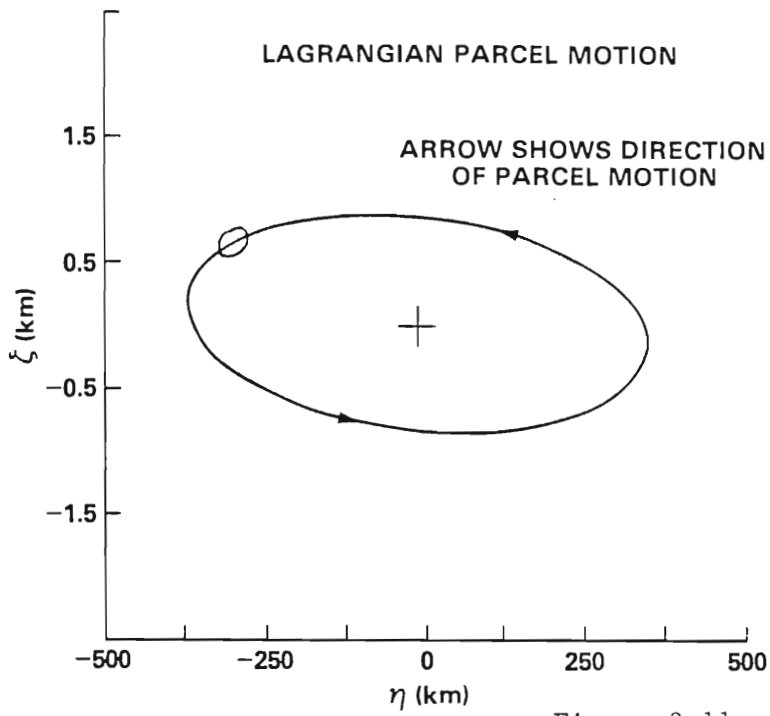


Figure 3.11

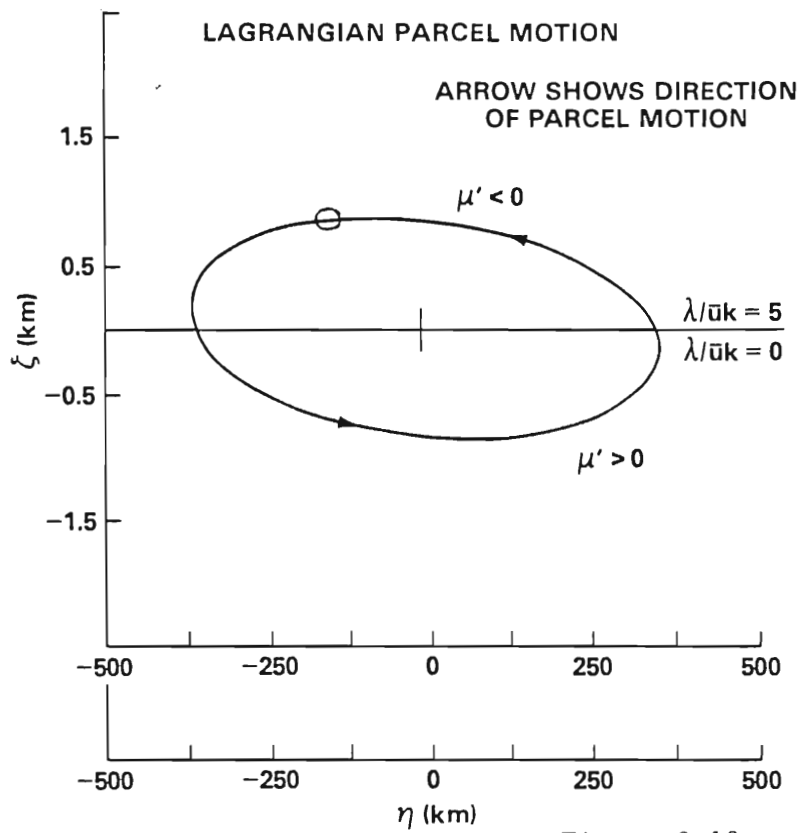


Figure 3.12

When chemistry is present μ' still changes due to the varying background field, but the chemistry tries to bring the parcel's ozone density towards the background value. The constituent density for the parcel is determined by

$$\frac{d\mu'}{dt} = S - \lambda\mu' \quad (3.27)$$

where S represents the effective source caused by the parcel moving through the varying background density. For elliptical trajectories S is a harmonic function in time, proportional to the magnitude of the velocity and the background constituent gradients. In general, as the parcel orbits the ellipse, it goes through varying photochemistry so that λ is also a function of time. In a reference frame moving with the zonal velocity of the parcel, (3.27) can be rewritten as

$$\frac{d\mu'}{dt} = S_0 \cos \omega t - \lambda(t)\mu' \quad (3.28)$$

where $\omega = k\bar{u}$.

If λ is constant, then the solution to (3.26) for large t can be written as

$$\mu' = \frac{S_0}{\lambda^2 + \omega^2} (\lambda \cos \omega t + \omega \sin \omega t) \quad (3.29)$$

$$\mu' = \frac{v}{\lambda^2 + \omega^2} (\lambda \cos \omega t + \omega \sin \omega t) \quad (3.29)$$

For large λ , μ' approaches zero which is equivalent to the previous result that the eddy fluxes disappear in the fast photochemical

region. For $\lambda = 0$ the solution reduces to the ozone density appropriate to the conservative problem. Note that the average of μ' over one period is zero.

In the regions where λ varies strongly over the extent of the ellipse, the perturbation can take on a different character. Such regions would be expected to exist in the lower parts of the transition layer and at the polar night boundary where the chemistry is nearly discontinuous. Figure 3.12 shows an extreme example where the chemistry is discontinuous across an ellipse. As the parcel travels through the conservative region the perturbation density varies as S . In the transition region ($\lambda/k\bar{u} = 5$) the perturbation is decreased by $\sim 80\%$. Assuming the background density increases with height, this behavior means that the negative perturbations are selectively damped while the positive perturbations are not. Therefore, the average value of μ' over one period, which was zero when λ did not vary, may become nonzero in the presence of extreme chemical gradients. Such regions would be expected to have a great effect upon transport calculations. This effect is analogous to mean density changes in a fluid tube as calculated by Hartmann (1981).

Figure 3.13. Solution, at large t , of perturbation ozone density for an elliptically orbiting parcel.

- a. constant photochemistry
- b. photochemistry at the bottom of
the transition layer

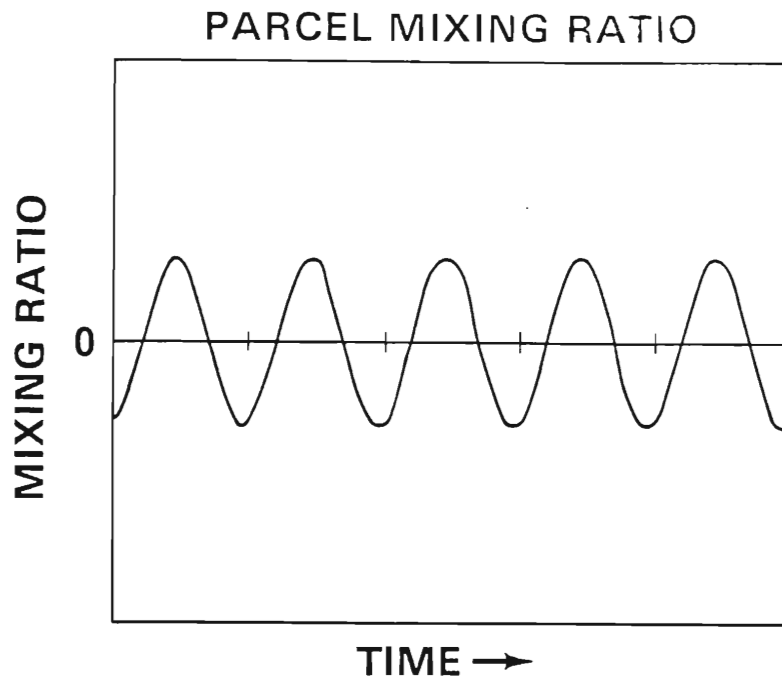


Figure 3.13a

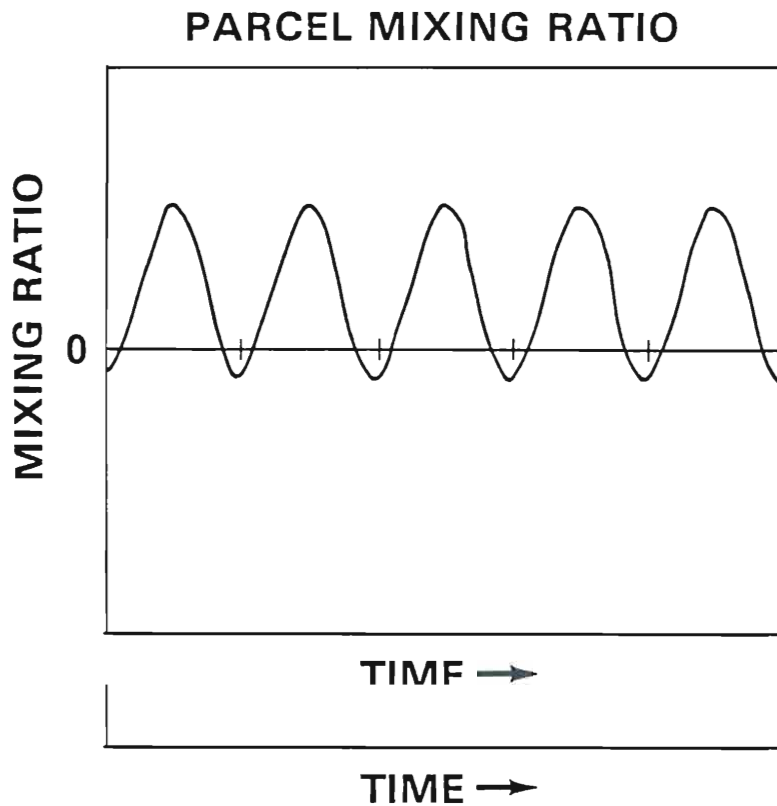


Figure 3.13b

Figure 3.13 demonstrates this effect for a more realistic problem. Figure 3.13a shows (3.29), the steady state solution to (3.28). This is a harmonic function with zero average. Figure 3.13b shows the numerical solution to (3.24) for an ellipse situated at the bottom of the transition layer with the model photochemistry. The steady state solution has a non-zero time average, as expected.

f. The effects of eddy transport on the mean field

Since the changes in the mean field have been assumed to be $O(a^2)$, the calculation of the steady state forcing by the eddies on the mean field is independent of the mean constituent density. Therefore, at any point in space it is possible to write the mean field equation (3.8) or (3.10) as

$$\frac{\partial \bar{\mu}}{\partial t} = -\lambda \bar{\mu} + F \quad (3.30)$$

where F is the eddy forcing which represents the divergence of both the horizontal and vertical fluxes. F is independent of time; therefore, the solution to (3.30) can be written as

$$\bar{\mu} = \frac{F}{\lambda} (1 - e^{-\lambda t}) \quad (3.31)$$

where it has been assumed that $\bar{\mu}$, the change in the equilibrium

where it has been assumed that $\bar{\mu}$, the change in the equilibrium field, is zero at time zero. As $t \rightarrow \infty$ the change in the mean field is F/λ .

In the conservative region the mean continuity equation can be written as $\frac{\partial \bar{\mu}}{\partial t} = F$ which yields

$$\bar{\mu} = Ft \quad (3.32)$$

In order to investigate the effect of the steady state waves on the mean field the appropriate equation (3.31) or (3.32) was solved at $t = 90$ days. This calculation would represent the effects of the waves if they persisted for the entire winter. The forcing is taken from the line in Fig. 3.7 through the region of maximum ozone increase.

Figure 3.14 shows the change in $\bar{\mu}$. The large rates of change that are calculated in the transition region are almost completely counterbalanced by the mean chemistry. At the altitude of maximum increase in Fig. 3.7 the actual change in the mean field is only .5 ppm for 90 days.

The largest changes in the mean field are in the lower stratosphere where changes of 1.4 ppm are seen at 90 days. These changes are comparable to those observed in the northern hemisphere. Immediately below the transition region is a region of depletion caused by the advection. This vertical structure of the changes in the mean field is unrealistic and due largely to the simplified representation of photochemistry and dynamics in the lower stratosphere.

simplified representation of photochemistry and dynamics in the lower stratosphere.

Figure 3.14. 90 day zonal mean ozone change, with the mean chemistry included, at the latitude of the maximum ozone increase in Fig 3.7 (ppm).

Figure 3.15. 90 day zonal mean ozone change, with the mean chemistry included, at the northern and southern extremes, as determined by Lagrangian-mean advection (LGM) and residual velocity advectons (+) (ppm).

a. Southern

b. Northern

CHANGE IN $\bar{\mu}$ AT 90 DAYS

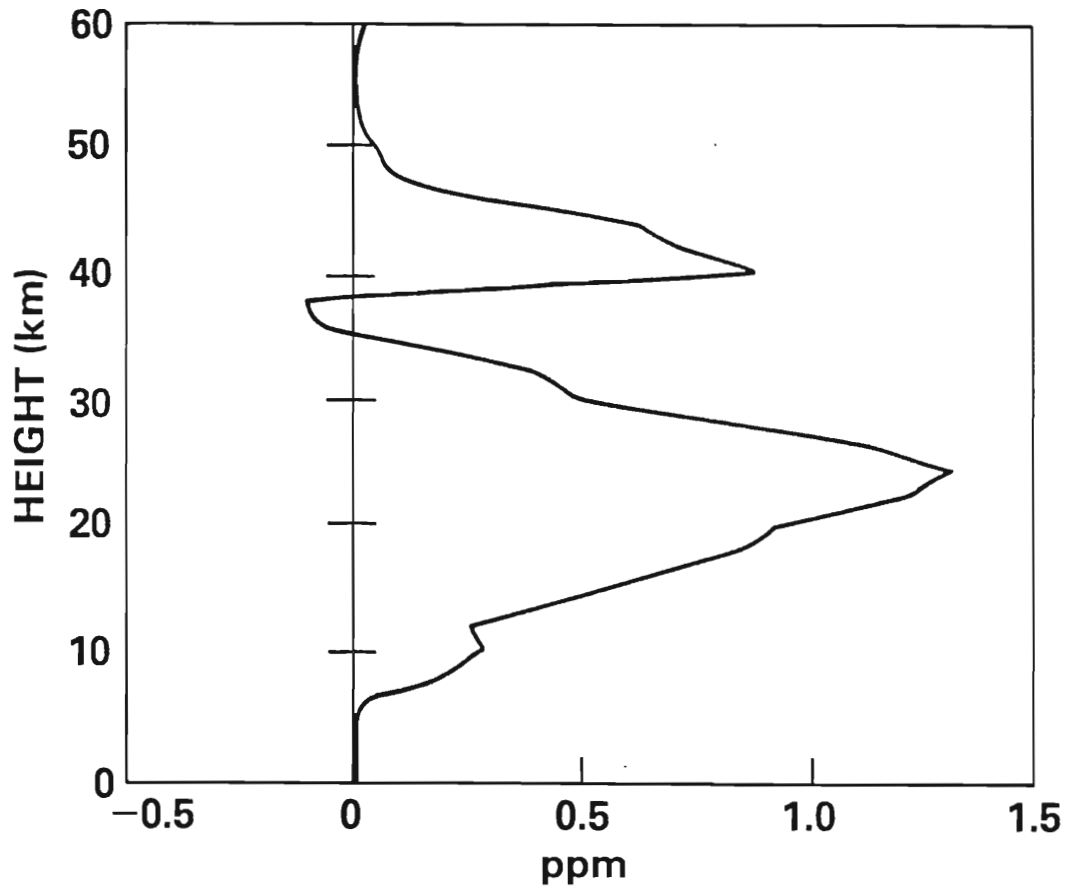


Figure 3.14

CHANGE IN $\bar{\mu}$ AT 90 DAYS

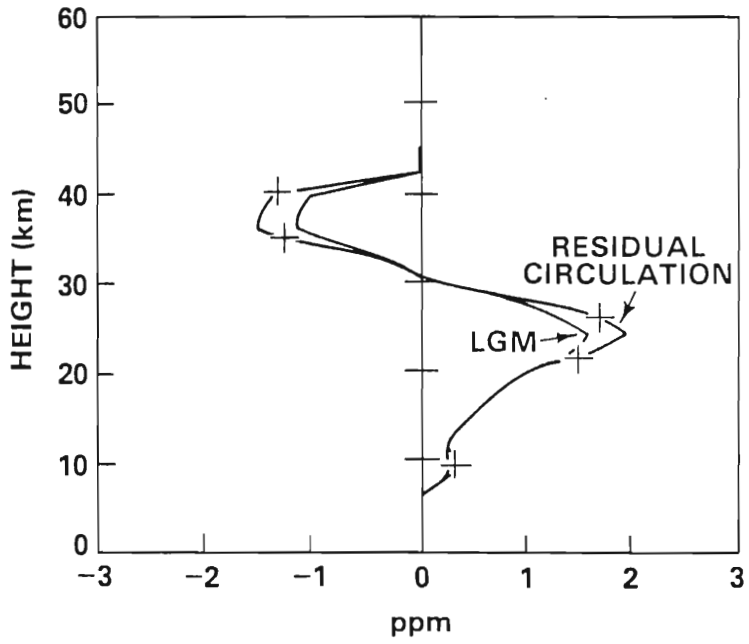


Figure 3.15a

CHANGE IN $\bar{\mu}$ AT 90 DAYS

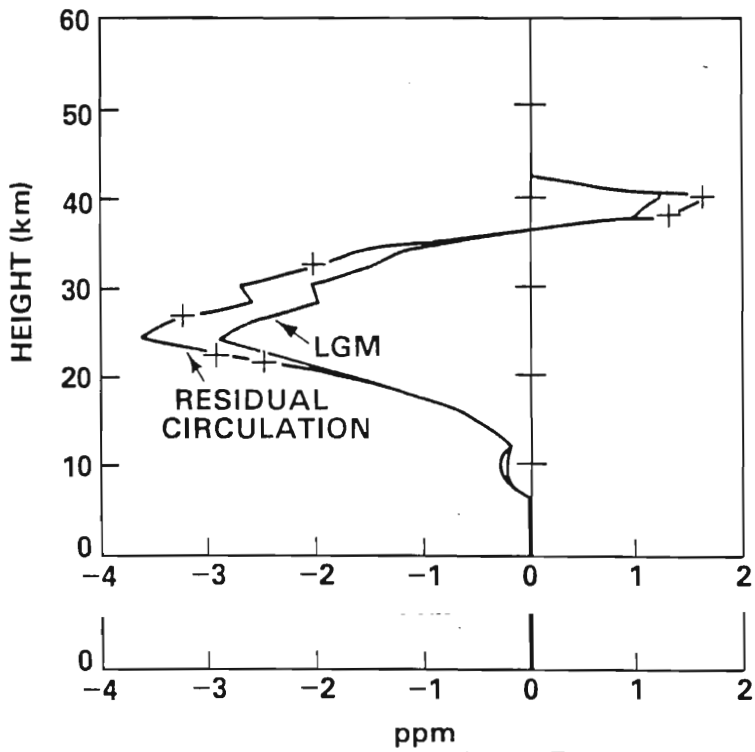


Figure 3.15b

The relatively large positive changes in the mean field at the bottom of the transition layer are in the region where the photochemistry gradients are large. This is the region where a parcel takes on a non-zero average during a parcel orbit. The equilibrium values at this altitude are reached after 5 days of integration. This region of large increase just above a region of decrease demonstrates an important model sensitivity to the chemical structure.

Since the advection term is responsible for all of the change in the mean field below the transition region it is worthy of further investigation. Mean field tendencies for 90 day periods were calculated 400 km from both the northern and southern boundaries using both the residual and Lagrangian-mean advection (Fig. 3.15). The large changes in the midlatitudes caused by meridional transport are largely negated by the photochemistry.

In the southern region the change in the mean field by advection is unlike that observed in the stratosphere. There is a depletion of nearly 4 ppm at 24 km and an enhancement of almost 2 ppm at 40 km. In the northern region the changes in the lower stratosphere are not unreasonable showing a 1.5 ppm increase at 24 km. However, at 36 km a 1 ppm depletion occurs. It is obvious that the modeling of the lower stratosphere is inadequate. Both small scale dynamics and photochemistry which may act to counter the tendencies shown here have been neglected. The advection calculated using the residual circulation produces larger changes in the mean field than that calculated using the Lagrangian-mean velocity. This

means, that in this model, the antisymmetric part of Holton's (1981) diffusion tensor is not negligible.

3.4 Conclusions

The changes in zonal mean ozone as forced by steady state planetary waves have been calculated using both a Lagrangian-mean and Eulerian formulation. Although the calculated results from the two methods are the same, the use of the two methods allows for increased interpretation of the results.

In the Eulerian formulation the tendency for the eddy and mean fluxes to cancel is well illustrated. Both the horizontal and vertical flux fields are complex and largest in the conservative region. However, the changes in the mean field in the absence of the mean photochemistry are largest in the transition region as found by Hartmann and Garcia (1979).

The problem of compensation by two large terms which appears in the Eulerian framework also appears in the calculation of the Lagrangian-mean velocity. If the Lagrangian-mean flow could be calculated directly, then it might be possible to avoid the numerical difficulties of compensation. There seems to be no computational advantage of the Lagrangian-mean method to calculate planetary wave transport as it requires the formulation of Eulerian quantities, their conversion to Lagrangian-mean quantities, and then the calculation of the transport. quantities, their conversion to Lagrangian-mean quantities, and then the calculation of the transport.

In the Lagrangian-mean formulation the stirring term is dominant in the absence of mean chemistry. The stirring is equal to

the chemical contribution of the divergence of the eddy flux when $\lambda/\bar{u}k < 1$. When λ is large the stirring term is equivalent to the Stokes advection. Using particle displacement fields it is possible to predict the type of eddy transport that is to be expected in a certain region. It was found that μ' has a non-zero time average in the presence of strong chemical gradients. Calculation of the mean field changes shows that the mean chemistry is able to compensate for the eddy chemistry changes except where the chemical gradients are large. This indicates that the interaction of steady planetary waves and photochemistry need only be modeled in the presence of large chemical gradients.

For seasonal integrations the largest changes in the mean field are caused by advection by the Lagrangian-mean velocity in the conservative region. The advection is so weak that in the chemical regions its effects are negligible. Using the residual circulation instead of the Lagrangian-mean circulation overestimates the advection by the planetary waves. In this particular model the largest differences occur between the Lagrangian-mean and residual circulations in chemically active regions and, hence, the difference between the ozone field changes calculated with Lagrangian-mean and residual circulations are small. This would not necessarily be true for constituents with different chemistry.

The transport mechanisms investigated here are probably not adequate to model planetary wave effects in the stratosphere.

The transport mechanisms investigated here are probably not adequate to model planetary wave effects in the stratosphere. Sudden warmings, which are highly transient, will certainly have a great effect upon the ozone distribution (Garcia and Hartmann,

1980). Therefore, steady state planetary wave transport models are probably only relevant in the late fall and early winter. The planetary wave transport would have to be supplemented by transport due to the diabatic circulation and small scale dynamics in the lower stratosphere. Transport by planetary waves during sudden warmings, transport by the diabatic circulation, and the relative importance of the two circulations will be presented in the next chapter.

Chapter 4

TRANSPORT BY TRANSIENT PLANETARY WAVES AND THE DIABATIC CIRCULATION

4.1 Introduction

In this chapter the transport of ozone by time dependent planetary waves on a β -plane is discussed. In Section 4.2 the results of the dynamic model for both 600 m and 900 m topographic forcing are presented. In Sections 4.3, 4.4, and 4.5 the transport of ozone by the diabatic circulation alone, by planetary waves alone, and by the combination of the diabatic and planetary wave circulations is discussed. The results are analyzed in Section 4.6.

4.2 Dynamics

Equations 2.3 and 2.4 are solved on a β -plane centered at 60° N for zonal wavenumber one perturbations. The wave is forced by zonal flow over a wavenumber one topography with a height of either 600 m or 900 m. With forcing of this magnitude there is at least one sudden warming accompanied by a reversal in the zonal mean wind field. For long integrations a steady state solution is reached sudden warming accompanied by a reversal in the zonal mean wind field. For long integrations a steady state solution is reached with permanent easterlies at some level. Schoeberl (1982b) presents a detailed analysis of the model dynamics.

During winter it is common to see distinct pulses of wave amplitude and either major or minor warmings (Labitzke and Goretzki, 1982). After a major or minor warming the stratosphere usually returns to its winter climatological state. If the warming occurs late in the winter, then the zonal mean circulation after the warming evolves into the summertime regime where easterlies are present throughout the entire stratosphere. This type of warming is called a final warming. The dynamical model used here does not attempt to represent all of the features of the winter stratosphere only to simulate warming events and their corresponding circulation patterns.

The details of the numerical scheme were given in Section 2.3b. Results will be presented as time-height cross sections at the center of the channel and at a northern and southern point, corresponding to 60° N, 46° N, and 74° N on the β -plane.

a. 600 m topography

Time series of 60 days for \bar{u} , the zonal mean wind, and the magnitude of ϕ' , the planetary wave geopotential, are shown at the channel center in Figures 4.1 and 4.2 for the 600 m orography. The wave amplitude increases at all altitudes until day 22 when it reaches a maximum of about 1.6 gpm. After day 22 the wave amplitude decreases rapidly until day 30 and continues to decrease more slowly until day 47. On day 47 the wave amplitude starts to amplitude decreases rapidly until day 30 and continues to decrease more slowly until day 47. On day 47 the wave amplitude starts to increase at high altitudes and is still increasing at the end of the time series.

Figure 4.1. Zonal mean wind for 600 m topography
at the channel center (m sec^{-1}).

Figure 4.2. Geopotential amplitude for 600 m topography
at the channel center (gpm).

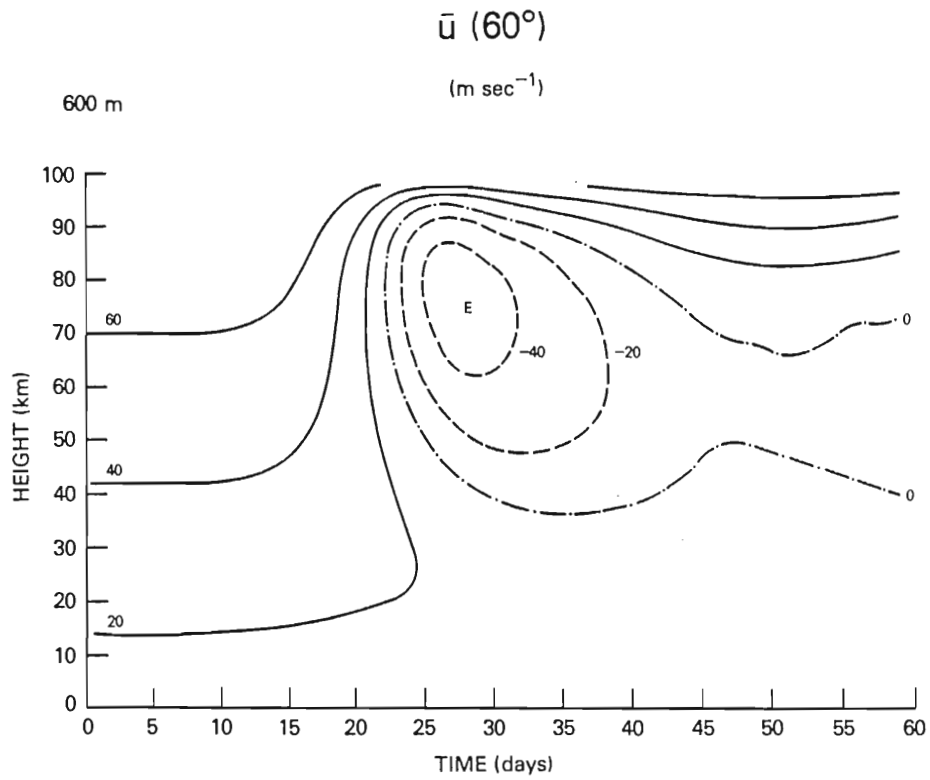


Figure 4.1

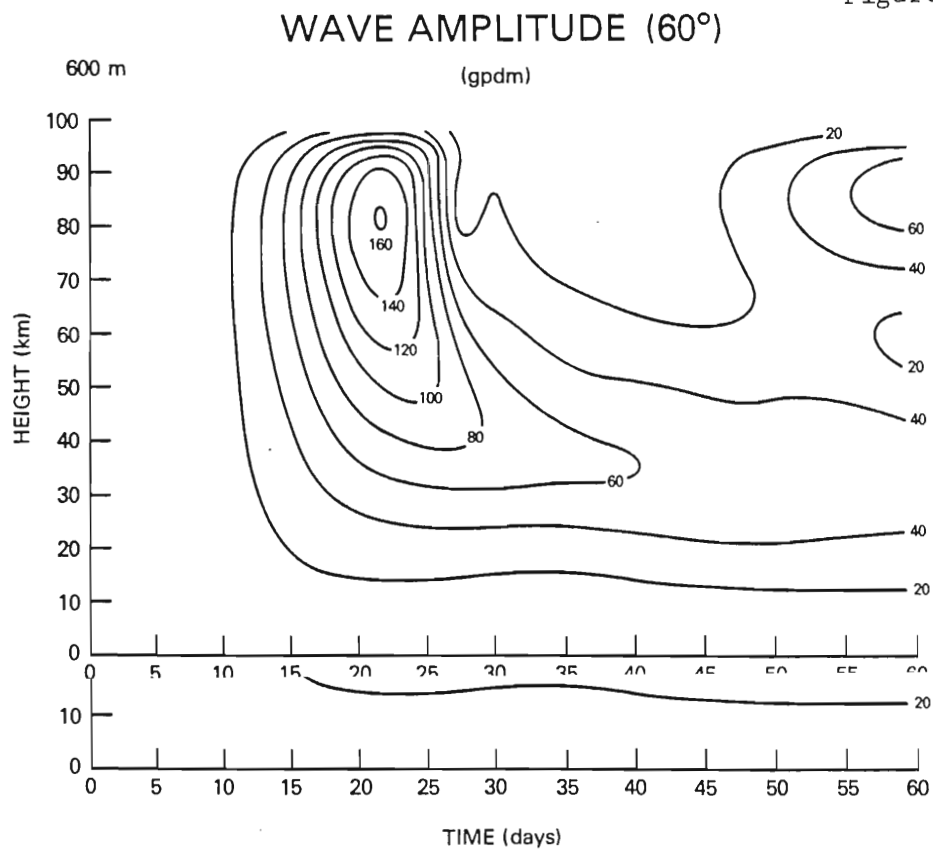


Figure 4.2

Coincident with the maximum in the wave amplitude field is the appearance of easterlies in the zonal mean wind field. The presence of easterlies prohibits further vertical propagation of the stationary wave (Charney and Drazin, 1961) and, hence, the rapid decrease of the wave amplitude. The easterly zonal wind reaches a maximum velocity of 53 m sec^{-1} on day 29 and then decreases in intensity until day 45 when westerlies begin to appear again at the edges of the channel. The reappearance of westerlies permits vertical planetary wave propagation subsequently leading to the second increase in wave amplitude at day 47.

Since it has been predicted that transport in the vicinity of critical lines might be large (Schoeberl, 1981b; Matsuno and Nakamura, 1979), the descent of the zero wind line (critical line for stationary waves) is of particular importance to the study of tracer transport. For the 600 m topography the critical line in the center of the channel has descended to 48 km on day 25 and reaches a minimum altitude of 36 km on day 35. The critical line remains in the neighborhood of 36 km and then starts to rise on day 40. This rise is related to the reappearance of westerlies at high and low latitudes. The critical line ascends to 50 km on day 45 and then starts to descend again as the wave amplitude increases.

Figure 4.3. Zonal mean wind for 900 m topography
at the channel center (m sec^{-1}).

Figure 4.4. Geopotential amplitude for 900 m topography
at the channel center (gpm).

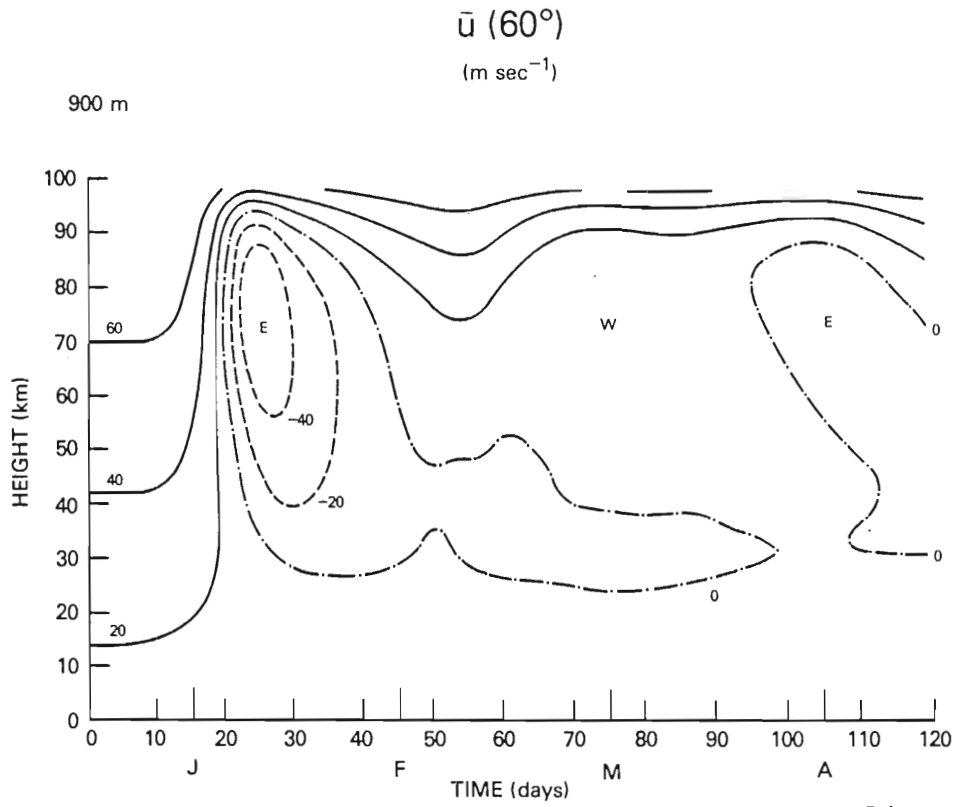


Figure 4.3

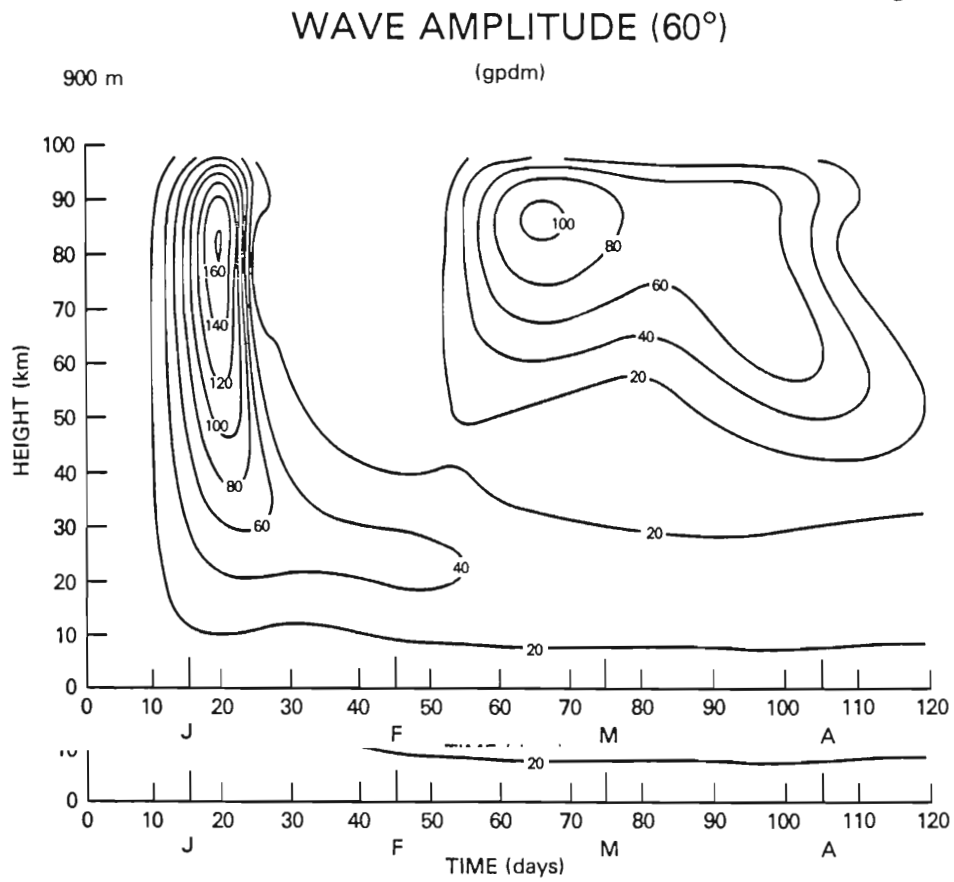


Figure 4.4

b. 900 m topography

The mean zonal wind field and the wave amplitude field associated with the 900 m topography are shown in Figures 4.3 and 4.4 for a 120 day integration. These fields are similar in many ways to the 600 m topography fields. The wave amplitude increases rapidly until about day 20 where it reaches a maximum of 1.6 gpkm. The fact that the forcing has been increased by 50% but the wave amplitude reaches the same maximum amplitude is consistent with the wave saturation theory of Schoeberl (1982a). The main effect of the increased forcing is to cause the wave maximum to be reached somewhat earlier. The wave amplitude rapidly decreases between days 20 and 30 after which it slowly decreases until day 50. There is another rapid increase in wave amplitude after day 50 which maximizes on day 65. The wave amplitude decrease following this maximum is not as rapid as that following the initial warming event.

Coincident with the first wave maximum is the rapid deceleration of the mean zonal wind and the formation of easterlies which reach a maximum velocity on day 26 of 57 m sec^{-1} . The second wave maximum on day 65 is not instantaneously associated with the onset of high level easterlies. The wave forcing of the mean flow from days 55-65 decelerates the mean zonal wind restoring the low level easterlies which then prohibit propagation of the wave into the stratosphere. The low level easterlies ultimately disappear about day 100 which allows the wave to once again propagate the stratosphere. The low level easterlies ultimately disappear about day 100 which allows the wave to once again propagate vertically. The zonal mean westerlies are so weak at this time that even the relatively weak forcing associated with the wave pulse at

day 100 is capable of producing easterlies throughout a deep portion of the atmosphere.

The zero wind line reaches minimum altitudes of 26 km on day 37 and 24 km on day 76. Between days 45 and 55 the critical line rises and the wave propagates and rebuilds the low level easterlies. The low level critical line is absent for a brief period beginning at day 100.

c. The diabatic circulation

As mentioned in the introduction, early theories of stratospheric circulation postulated a direct cell with rising motion in the equatorial region and sinking motion in the polar region. This circulation was thought to describe the dryness of the stratosphere and the buildup of ozone at high latitudes (Brewer, 1949; Dobson, 1956). Observations during the 1960's showed, however, that the northern hemisphere stratospheric mean circulation consisted of two cells with rising motion over the pole and the equator. Dunkerton (1978) pointed out that in the absence of waves the diabatically driven zonal mean field is a good approximation to the Lagrangian-mean velocity field and is consistent with the Brewer-Dobson circulation. Hence, the large scale mass transport associated with radiative forcing is described by a one cell circulation as originally postulated.

The diabatic circulation used here is derived from Dunkerton circulation as originally postulated.

The diabatic circulation used here is derived from Dunkerton (1978) and the more detailed calculations of Murgatroyd and Singleton (1961). The circulation appropriate for the winter

solstice is shown in Fig. 4.5. The time variation is assumed to be harmonic such that the intensity of the flow reaches a maximum shortly after the winter solstice and then decreases and reaches a minimum in the spring.

d. Initialization

The zonal mean ozone field used to initialize the transport model is shown in Fig. 4.6. This field is derived from the data of Dütsch (1969) and is representative of mid-November. Data north of 70° and above 45 km are scarce and of low quality. In these regions the prescribed ozone field is based on the vertical profile derived by Kreuger and Minzner (1976) and the ozone field used by Fels et al. (1980). The eddy ozone field is initially assumed to be zero.

A review of stratospheric warming data indicates that there is either a major or minor warming during the first or second week of January. Since the model warmings occur about three weeks after the planetary waves are turned on, December 15 has been chosen as the initialization date. In order to properly correlate the ozone field with the planetary wave dynamics the initial ozone field is advected with the diabatic circulation until Dec 15.

Figure 4.5. Diabatic circulation
at the winter solstice (cm sec^{-1}).

a. meridional component

b. vertical component

Figure 4.6. Initial ozone profile (ppm).

\bar{V}
(cm sec⁻¹)

DIABATIC

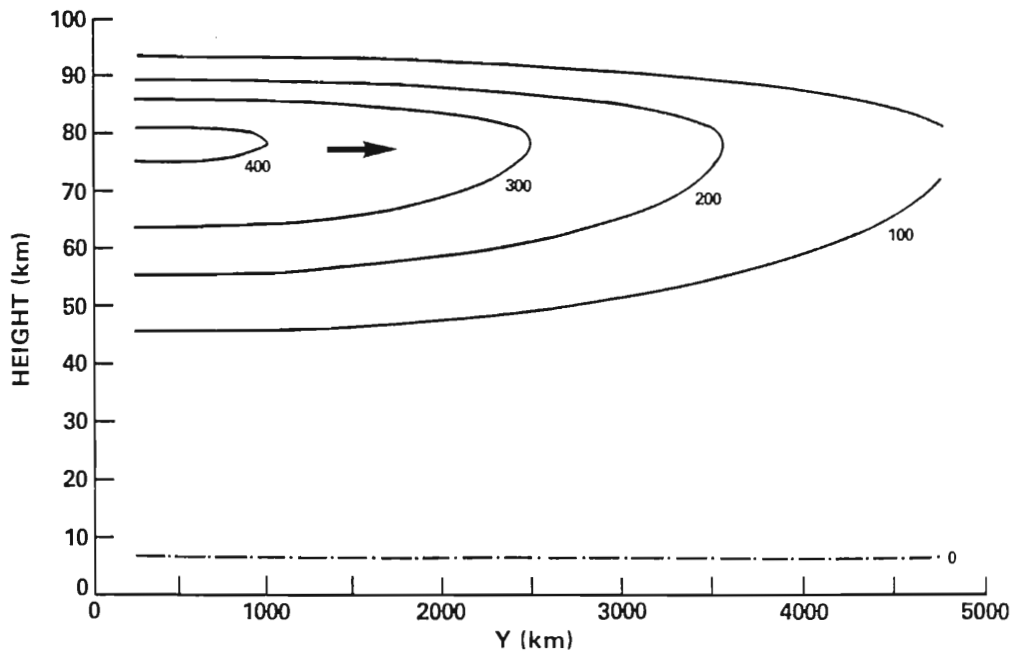


Figure 4.5a

\bar{W}
(cm sec⁻¹)

DIABATIC

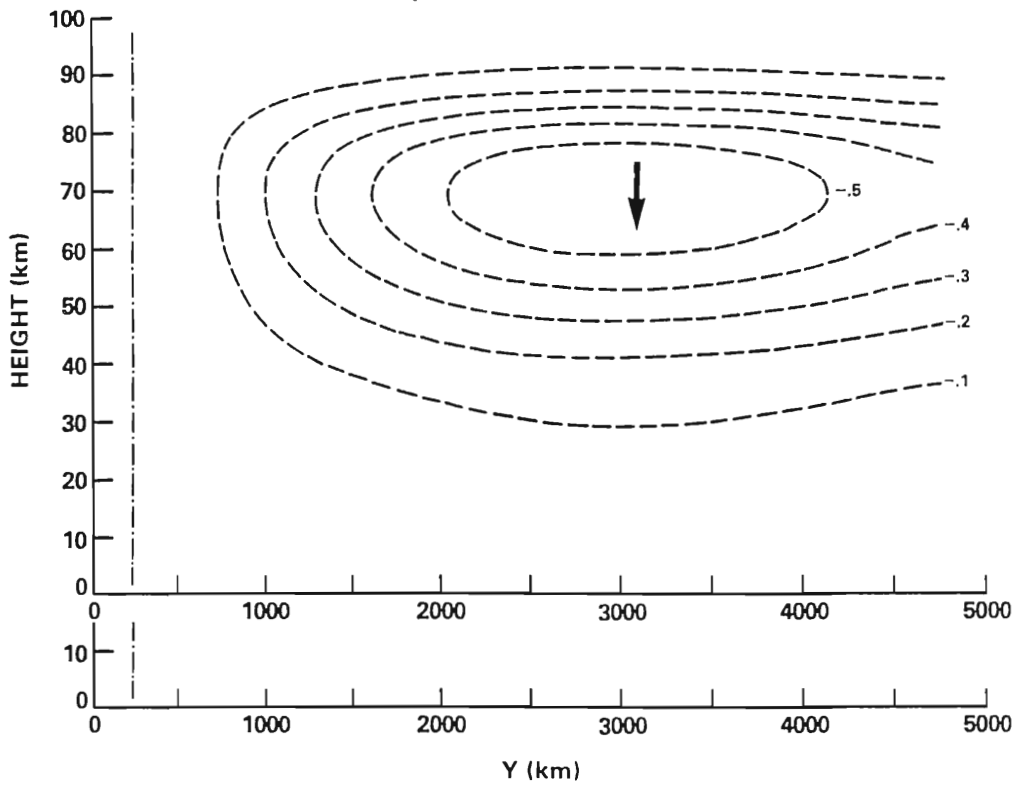


Figure 4.5b

OZONE (ppm)

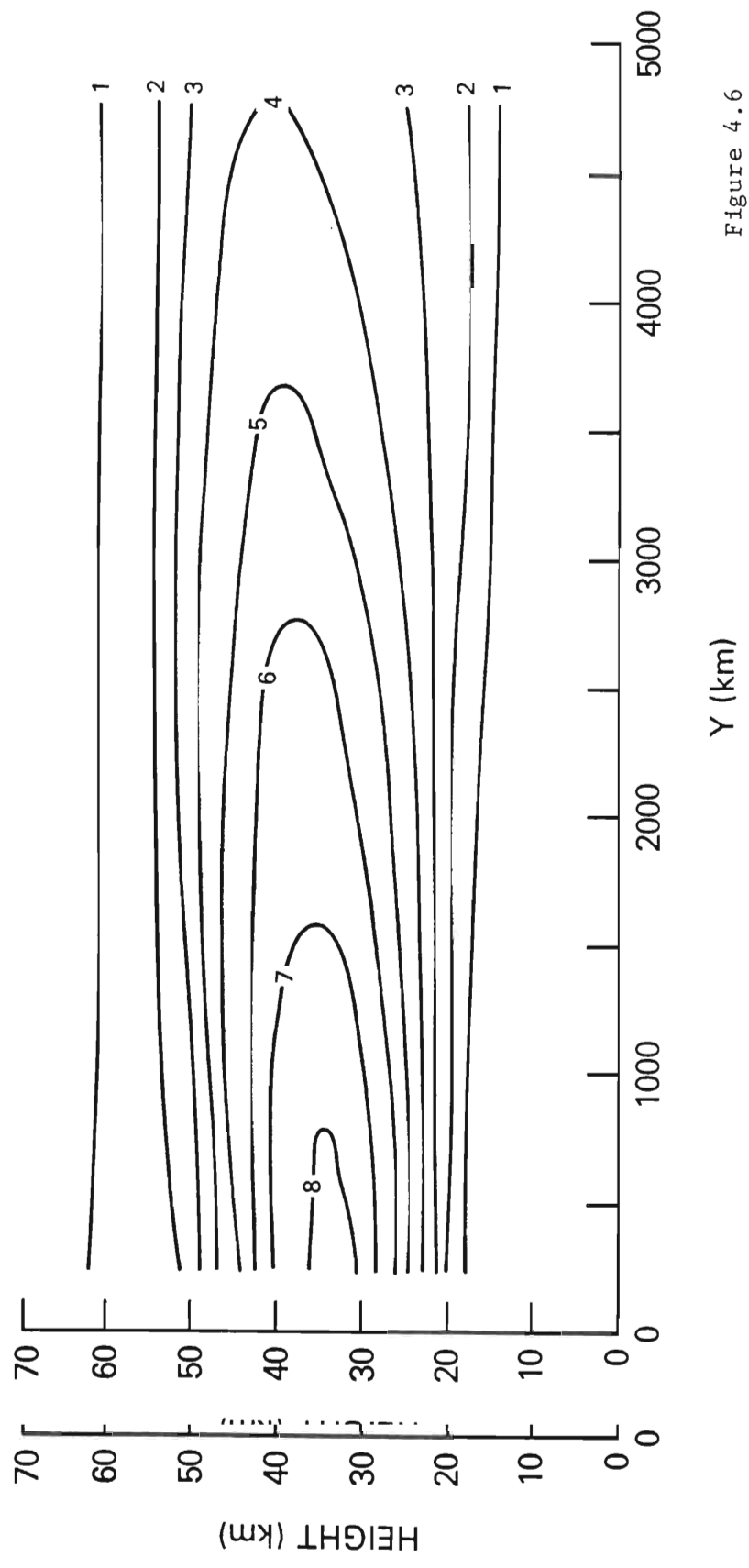


Figure 4.6

4.3 Transport by the diabatic circulation

The change in the mean ozone field (anomaly) due solely to the diabatic circulation is presented in one year time series in Figures 4.7 and 4.8. In general there is a positive anomaly in the lower stratosphere (20-30 km) for much of the year and a negative anomaly in the autumn. Since the ozone is in near equilibrium above 35 km, a positive (negative) anomaly is associated with an increase (decrease) in total ozone. Using this correlation it is seen that the total ozone reaches a maximum in early April and a minimum in October as opposed to an observed March maximum and October minimum.

There is a strong latitudinal dependence of the anomaly. The wintertime increase is larger and reaches lower altitudes at high latitudes. In the northern region (Fig. 4.8) a maximum increase of 3.5 ppm is centered around 26 km, and increases greater than 1 ppm are seen as low as 15 km. At the center of the channel (Fig. 4.7) an anomaly of 3 ppm is centered at 30 km, while in the southern region (not shown) a maximum increase of .5 ppm is centered around 32 km. The largest increase in the entire domain, 4.25 ppm, occurs at 70°.

The computed total ozone field (Fig. 4.9) differs considerably from observations. The time series for Dec.15-Apr.15 shows a maximum of 538 DU, an overestimate of 20%, which is reached about the first of April at 70°. Observations of ozone in the stratosphere (Fig. 2.11) show a maximum near the pole about March 1 the first of April at 70°. Observations of ozone in the stratosphere (Fig. 2.11) show a maximum near the pole about March 1 of approximately 450 DU.

Figure 4.7. Change in ozone at the center of the channel (60°) for transport by the diabatic circulation alone (ppm).

Figure 4.8. Same as Fig. 4.7 but at 74° .

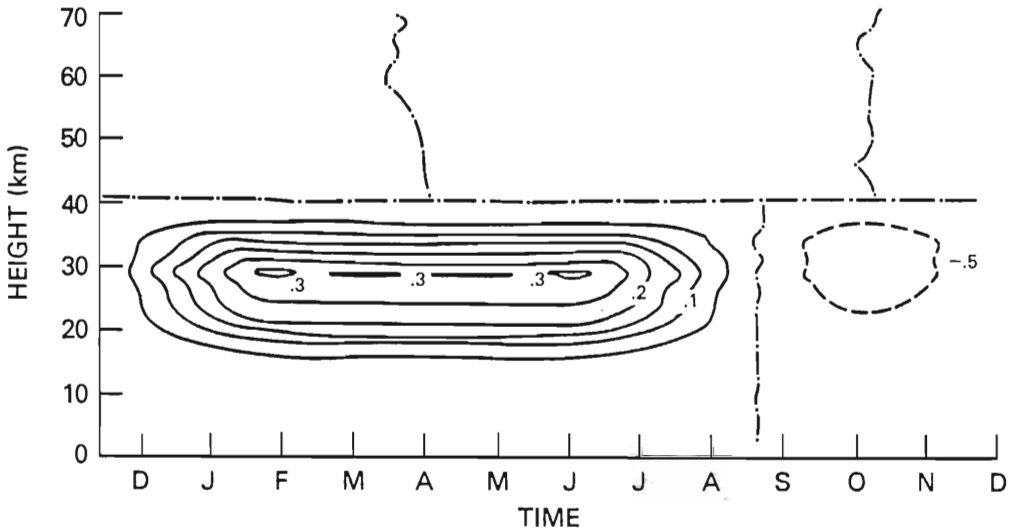
Figure 4.9. Latitude-time cross section of total ozone as calculated with the diabatic circulation (DU).

CHANGE IN $\bar{\mu}$ (60°)

(ppm)

Figure 4.7

DIABATIC, CHEMISTRY

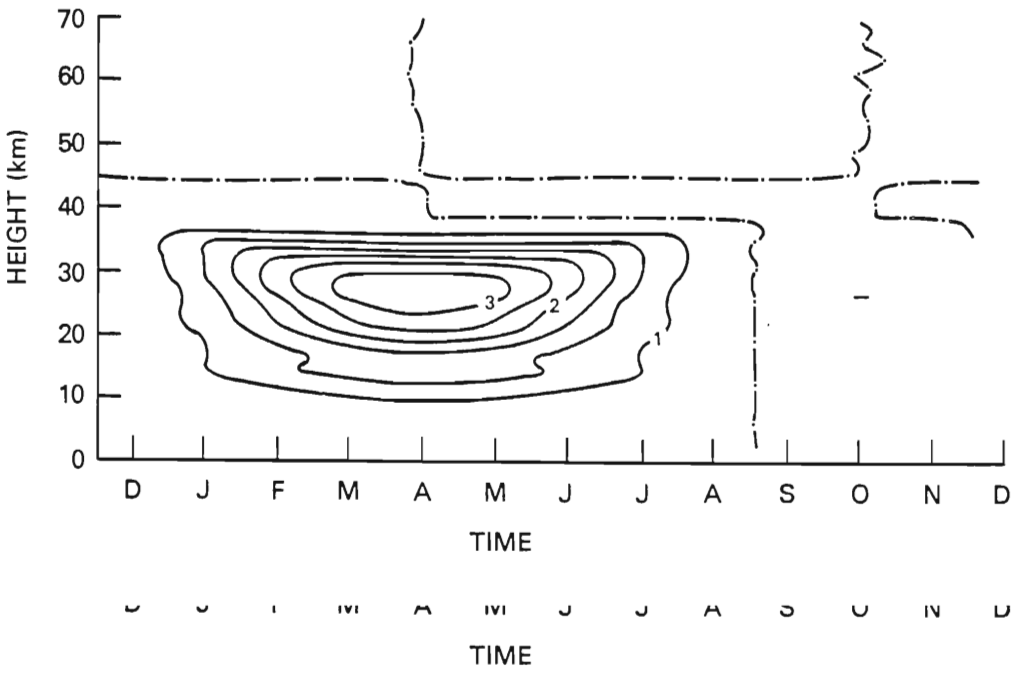


CHANGE IN $\bar{\mu}$ (74°)

(ppm)

Figure 4.8

DIABATIC



TOTAL OZONE

D.U.

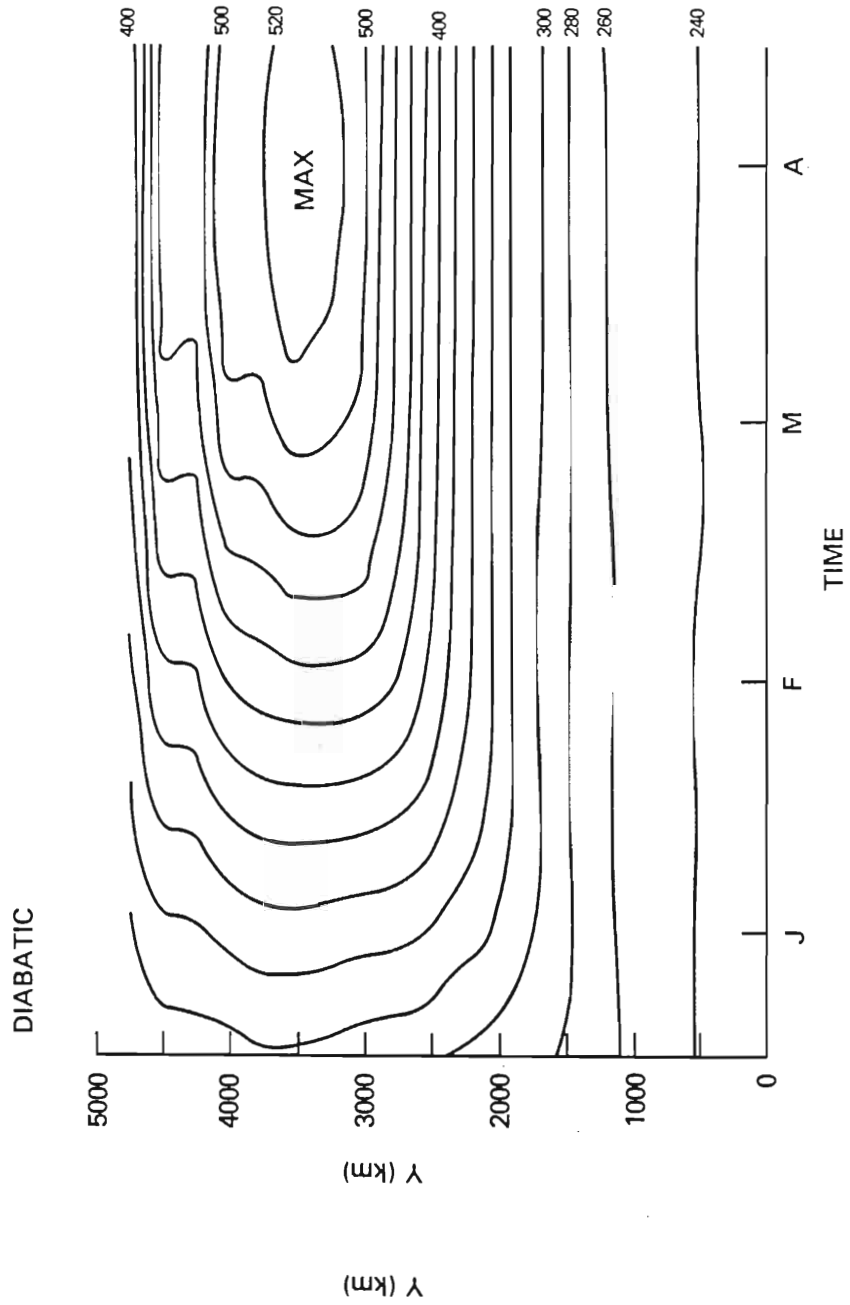


Figure 4.9

The changes in ozone above 45 km in Figures 4.7 and 4.8 are negligible due to the strong photochemistry. Therefore, where the diabatic circulation is strongest no changes in the ozone field are found. The transport effects by the diabatic circulation are most notable in the transition and conservative regions and are due primarily to the vertical velocity which is downward at all latitudes and constantly advecting ozone into the lower stratosphere. The maximum anomaly occurs about 500 km north of the maximum vertical velocity indicating the relative ineffectiveness of the meridional velocity ($<.3 \text{ m sec}^{-1}$) at transporting ozone northward.

Because insolation is weak during the winter the ozone photochemistry is much slower than modeled here at high latitudes. The overestimation of the photochemical source term may be responsible for the unrealistic buildup in the northern region. The results from two experiments where latitudinal variation of the chemistry is included are shown in Fig. 4.10. In the first experiment the photochemistry is given a cosine of latitude dependence such that the chemical relaxation weakens and disappears at the northern boundary. This is the same latitudinal dependence as used by Garcia and Hartmann (1980). Comparing Figures 4.8 and 4.10a indicate there is no significant difference in the results from the case with no latitudinal variation of the chemistry. Apparently, the diabatic circulation is so weak that even with much from the case with no latitudinal variation of the chemistry. Apparently, the diabatic circulation is so weak that even with much slower photochemistry the ozone never varies much from its equilibrium value.

In the second experiment (Fig 4.10b) the photochemistry is set exactly equal to zero north of 67.5° for the entire time integration. The positive anomaly in the lower stratosphere remains the same as in the other experiments, but there is a negative anomaly around 50 km of more than 1 ppm. This region of depletion is due to the inability of the ozone to return to its equilibrium state. Since the increase in the lower stratosphere remains the same, some other process besides the latitudinal variation of the photochemistry must be responsible for prohibiting the excessive buildup of ozone at 70° .

In summary, the diabatic circulation during winter is directed such that transport is poleward and downward. The northward component of the velocity is too small to effectively transport ozone to polar regions; however, the vertical component acts over a considerable depth of the stratosphere and transports significant amounts of ozone into the lower stratosphere. The total ozone calculated using the diabatic circulation alone is too large in magnitude. In addition, the maximum amounts occur too far south and about 1 month too late.

Figure 4.10. Change in ozone at 74° with horizontally varying chemistry (ppm).

a. cosine of latitude dependence

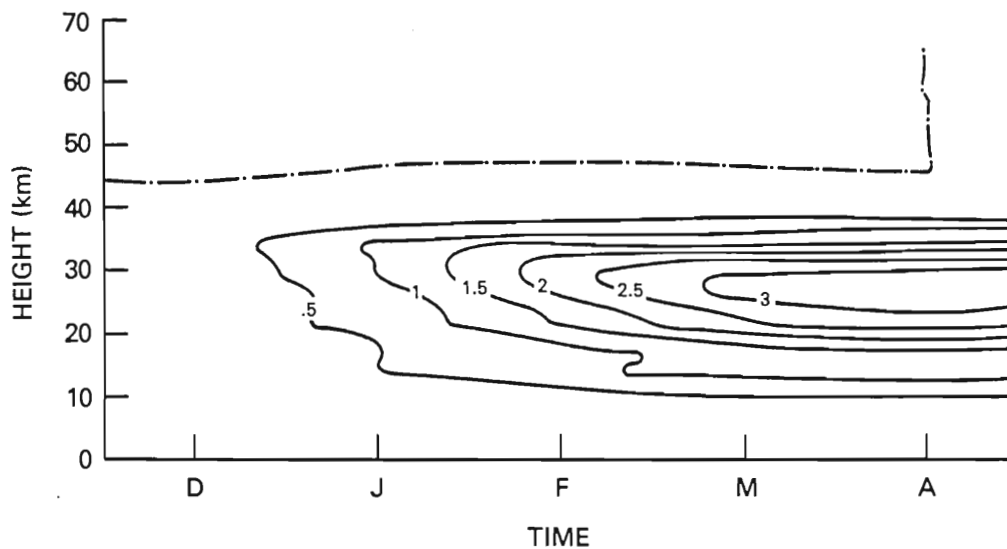
b. $\lambda=0$ north of 67°

CHANGE IN $\bar{\mu}$ (74°)

(ppm)

Figure 4.10a

DIABATIC, $\cos(\text{LAT})$

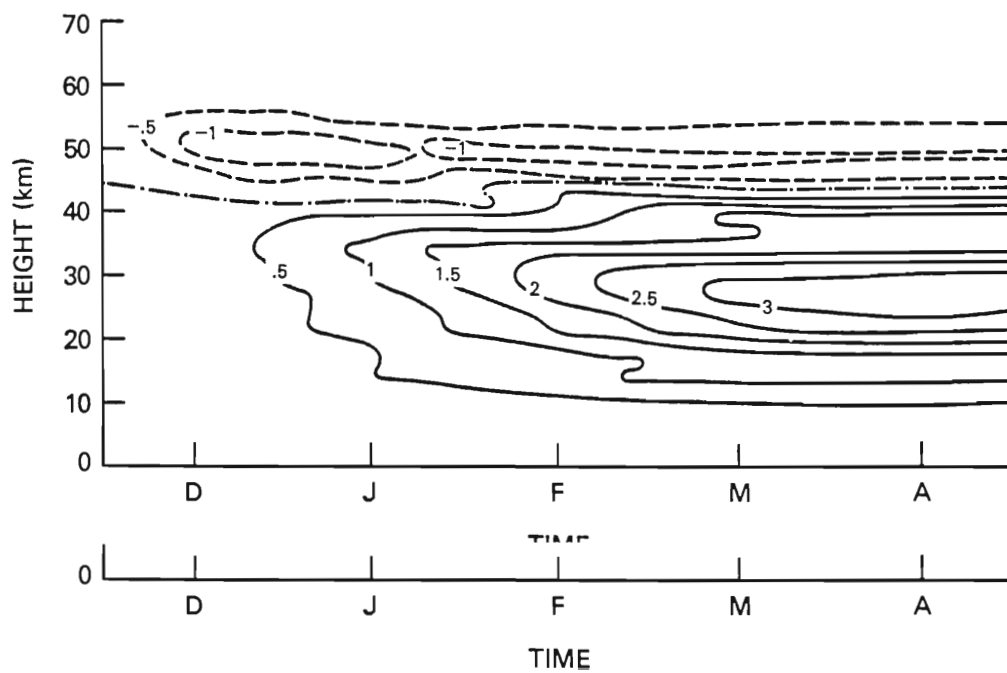


CHANGE IN $\bar{\mu}$ (74°)

(ppm)

Figure 4.10b

DIABATIC, POLAR NIGHT



4.4 Planetary wave transport

Transport by steady, stationary, dissipative planetary waves was discussed in Chapter 3. It was found that in the conservative region of the stratosphere planetary waves tended to advect ozone from low latitudes towards the pole. In the transition region it was found that stirring of parcels by the waves across regions of widely varying photochemistry could produce changes in the mean field that the mean chemistry could not completely counterbalance. In this section the results of transport by transient planetary waves will be presented. In order to study transport mechanisms it is useful to study both conservative transport (chemically inactive) and chemical transport.

a. Conservative transport

The changes in the mean ozone field for conservative transport by planetary waves forced with 600 m orography is shown in Figures 4.11 and 4.12 for the southern and northern points. Centered around 40 km is a zone of poleward ozone transport and just above this zone, centered at 50 km, is a region of equatorward transport. With the 900 m orography (Fig. 4.13), similar structure is evident with the northward transport centered at 35 km and the southward transport centered at 50 km. The maximum positive change at the northern point for the 900 m case is 2.2 ppm and occurs on day 32; for the 600 m case a maximum of slightly more than 1 ppm occurs on northern point for the 900 m case is 2.2 ppm and occurs on day 32; for the 600 m case a maximum of slightly more than 1 ppm occurs on day 35. For both cases there is relatively little change at the center of the channel.

Figure 4.11. Change in ozone for 600 m topography
at 46° with no chemistry (ppm).

(bold solid line is the critical line)

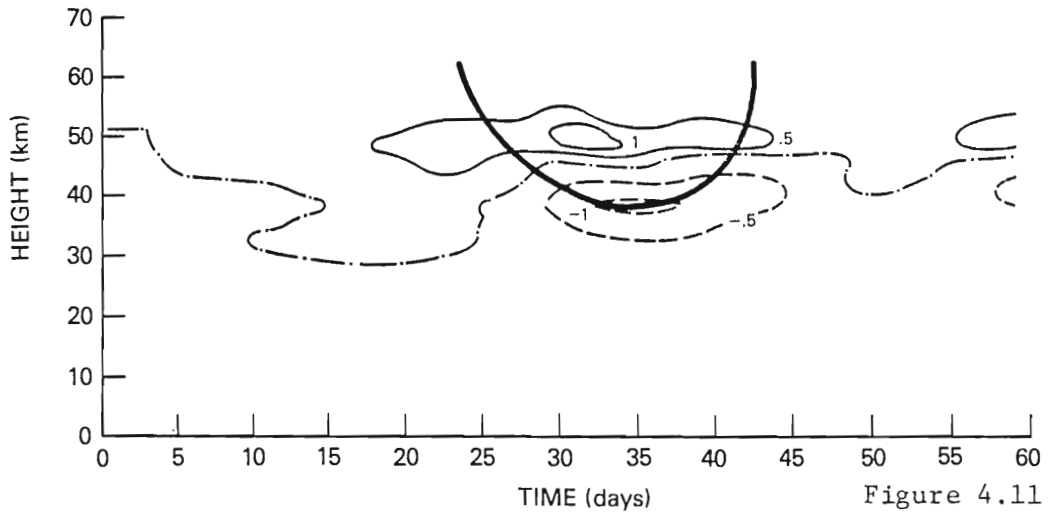
Figure 4.12. Same as Fig. 4.11 but at 74° .

Figure 4.13. Same as Fig. 4.12 but for 900 m topography.

CHANGE IN $\bar{\mu}$ (46°)

(ppm)

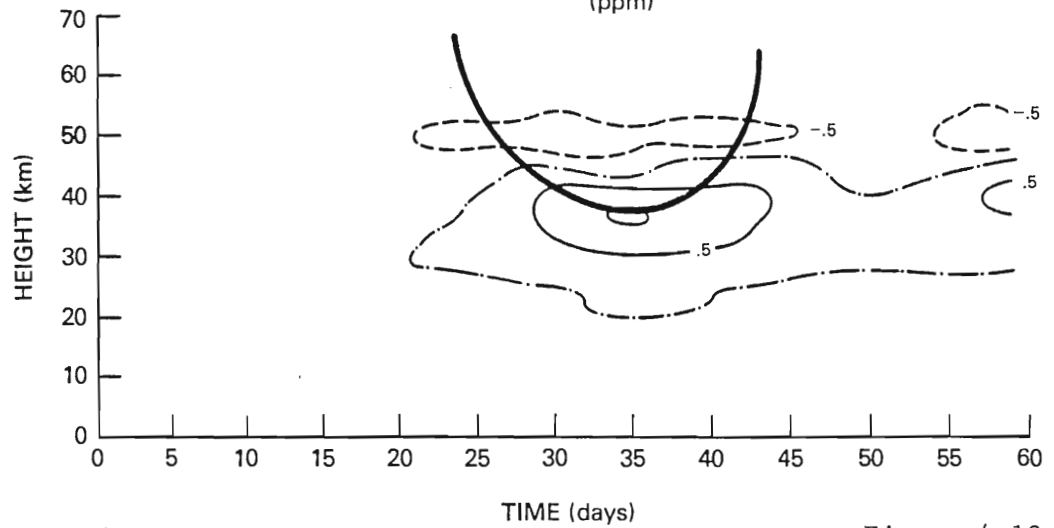
600 m, CONSERVATIVE



CHANGE IN $\bar{\mu}$ (74°)

(ppm)

600 m, CONSERVATIVE



TIME (days)

Figure 4.12

CHANGE IN $\bar{\mu}$ (74°) (ppm)

900 m, CONSERVATIVE

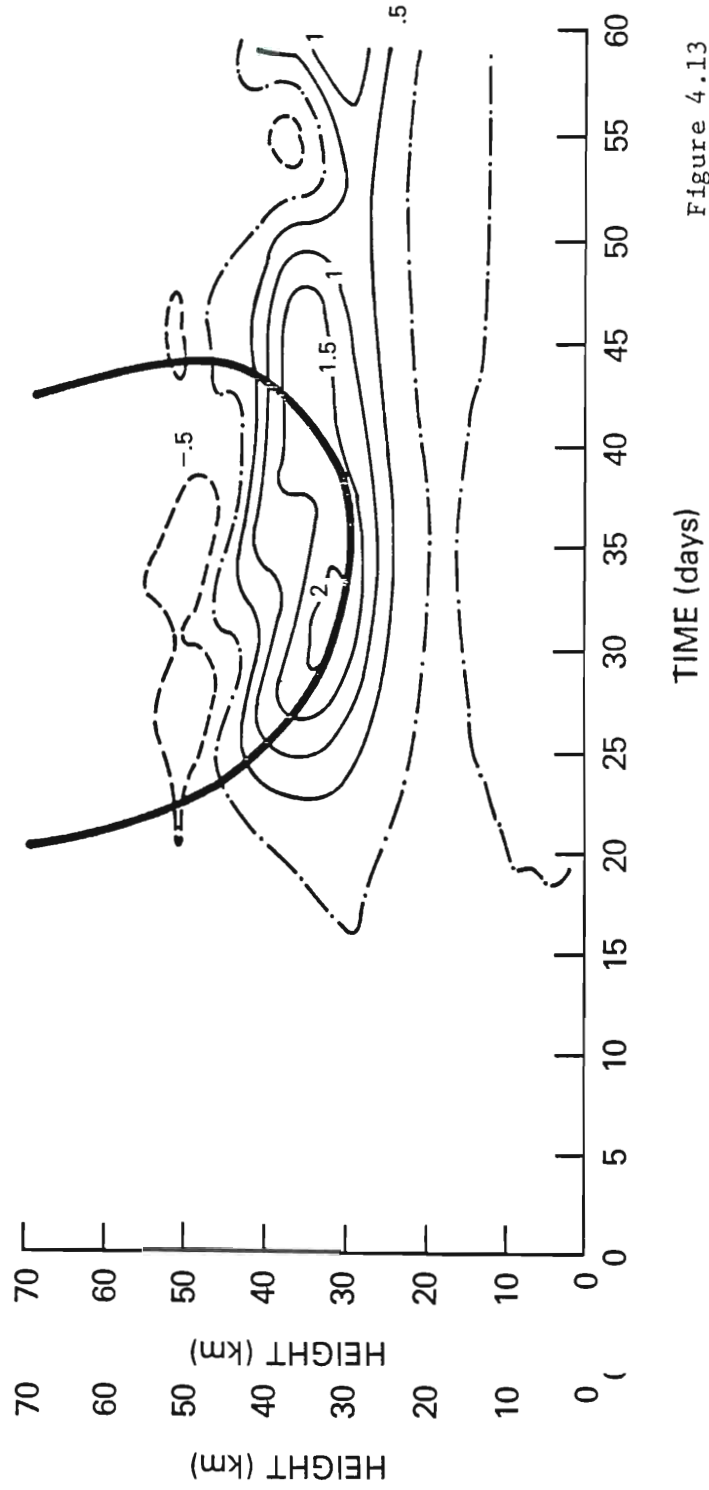


Figure 4.13

Superimposed on Figures 4.11-4.13 is the location of the critical line at the appropriate latitude. For all cases the level of maximum northward transport is coincident with the minimum descent of the critical line. The layer of southward transport is above the critical line. The transport calculated here supports the theory of Schoeberl (1981b) which predicts that a wave energy absorbing critical line will produce a jet of northward transport at the critical line. This transport mechanism will be discussed further in Section 4.6.

b. Chemical transport

The transport of ozone for both 600 m and 900 m orography with photochemistry is presented in Figures 4.14-4.16. There is the general tendency for the upper region of equatorward transport to be significantly reduced in all cases due to the photochemistry. With photochemistry the transport appears to occur in a thin layer in the conservative region and at the bottom of the transition region.

For the 600 m orography at the southern point (Fig 4.14) the magnitude of the depletion at 40 km has decreased by 35% with the addition of photochemistry (compare to Fig. 4.11). This might be expected since the chemistry would tend to moderate large differences from equilibrium. The magnitude of the positive anomaly at the northern grid point (Fig. 4.15) on the other hand has not moderated with the addition of chemistry but has increased by 14%. at the northern grid point (Fig. 4.15) on the other hand has not moderated with the addition of chemistry but has increased by 14%.

At the northern point, with the 900 m orography (Fig 4.16), the anomaly field is once again more jet like than without chemistry,

but the magnitude has remained the same. The transport calculated at the southern point shows similar behavior with the low level negative anomaly maintaining the same magnitude with the addition of photochemistry. The level of maximum northward transport for the 900 m case occurs significantly lower in the stratosphere than with the 600 m forcing; therefore, the addition of chemistry would be expected to have relatively little effect on the transport.

It is of interest to examine the extended time series of the 900 m forcing (Fig. 4.16). In this figure the solid heavy line is the critical line at the latitude of the figure and the heavy dashed line is the critical line at the center of the channel. While the critical line at high and low latitudes ascends and dissipates, there is still intense south to north transport centered around 35 km. This transport is obviously associated with the critical line at the center of the channel. The anomaly decreases and increases coincident with the ascent and descent of the critical line.

The largest northern anomaly during the entire time integration occurs on day 70 when the critical line reaches its lowest altitude at the center of the channel. At this time there is no critical line present at any altitude at the northern point. This result shows that the horizontal extent of the transport associated with the critical line at the center of the channel is significant.

Figure 4.14. Change in ozone for 600 m topography
at 46° with chemistry (ppm).

(bold solid line is the critical line)

Figure 4.15. Same as Fig. 4.14 but at 74° .

Figure 4.16. Same as Fig. 4.15 but for 900 m topography.

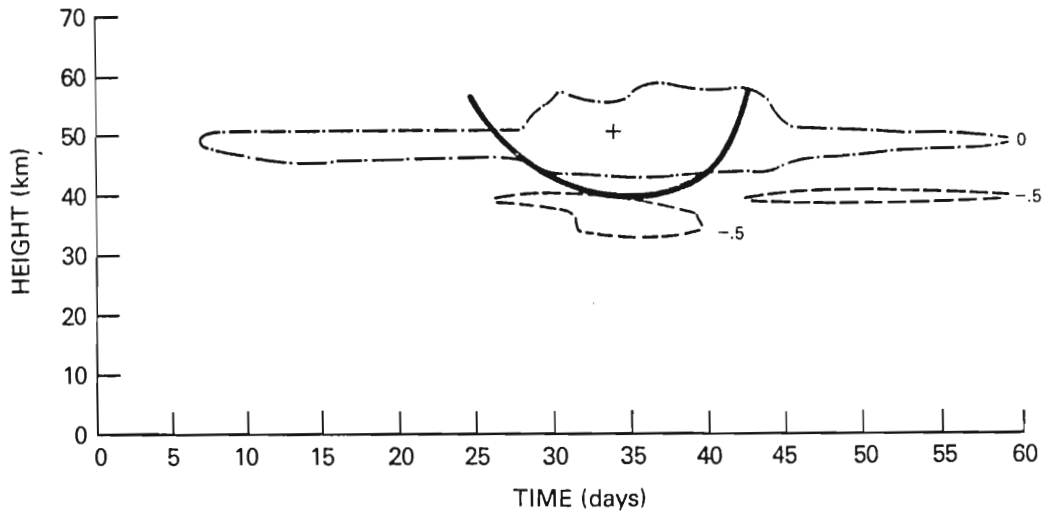
(bold dashed line is the critical line
at the center of the channel)

CHANGE IN $\bar{\mu}$ (46°)

(ppm)

Figure 4.14

600 m, CHEMISTRY

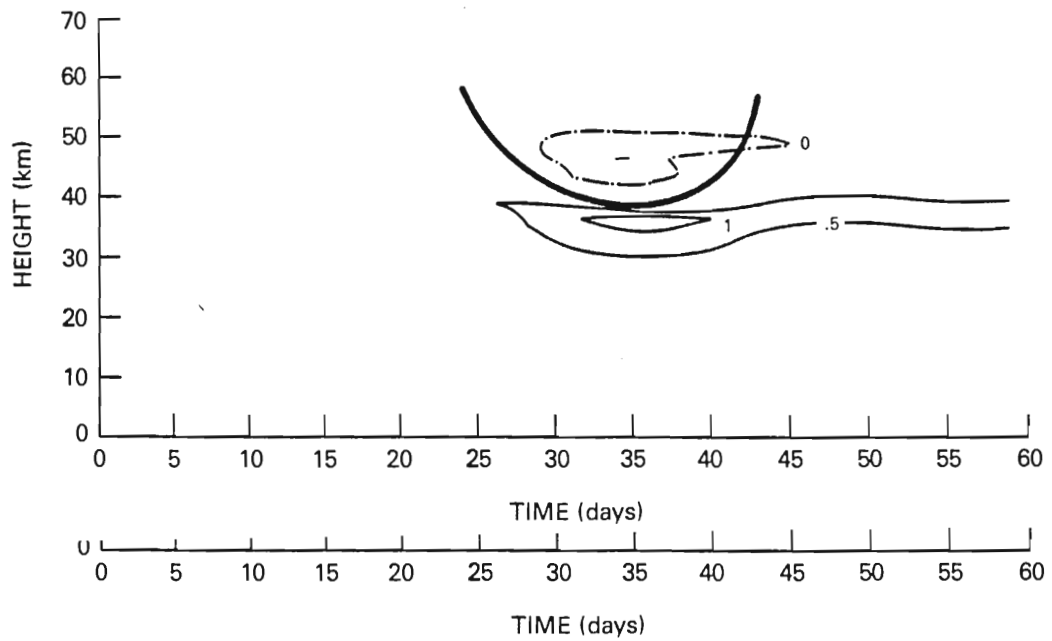


CHANGE IN $\bar{\mu}$ (74°)

(ppm)

Figure 4.15

600 m, CHEMISTRY



CHANGE IN $\bar{\mu}$ (74°)

(ppm)

900 m, CHEMISTRY

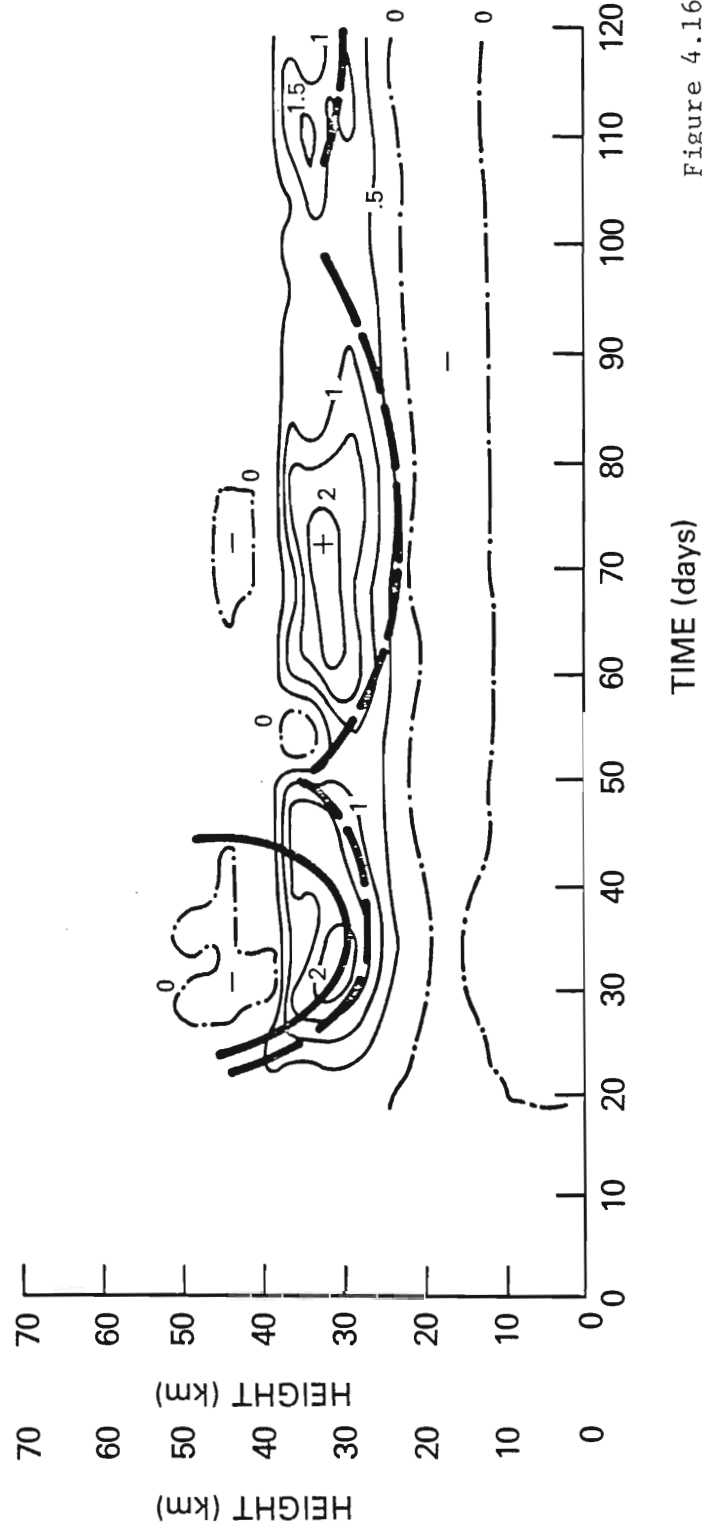


Figure 4.16

4.5 Transport by both waves and the diabatic circulation.

The change in the zonal mean ozone field associated with the diabatic circulation superimposed on the 900 m topography dynamics is shown in Figures 4.17-4.19. The 900 m topography was chosen for these experiments since this amplitude forcing is more consistent with the terrestrial topography (Berkofsky and Bertoni, 1955), and the critical line for this case descends below 32 km. One of the WMO criteria for the classification of a major stratospheric warming is that the wind reversal descends below 10 mb which is approximately 32 km. The transport by the combined circulations is much different from the transport by each individual type of circulation indicating that both the wave and diabatic transport regimes are important in the lower stratosphere.

At the center of the channel (Fig. 4.18) there is a maximum increase between 25 and 30 km of 1.25 ppm in late March. There is a series of short term decreases around 40 km with the most intense decrease of 1.25 ppm also occurring in late March. The region of steady increase is due to the downward transport by the diabatic circulation. The intermittent nature of the ozone depletion at 40 km is associated with the wave transport. With the combined circulation the increase in ozone at the channel center is reduced by more than 50% when compared to the changes caused by the diabatic circulation alone (Fig. 4.7), which indicates that the planetary waves are transporting ozone out of the center of the channel.

----- (Fig. 4.7), which indicates that the planetary waves are transporting ozone out of the center of the channel.

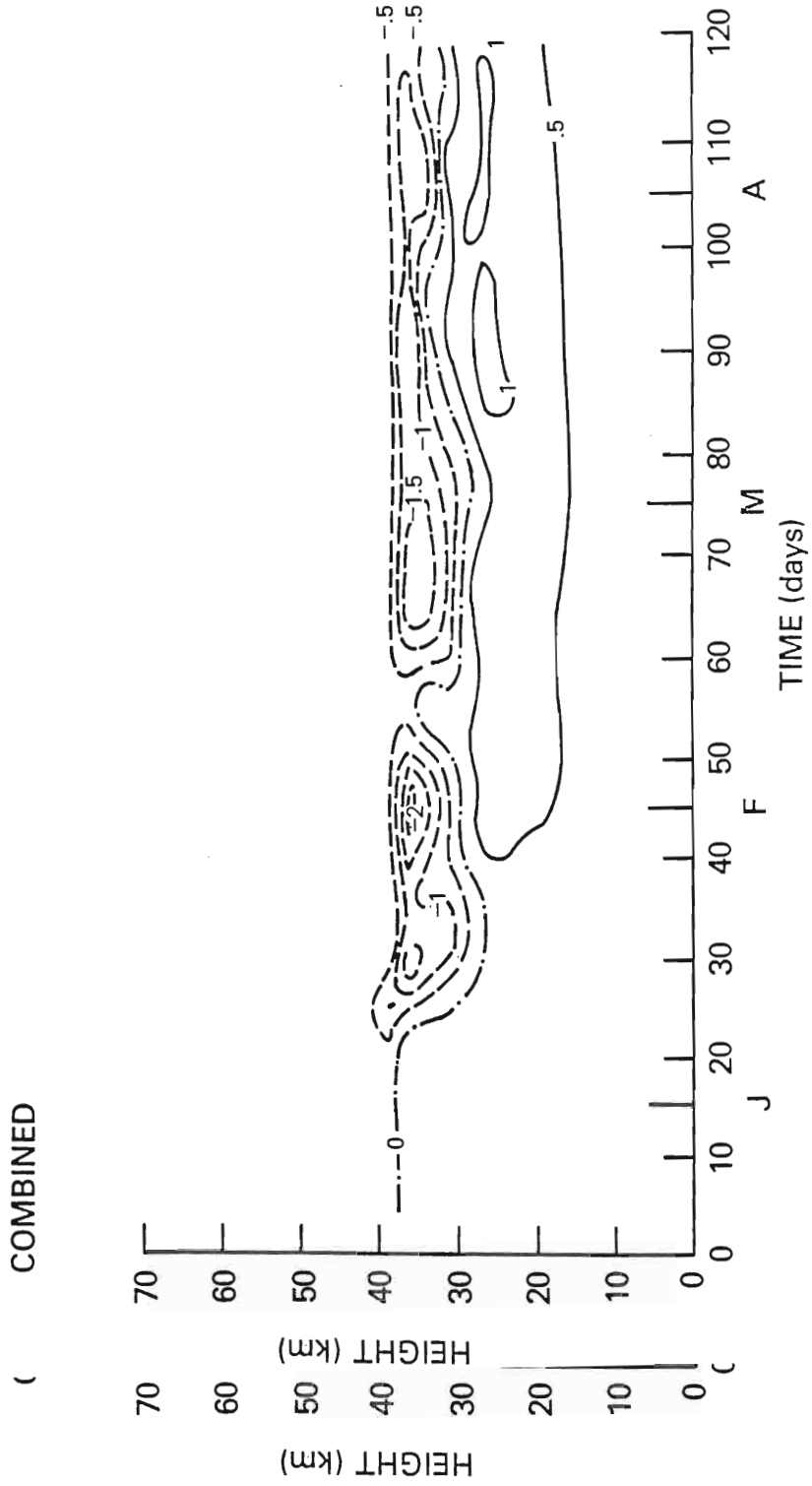
Figure 4.17. Change in ozone for the combined planetary wave (900 m) and diabatic circulations at 46° with chemistry (ppm).

Figure 4.18. Same as Fig. 4.17 but at 60° .

Figure 4.19. Same as Fig. 4.17 but at 74° .

CHANGE IN $\bar{\mu}$ (46°) (ppm)

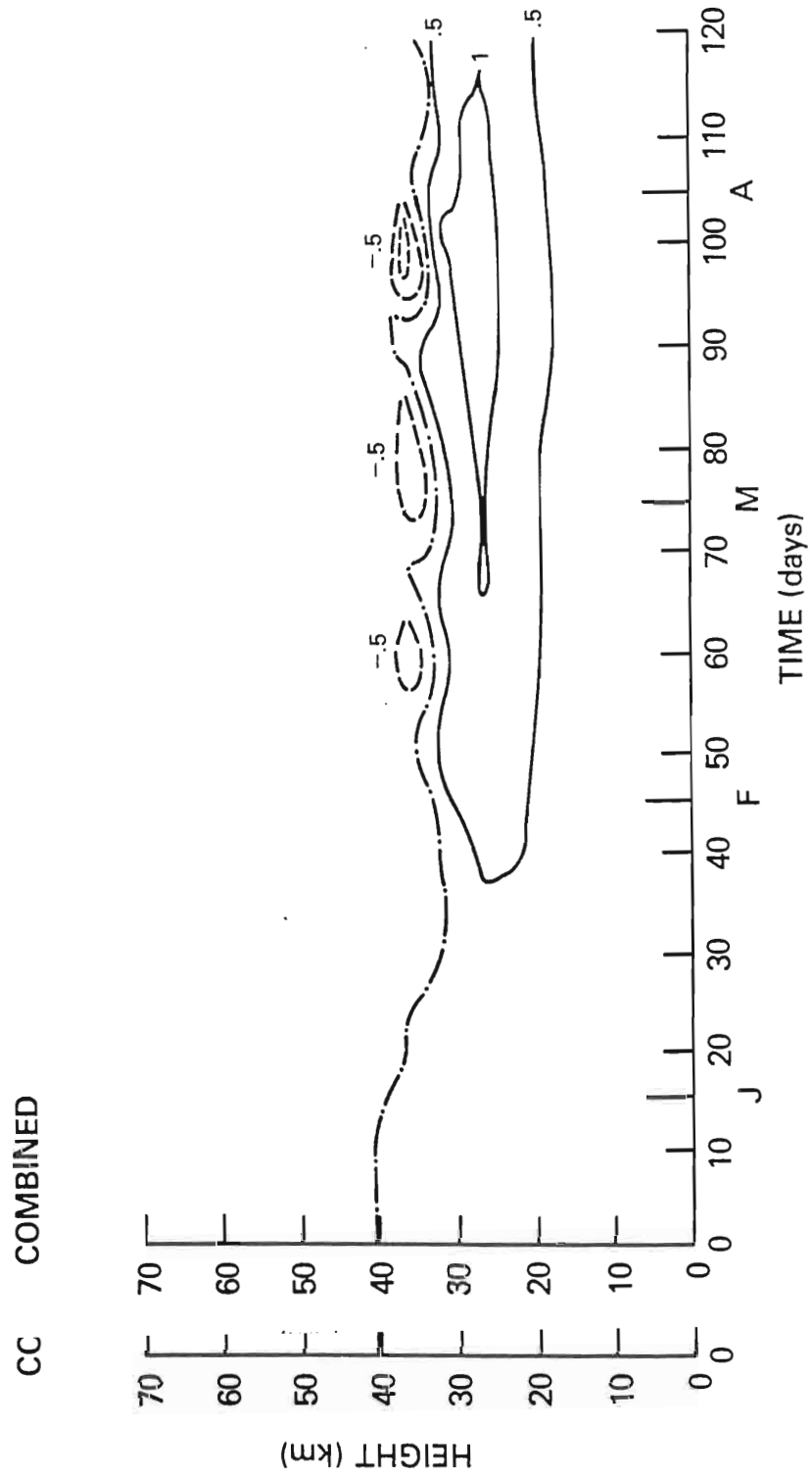
Figure 4.17



CHANGE IN $\bar{\mu}$ (60°)

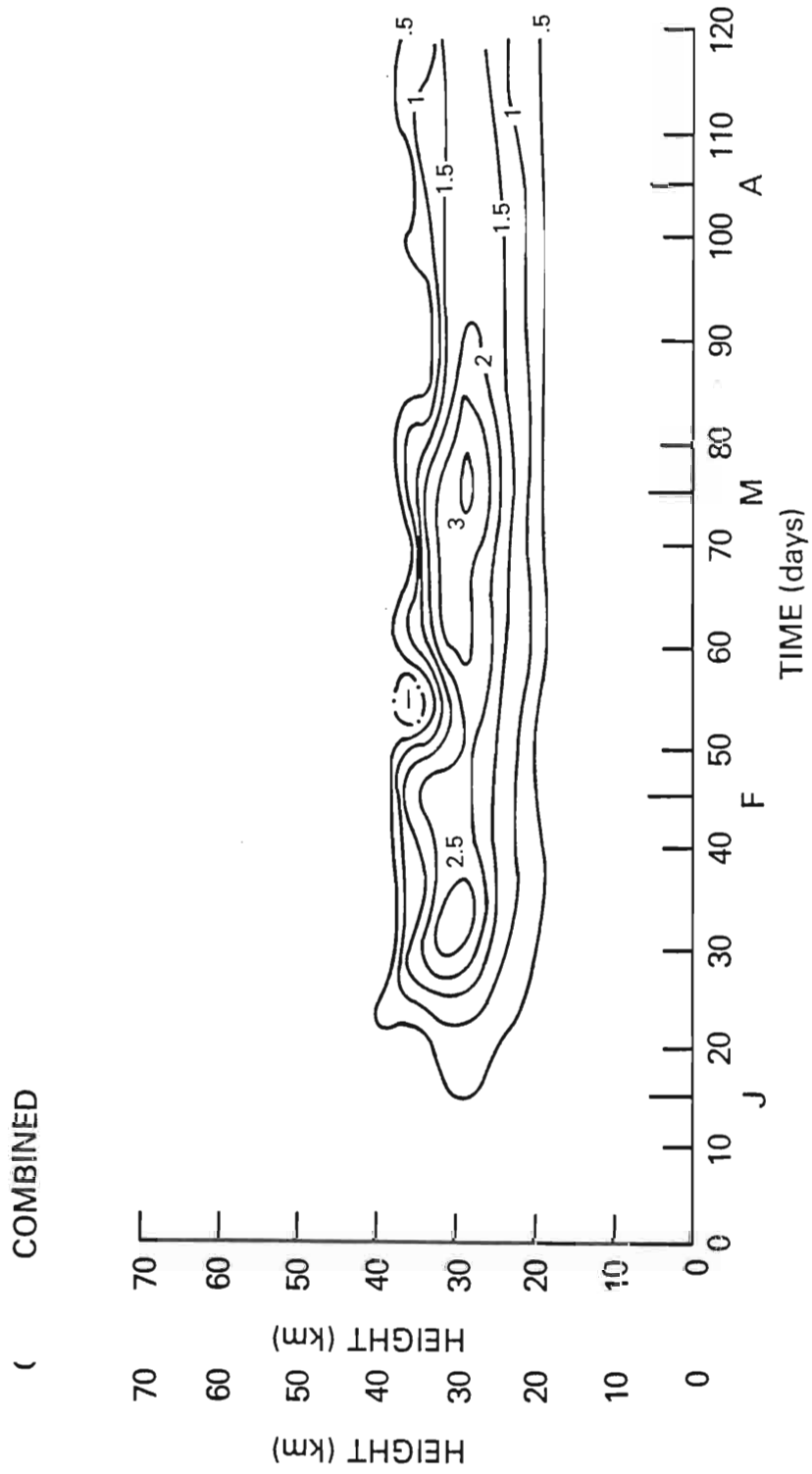
(ppm)

Figure 4.18



CHANGE IN $\bar{\mu}$ (74°) (ppm)

Figure 4.19



At the northern latitude (Fig. 4.19) there is a uniform increase of ozone at all levels with the maximum increase of 3.12 ppm occurring close to 30 km, about 4 km lower than the maximum associated with the planetary waves alone (Fig. 4.16) and 4 km higher than that associated with the diabatic circulation alone (Fig. 4.8). An anomaly of 1 ppm is evident at 25 km, which is 10 km higher than a similar anomaly calculated using only the diabatic circulation (compare to Fig. 4.8). The largest anomaly occurs in early March and is coincident with the lowest altitude of the critical line. Following the maximum in early March the positive anomaly remains relatively stable at a maximum value somewhat greater than 2 ppm.

At the southern latitude (Fig. 4.17) there is a region of relatively strong poleward transport between 35 and 40 km and below this layer is a region of increase. As at the center of the channel, the region of increase is associated with the diabatic circulation and the decrease is associated with the planetary wave. Such large depletions are not observed at this latitude (44°) in the stratosphere.

The total ozone time series (Fig. 4.20) shows much better agreement with observation at high latitudes than the total ozone field calculated with the diabatic circulation (Fig 4.9). A late winter maximum of almost 440 DU occurs during early March at the most northern latitudes. There is an earlier maximum of slightly winter maximum of almost 440 DU occurs during early March at the most northern latitudes. There is an earlier maximum of slightly more than 420 DU coincident with the initial descent of the critical line. This earlier maximum produces a wave like feature that is

similar to the wave structure shown in Fig 2.10. Both maxima are associated with the critical line descent after the first warming event (Fig. 4.3).

In the southernmost section of the model there is too little ozone from the beginning of the combined planetary wave-diabatic integration (Dec. 15). Furthermore, during the initial descent of the critical line there is excessive transport out of the south. The excessive transport occurs at the time that the critical line descends to low altitudes at the northern and southern points.

Figure 4.20. Time-latitude cross section of total ozone as calculated with the combined planetary wave-diabatic circulation (DU).

TOTAL OZONE

D.U.

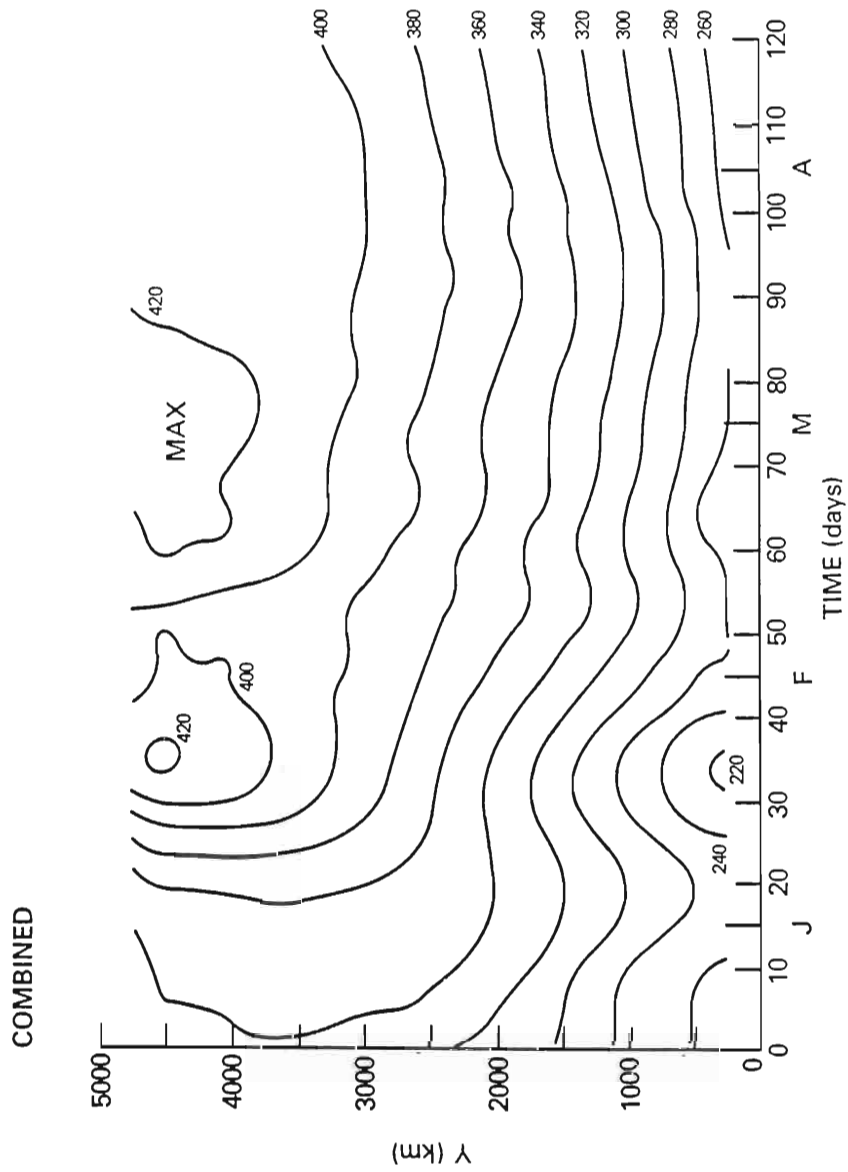


Figure 4.20

4.6 Discussion.

The transports associated with the diabatic and planetary wave circulations are fundamentally different from each other and of equal importance. The diabatic circulation is primarily responsible for transport of ozone downward from the photochemical source region while the planetary wave circulation is responsible for north-south transport. The combined circulations do a particularly good job of reproducing the features of the total ozone distribution at high latitudes.

The vertical structure of the winter ozone field is not as well simulated as the total ozone distribution. The computed increase of more than 3 ppm at high latitudes is concentrated at 30 km which is larger than observed at this altitude. The increase between 20 and 25 km is significantly smaller than is observed. The increase in ozone at high latitudes is due largely to the downward transport of ozone out of the photochemical region by the diabatic circulation at 70° and the subsequent northward transport of this ozone to high latitudes by the planetary waves.

Enough ozone is transported out of the source region to high latitudes to model the total ozone maximum; however, redistribution of ozone within the conservative region is needed to accurately reproduce the ozone distribution. Synoptic scale disturbances are probably instrumental in determining the vertical structure of ozone within the lower stratosphere. probably instrumental in determining the vertical structure of ozone within the lower stratosphere.

In the southern region of the channel and to a lesser degree in the middle of the channel the vertical structure is more poorly

represented. There is excessive transport out of the south by the planetary waves between 35 and 40 km which leads to unrealistic vertical profiles. This excessive transport is also evidenced by the underestimation of total ozone at low latitudes during mid-January. The overestimation of transport out of the southern region might be due to an inadequate representation of chemistry at low altitudes; the underestimation of the transport by the diabatic circulation into the south from either high altitudes or lower latitudes; geometric effects of the β -plane transport; and/or to the neglect of small scale dynamics.

In order to understand the particular nature of the transport, it is necessary to further analyze the transport mechanisms involved. It was mentioned in Chapter 3 that even for steady, stationary, dissipative planetary waves, there were computational difficulties in calculating Lagrangian-mean quantities. In the presence of highly transient dynamics these difficulties are more severe, and the calculation of Lagrangian-mean velocities is time consuming with the result being uncertain (McIntyre, 1980). Furthermore, in the vicinity of the critical lines, the displacement vectors are nearly singular and their calculation is difficult. Dunkerton et al. (1981) also experienced difficulty in the calculation of Lagrangian-mean quantities with realistic dynamical models. Therefore the transport will be analyzed in the Eulerian framework with comments made on the Lagrangian-mean interpretation models. Therefore the transport will be analyzed in the Eulerian framework with comments made on the Lagrangian-mean interpretation where it is appropriate.

a. Diabatic circulation

At all times during the winter at extratropical latitudes the flux due to the diabatic circulation is northward and downward. The northward transport is quite weak and does little to change the ozone distribution. The vertical transport is effective at transporting ozone from the photochemical and transition regions into the upper part of the conservative region.

While the diabatic circulation does transport ozone northward and downward it is inadequate alone to explain the wintertime polar ozone buildup. The meridional component of the diabatic circulation is large enough to cause significant transport only at high altitudes where the photochemistry is dominate. Therefore Brewer-Dobson circulations, which involve the upward transport of ozone at low latitudes; northward transport at high altitudes in the midlatitudes; and subsidence at high latitudes, cannot explain ozone transport.

b. Planetary waves

The planetary wave transport is more complex than that presented in Chapter 3 for steady-state transport. Examination of Fig. 4.16, for instance, shows that the transport is highly time dependent with strong pulses of northward transport. The planetary wave transport was demonstrated to be directly related to the descent of the critical line in the previous section.

The transport was demonstrated to be directly related to the descent of the critical line in the previous section.

According to theory (Charney and Drazin, 1961), it is impossible for stationary planetary waves to propagate vertically in

an easterly mean zonal flow; that is, through a critical line. Therefore, when a propagating wave is incident upon a critical line the wave energy must be absorbed, reflected, or possibly overreflected if the critical line is in a region of negative \bar{q}_y (Lindzen et al., 1980). In general, the vicinity of the critical line is a region of strong wave transience and dissipation (Matsuno and Nakamura, 1979).

In this model the critical region is generally a region of partial if not full absorption of wave energy. This fact is demonstrated by the persistence of the critical line. The Rayleigh friction incorporated into the model tends to force the mean flow back to its equilibrium state. Since the critical line remains persistent for such long periods, as is evidenced in Fig 4.3, some wave energy must be absorbed at the critical level in order to maintain the critical level.

Matsuno and Nakamura (1979) and Schoeberl (1980, 1981b) have discussed the Eulerian and Lagrangian-mean circulations associated with an idealized absorbing critical line oriented at various angles with the vertical. In Fig 4.21 are shown the mass stream functions associated with the two different formulations as taken from Matsuno and Nakamura (1979) for a horizontal critical line. In the Eulerian mean formulation there is rising motion in the north with descending motion in the south and a general southward transport. This flow regime is viewed as the mean field response to the northward heat flux of the planetary waves.

Figure 4.21. Stream functions for a horizontal critical line
(from Matsuno and Nakamura, 1979).

- a. Eulerian mean
- b. Lagrangian-mean

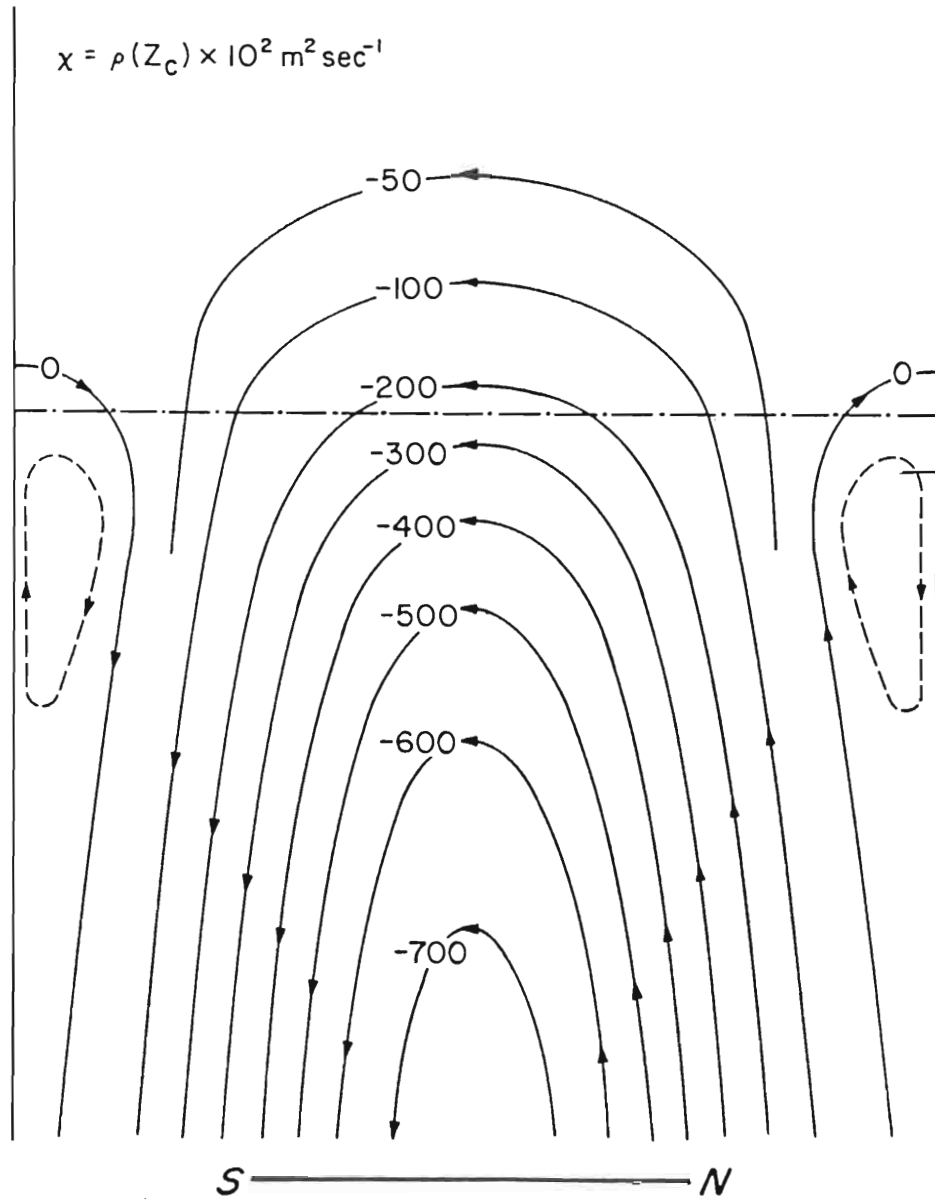


Figure 4.21a

Figure 4.21a

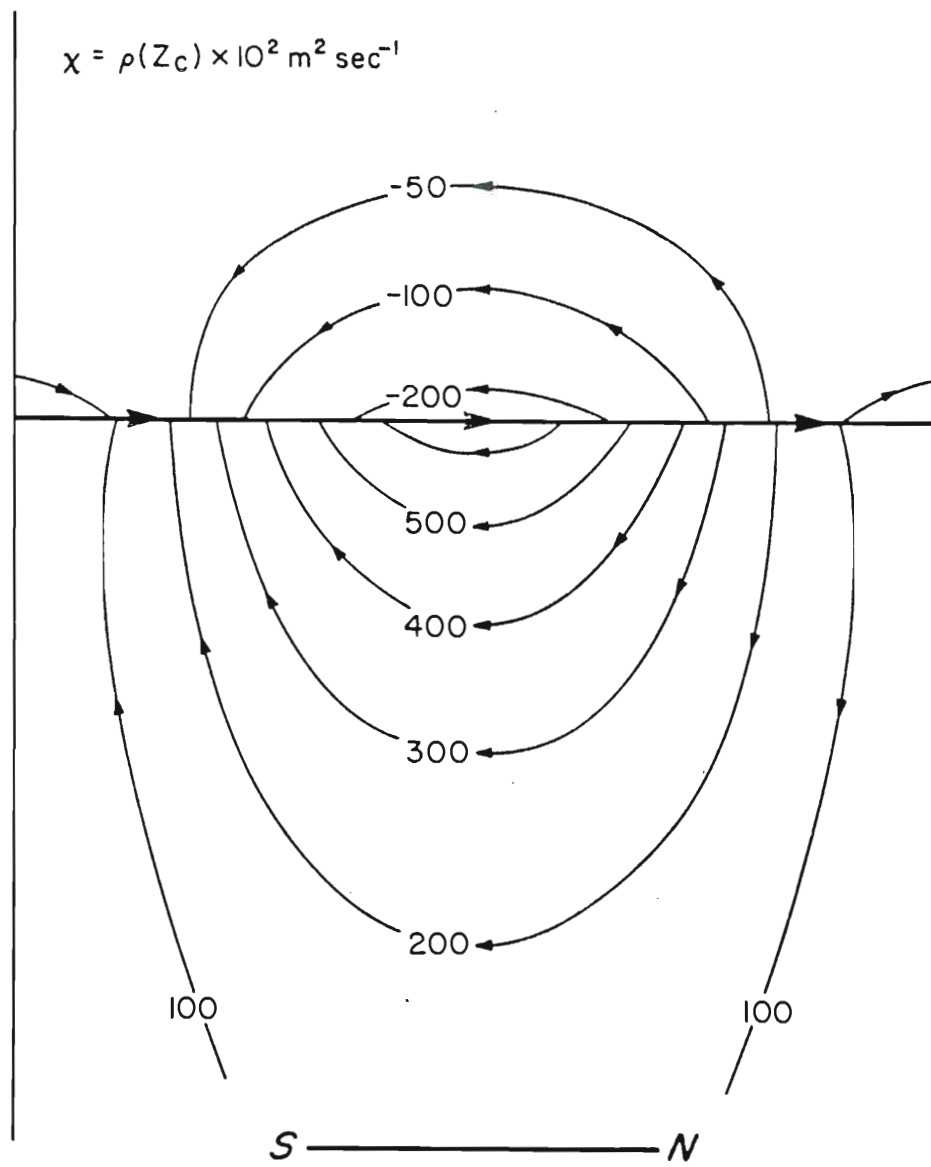


Figure 4.21b

The Lagrangian-mean stream function is much different with singular northward flow at the critical line and weaker return flow both above and below the critical line. Schoeberl (1981b) found that, except for vertical critical lines, there is always singular flow at a purely absorbing critical line. These authors use these idealized models to explain stratospheric warming phenomena and commented on the consequences of critical line flows on the distribution of minor constituents in the stratosphere. Schoeberl (1981b) predicted that where the critical line changes its orientation with the vertical, the constituent flux will be highly divergent and these regions will be an area of large constituent density changes.

In Schoeberl's study it was assumed that the critical line movement was so slow that it was not necessary to recalculate the zonal mean wind field. Nevertheless, it is possible to calculate the acceleration of the mean zonal wind which was found to be negative. That is, for the case of an absorbing critical line there is a tendency for the critical line to descend. Therefore the transport described above occurs when the mean zonal flow is being decelerated at the critical line and the critical line is descending.

For the case of an ascending critical line the flow is accelerating rather than decelerating at the critical line. This being the case the sign of Eq. (7) in Schoeberl (1981b) can be accelerating rather than decelerating at the critical line. This being the case the sign of Eq. (7) in Schoeberl (1981b) can be changed to indicate that the critical region is forcing the mean flow to become more westerly. With this sign change a strong

southward Lagrangian-mean jet is found at the critical line.

Both the models of Schoeberl (1980, 1981b) and Matsuno and Nakamura (1979) assume the interaction of the wave with the critical line can be modeled as a step function so that the Eliassen-Palm (EP) flux is discontinuous across the critical line. With such a functional dependence of the wave forcing, the EP flux divergence is proportional to a delta function and, therefore, the Lagrangian-mean flow is singular at the critical line. The delta function dependence is equivalent to putting all of the wave transience at the critical line. In the real atmosphere and in numerical models the forcing is not so abrupt; hence, the effects of the critical line are spread out over a thin layer of the atmosphere.

In the Lagrangian-mean framework one would expect to see large northward fluxes at the critical line with the changes in the mean field being proportional to the divergence of the flux. In the Eulerian formulation, since the mean velocity is generally southward, the strong transport at the critical line should manifest itself as strong eddy flux oriented with the critical line. The direction of the eddy flux will depend on the background constituent density.

In the following, the transport for 900 m planetary waves will be discussed for both chemical and conservative transport. It is desirable to study the transport for conservative tracers because the chemistry tends to counter any changes in the upper stratosphere desirable to study the transport for conservative tracers because the chemistry tends to counter any changes in the upper stratosphere and might conceal transport mechanisms which would be important or incorrect for other chemical species. The transport will be

discussed with regard to the time scale in Fig. 4.3 measured from the beginning of the model integration.

The mean flux is shown at day 25 in Fig 4.22. At all times the Eulerian mean flux is from north to south with upward flux at high latitudes and downward flux at low latitudes. This flux field is consistent with that expected for a wave interacting with a critical line.

The eddy horizontal flux at day 25 is shown in Fig. 4.23 for conservative transport by the planetary waves alone. At this time the critical line has descended to approximately 40 km and is still descending. Centered at the critical line is a region of strong northward transport which has a strong meridional derivative in both the north and the south. This region of northward transport is responsible for the positive anomaly centered at 40 km seen in Fig. 4.13. The region of southward transport centered at 50 km is responsible for the negative anomaly at 50 km in Fig. 4.13. The transport shown here is consistent with the transport as predicted by Schoeberl (1981b) and Matsuno and Nakamura (1979) with strong northward transport at the critical line and return flow above.

Figure 4.22. Eulerian mean flux at day 25 (ppm m sec^{-1}).

a. horizontal

b. vertical

Figure 4.23. Horizontal eddy flux at day 25
conservative transport (ppm m sec^{-1}).

(bold solid line is the critical line)

Figure 4.24. a. Same as Fig. 4.23 but at day 31.

b. Wave transience at day 31.

c. \bar{q}_y at day 31.

(chain-dot = 0, dash < 0, solid > 0)

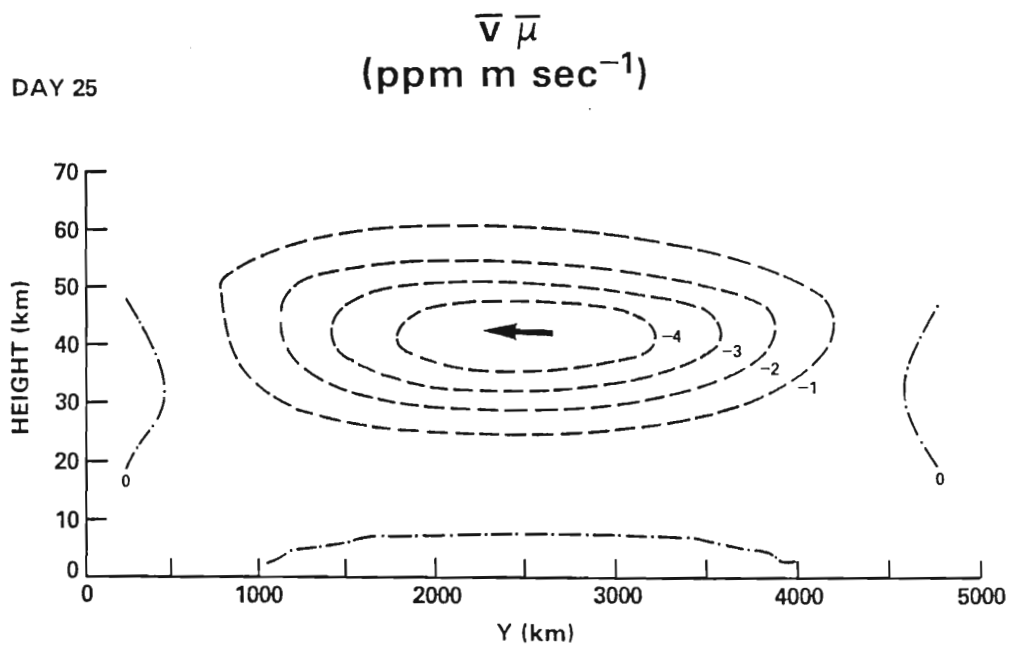


Figure 4.22a

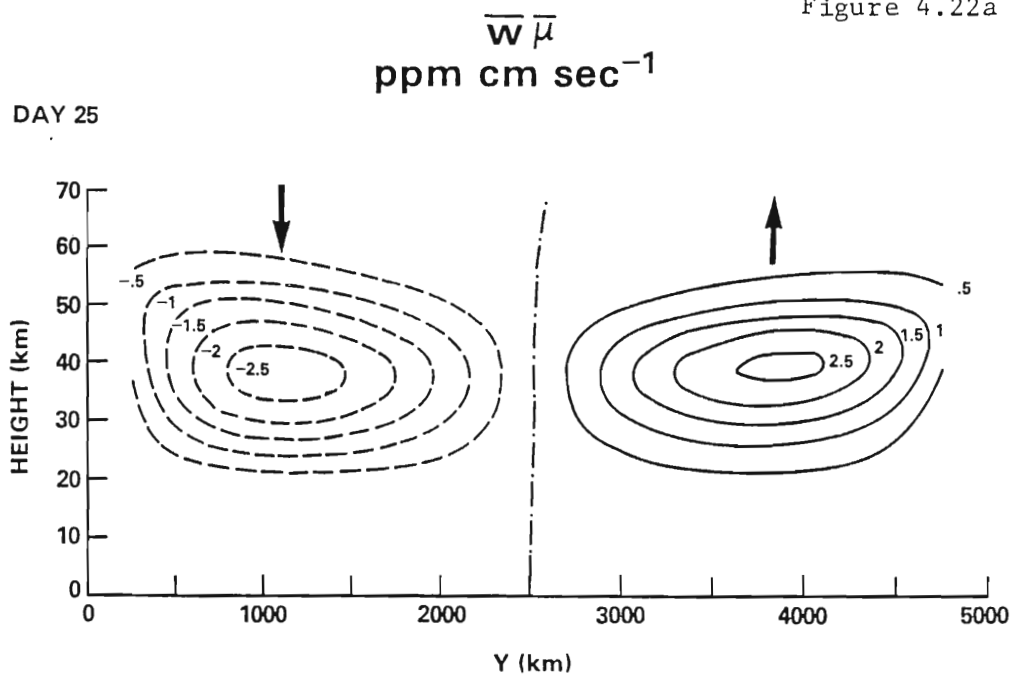


Figure 4.22b

Y (km)

Figure 4.22b

$\overline{v' \mu'}$
(ppm m sec⁻¹)

DA DAY 25, CONSERVATIVE

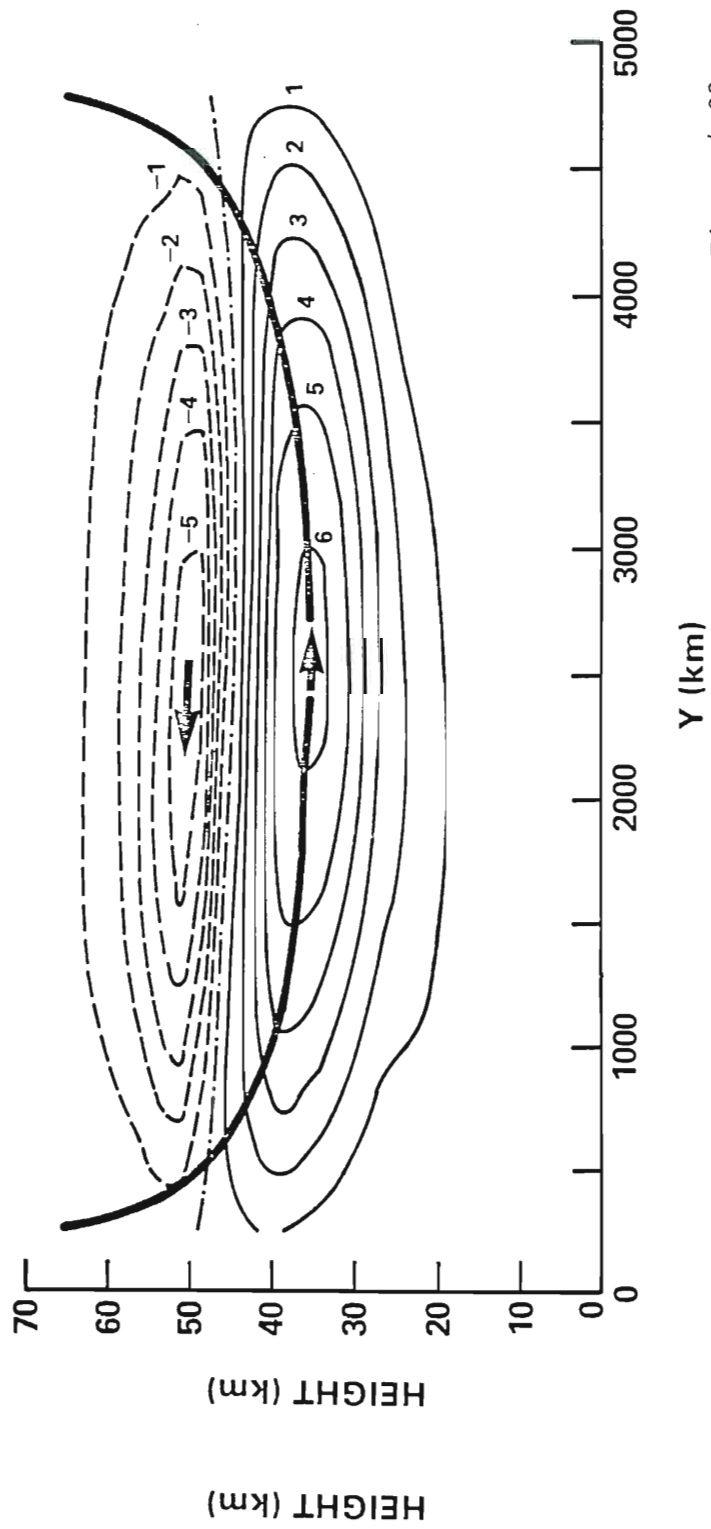


Figure 4.23

$\overline{v' \mu}$
(ppm m sec⁻¹)

D/ DAY 31, CONSERVATIVE

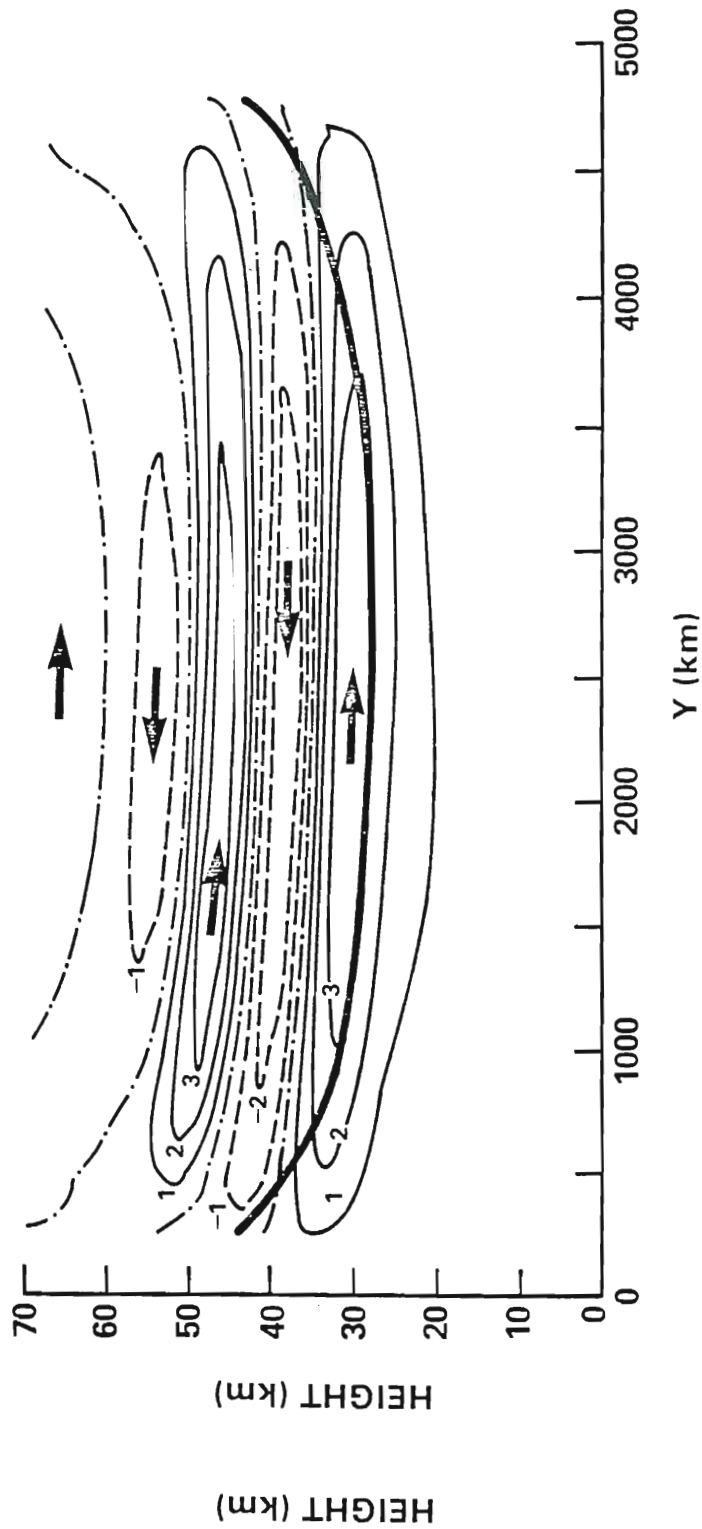


Figure 4.24a

WAVE TRANSIENCE

DAY 31

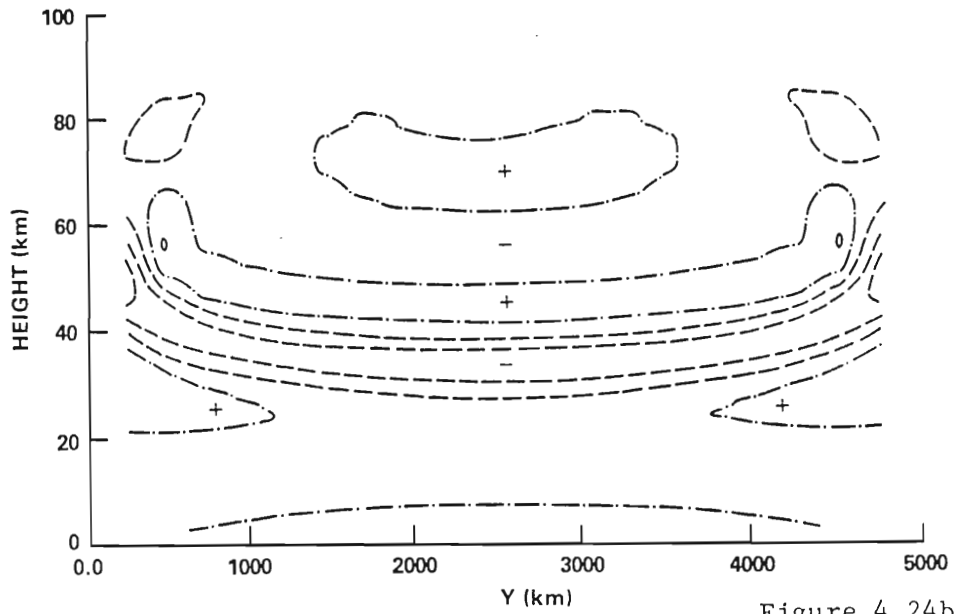


Figure 4.24b

DAY 31

$$\frac{\partial \bar{q}}{\partial y}$$

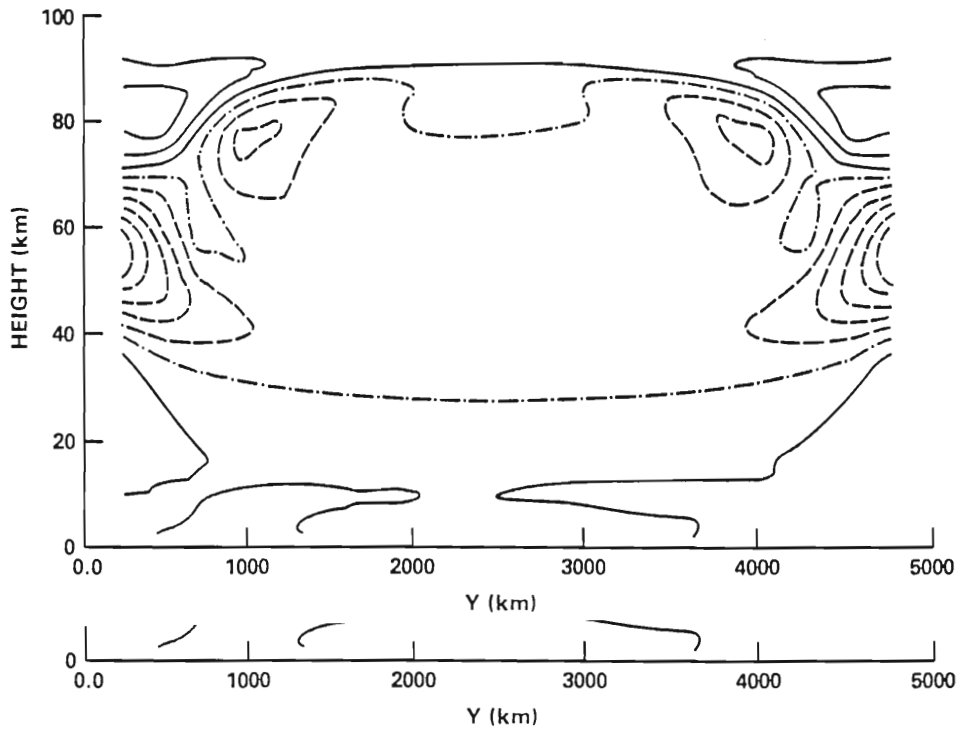


Figure 4.24c

By day 31 (Fig 4.24a) the eddy transport has changed considerably with the formation of several layers of northward and southward flux above the two layers that existed on day 25. The lowest level of northward transport has decreased in magnitude by half and is still centered at the critical line which is now near its maximum descent. At 50 km where there was strong southward transport on day 25 there is now predominately northward transport. This reversal of transport is responsible for the decrease in the magnitude of the anomaly at 50 km around day 30 in Fig. 4.13. It is obvious from Fig. 4.13 that the eddy flux at high altitudes has relatively little effect on the mean constituent field, indicating that the eddy and mean fluxes are nearly compensating away from the critical line.

In order to understand the mechanisms that are responsible for the formation of this layered transport structure it is useful to consider the following form of the horizontal eddy flux which can be derived from the perturbation continuity equation (Eq. 3.6) assuming that the perturbation experiences exponential growth or decay and that the chemistry is zero.

$$\overline{v' \mu'} = \frac{-c_i}{c_i^2 + (k\bar{u})^2} \left\{ \overline{\text{Re}(v')}^2 \frac{\partial \bar{\mu}}{\partial y} + \overline{\text{Re}(v') \text{Re}(w')} \frac{\partial \bar{\mu}}{\partial z} \right\} \\ - \frac{\bar{k}u}{c_i^2 + (k\bar{u})^2} \left\{ \overline{\text{Re}(v') \text{Im}(w')} \frac{\partial \bar{\mu}}{\partial z} \right\} \quad (4.1)$$

$$- \frac{\bar{k}u}{c_i^2 + (k\bar{u})^2} \left\{ \overline{\text{Re}(v') \text{Im}(w')} \frac{\partial \bar{\mu}}{\partial z} \right\} \quad (4.1)$$

C

This equation is useful for diagnostics away from the critical line.

At the critical line many of the terms in the denominator are nearly zero so that (4.1) would be singular. c_i is positive for a growing wave.

The transience at day 31 is shown in Fig. 4.24b. Positive transience is associated with a growing wave and negative transience is associated with a decaying wave. There is a strong correlation of the sign of the transience with the correlation in term C in Eq. 4.1. When the wave is growing (decaying) the correlation of $\overline{\text{Re}(v')\text{Im}(w')}$ is negative (positive); the vertical gradient of ozone is negative above 40 km, and the sign of \bar{k}_u in the region of the layering is negative. The horizontal eddy transport in the region where it is layered is dominated by term C. The horizontal eddy flux in this region is proportional to the vertical constituent derivative. This dependence is proven by an experiment where the horizontal gradient of ozone was reversed and the vertical gradient held constant. In this experiment the layering structure remained the same while the eddy flux at the critical line reversed direction.

The meridional gradient of the zonal mean potential vorticity, \bar{q}_y , is shown in Fig 4.24c. A necessary condition for baroclinic instability is that this gradient changes sign (Charney and Stern, 1962). The potential vorticity gradient is negative in a large area above the critical line, but there are three regions where it changes sign within the zone of easterlies. The positive above the critical line, but there are three regions where it changes sign within the zone of easterlies. The positive transience in Fig. 4.24b is localized near these gradient changes. Thus, the layered structure appears to be due to the

transport by an unstable mode in the zone of easterlies.

The positive anomaly in the ozone field is persistent until about day 47 when the anomaly begins to decrease and nearly disappears (Figures 4.13 or 4.16). This feature is coincident with the rise in the critical line which occurs around day 50. The horizontal eddy flux shown in Fig. 4.25 indicates that there is large southward flux associated with the rising critical line. As the critical line descends again after day 50 strong northward flux is once again associated with the critical line.

In actuality the critical line rises slowly for two weeks before rising rapidly on day 47. During the time the critical line is nearly stationary and rising slowly, there is a small flux in the southward direction. This explains why there is not enormous buildup in the northern region while the critical line is nearly steady.

The forcing of the mean flow in the vicinity of the critical line is shown in Fig. 4.26 where the EP flux divergence and critical line at the center of the channel is shown for a dynamics run similar to the one used in the transport study. Different dynamics were used here merely to conserve computer resources and all of the essential features of the transport dynamics are represented. While the critical line is rising there is convergence in the critical region which tends to accelerate the mean zonal flow in a westerly fashion. When the critical line is at its peak on day 42 the EP region which tends to accelerate the mean zonal flow in a westerly fashion. When the critical line is at its peak on day 42 the EP flux divergence is small and as the critical line descends the EP flux divergence becomes positive indicating absorption of wave

energy and a deceleration of the mean flow.

The effects of photochemistry are clearly exhibited in Fig. 4.27 which shows the horizontal eddy flux at day 31, the same time as Fig 4.24a. The multilayer structure which was present in the conservative experiment is not present due to the strong photochemistry above 40 km. This indicates that caution must be exercised if the current dynamics were to be applied to other gases with different chemistries. If, for instance, the transition layer were located in the region where the unstable mode was present large unrepresentative mean field changes might be calculated.

The strong poleward transport at the critical line is enhanced by the photochemistry because the weaker equatorial return transport is largely countered by the photochemistry. The photochemistry limits the transport largely to the conservative region and the lower part of the transition region for the 900 m topography. The importance of the critical line descending below the transition region is demonstrated by the transport with the 600 m topography which is only a third of that associated with the 900 m topography. The mechanism of transport when photochemistry is included is consistent with the critical line transport discussed above. The high latitude maximum in Fig. 4.20 on March 1 is associated with jet like transport of ozone as the critical line descends on day 70.

descends on day 70.

Figure 4.25. Eddy horizontal flux at day 47 for conservative transport during the rise of the critical line (ppm m sec^{-1}).

(bold solid line is the critical line)

Figure 4.26. Eliassen-Palm (EP) flux divergence during the rise of the critical line.

(negative values correspond to westerly acceleration)

solid lines > 0

dashed lines < 0

chain-dot $= 0$

Figure 4.27. Horizontal eddy flux on day 31 for chemical transport (ppm m sec^{-1}).

(bold solid line is the critical line)

(bold solid line is the critical line)

$\overline{v' \mu}$
(ppm m sec⁻¹)

DA DAY 47, CONSERVATIVE

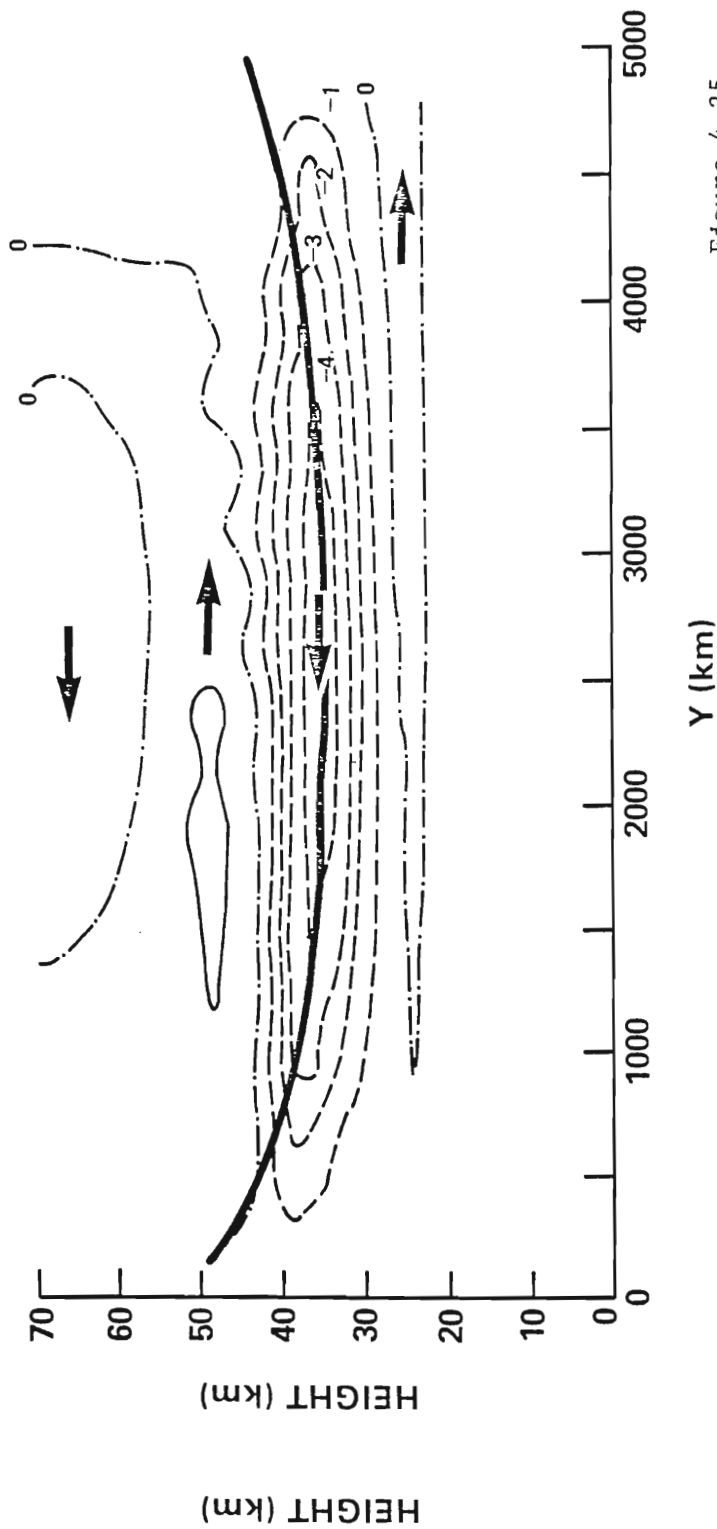


Figure 4.25

EP FLUX DIVERGENCE

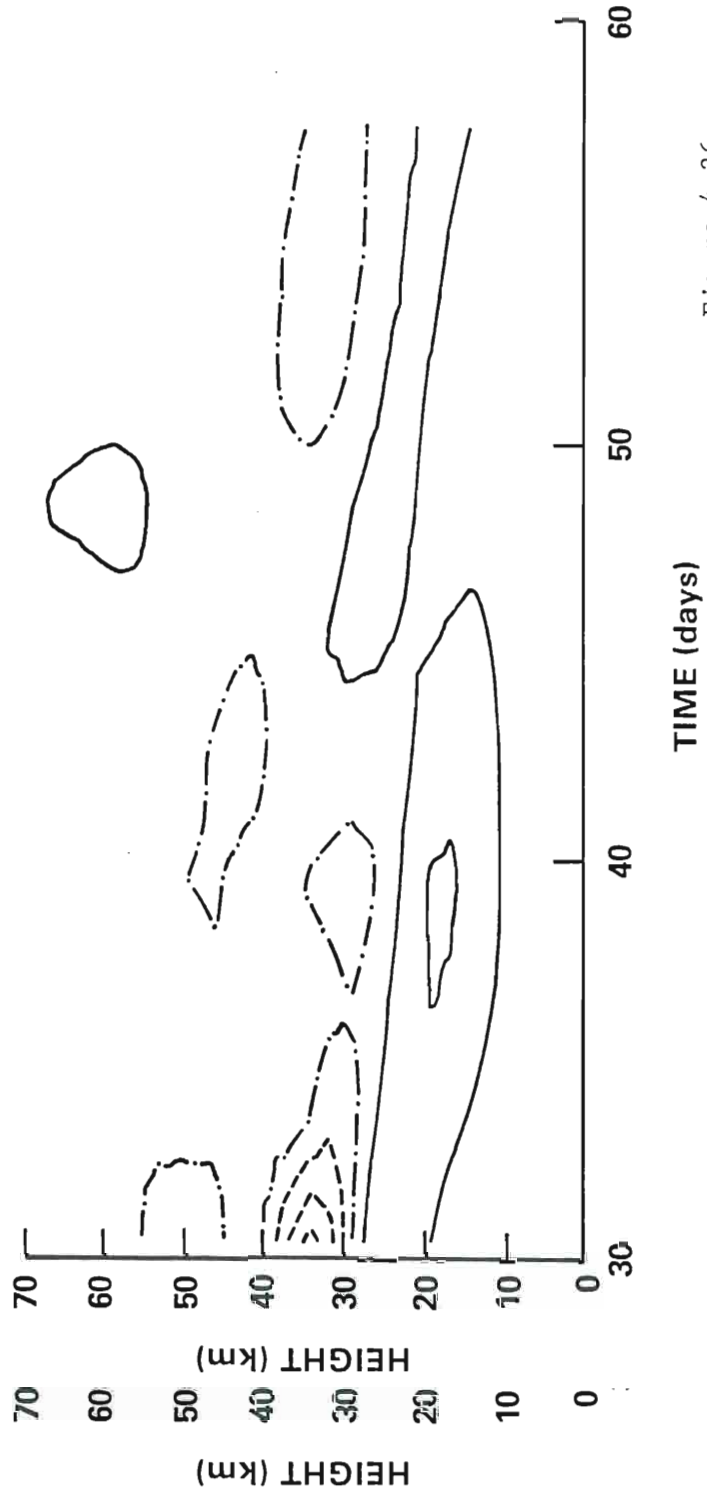


Figure 4.26

$\overline{v' \mu'}$
 (ppm m sec⁻¹)

DA DAY 31, CHEMISTRY

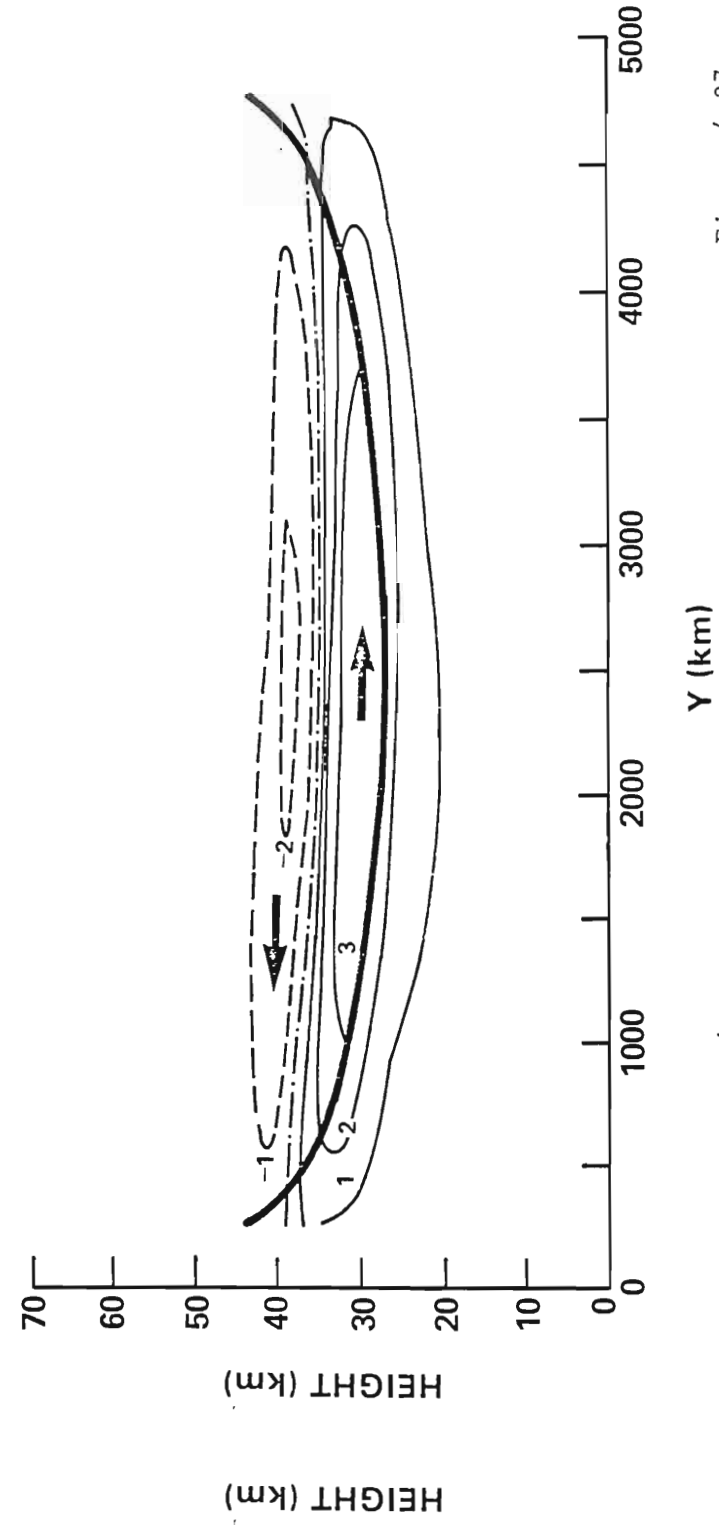


Figure 4.27

4.7 Summary

The effect of the planetary waves during a sudden warming is to transport ozone poleward. This transport is explained by the mechanisms revealed by Matsuno and Nakamura (1979) and Schoeberl (1981b). The transport by such strongly transient waves is much more vigorous and confined to a smaller vertical area than transport by steady state waves.

Northward transport coincides with a descending critical line. Southward transport occurs when the critical line ascends. The magnitude of the transport varies with the rate of ascent or descent, an indicator of the wave absorption properties of the critical line. When the critical line is stationary the transport is small.

Photochemistry enhances the buildup of ozone near the pole by reducing the return flux associated with the Lagrangian-mean jet at the critical line. The magnitude of the poleward transport is highly dependent on the critical line descending from the photochemical region into the transition and conservative regions.

The diabatic circulation transports ozone northward and downward but the northward transport is relatively ineffective. The downward transport produces increases in ozone in the lower stratosphere and replenishes the ozone in the southern region that is transported northward.

The β -plane model predicts a total ozone distribution at high latitudes consistent with observations but is less accurate at reproducing the vertical structure of ozone. Much of the discrepancy

can be attributed to the lack of small scale dynamics in the model lower stratosphere. In the next chapter the effects of the simplifying assumptions on the calculated transport as well as the applicability of the steady state and time dependent model to the real atmosphere will be discussed.

Chapter 5

SUMMARY AND A POSSIBLE OZONE TRANSPORT SCENARIO

5.1 Introduction

In the preceding chapters ozone transport by the diabatic circulation and both steady state and time dependent planetary waves on a β -plane has been described. The results simulate many of the large scale features of the wintertime ozone distribution with surprising accuracy. In this chapter the effects of some of the simplifying assumptions incorporated into the model will be evaluated, and the results will be interpreted with regard to their applicability to the atmosphere. It should be remembered that the purpose of the study is primarily to investigate transport mechanisms, not to accurately model all aspects of the ozone distribution.

Many simplifications were made both tacitly and explicitly in order to facilitate both the execution and the interpretation of the models. These specifically include the omission of small scale dynamics in the lower stratosphere; the lack of temporal and realistic latitudinal variation in the photochemistry; the specification, rather than the calculation, of the diabatic realistic latitudinal variation in the photochemistry; the specification, rather than the calculation, of the diabatic circulation; and the many assumptions incorporated in applying

quasigeostrophic planetary waves on a β -plane to a spherical atmosphere. The effects of these assumptions on the final results are varied and difficult to evaluate quantitatively but in some instances their qualitative influences can be described.

5.2 Low latitude ozone

One of the most serious inadequacies of the model is the overestimation of planetary wave transport out of the southern region of the model during sudden warmings. This excessive transport is exacerbated by the underestimation of the total ozone south of 50° on Dec. 15, the time when the planetary waves are turned on.

a. The diabatic circulation and the initial ozone distribution

The problem of too little ozone on Dec. 15 might be attributed to the initial ozone distribution being in error either with regard to total amount or the specification of mean gradients (see Section 4.2d). If the initial distribution is assumed to be correct, then the underestimation of ozone on Dec. 15 might be due to the improper designation of either the horizontal or the vertical diabatic velocity in the southern region. If the vertical velocity is too small, the transport from high altitude source regions to low altitudes would be underpredicted.

At the southern boundary there is a northward flux of ozone altitudes would be underpredicted.

At the southern boundary there is a northward flux of ozone associated with the meridional component of the diabatic velocity during fall and winter. If this component is too small then the flux

across the southern boundary may be underestimated. Furthermore, the ozone has been assumed to be constant at the southern boundary point (37.5°); when in fact, there is a 10% increase of total ozone mixing ratio during the winter (see Fig. 2.8). The specification of a constant mixing ratio at the southern boundary is, therefore, not strictly correct.

The inclusion of planetary waves in forming the Dec. 15 ozone field would tend to increase the total ozone error at low latitudes since both steady state and transient waves cause a depletion of ozone in the southern part of the β -channel. Even with an improved estimate of the ozone field, the transport of ozone out of the south during the initial warming is too strong. There is a large poleward transport out of the southern region associated with the initial warming which causes a more than 20 DU decrease in total ozone. Any decrease of ozone at 40° N during winter is unrealistic.

b. Geometric effects

The geometric effects of the β -plane would also contribute to the overestimation of transport out of the south. Figure 5.1 shows a spherical atmosphere divided into cells and the corresponding cells on a β -plane. The high latitude cells on the sphere contain less volume than the low latitude cells; in fact, a latitude band 2.15° wide (the approximate horizontal grid length) at 82.5° contains less than a third the volume of a similar cell centered at 37.5° . Likewise, a cell at 60° contains only 64% of the volume of a cell at 37.5° . Since the β -plane geometry assumes a constant cell

volume, the constituent divergence at low latitudes is overestimated while the constituent convergence at high latitudes is underestimated. In other words, the ozone transported north should be distributed over a smaller volume than it is, and the ozone removed from the south should be drawn from a larger volume than it is.

In order to understand the nature of this error consider the meridional term of the mean constituent divergence

$$\frac{1}{a \cos\theta} \frac{\partial}{\partial\theta} (\overline{v_{\mu}} \cos\theta) = \frac{1}{a} \frac{\partial}{\partial\theta} \overline{v_{\mu}} - \frac{\overline{v_{\mu}}}{a} \tan\theta \quad (5.1)$$

In the β -plane approximation $\cos\theta$ is replaced by $\cos\theta_0$, where θ_0 is the latitude of the center of the channel, and (5.1) becomes

$$\frac{1}{a \cos\theta} \frac{\partial}{\partial\theta} (\overline{v_{\mu}} \cos\theta) \approx \frac{\partial}{\partial y} \overline{v_{\mu}} \quad (y=a\theta) \quad (5.2)$$

So it is seen that the β -plane estimate is exact only at the center of the channel. The error due to the geometric effect is related to the second term on the right hand side of (5.1), and is proportional to the tangent of the latitude and the magnitude of the flux. At very high latitudes the tangent term would become very large. In this model both the mean and eddy horizontal fluxes approach zero at the northern boundary (82.5°); so that, the errors remain small. At low latitudes, the tangent term is smaller than that at the channel center; therefore, the divergence would be overestimated on the β -plane. The fluxes associated with the planetary wave dynamics

are small at the southern boundary because the wave amplitude is assumed to be zero. However, the flux associated with the diabatic circulation at the southern boundary is relatively large and could contribute to the underestimation of the ozone in the south.

c. Photochemistry

The photochemistry is not truly conservative in the lower stratosphere, and sufficiently rapid photochemistry might exist at southern latitudes to affect the transport. Figure 5.2 from Gille et al. (1980) shows an observational estimate of the transition region based on the phase between the geopotential and the ozone wave (Hartmann and Garcia, 1979). In the southern parts of this figure the transition region descends to nearly 20 km. Inclusion of chemistry between 28 and 30 km would help to alleviate the severe reduction calculated in the southern part of the model by generating new ozone to replace that transported northward.

Figure 5.1. Comparison of spherical and β -plane geometry.

Figure 5.2. Latitudinal dependence of the lower boundary of the photochemically controlled region (circles) and the upper boundary of the dynamically controlled region (squares), for November and December (from Gille et al., 1980).

Figure 5.3. Meridional cross section of the zonal mean wind velocity (m sec^{-1}).

a. 17 February 1979

b. 19 February

c. 20 February

d. 21 February

e. 23 February

f. 27 February

(from Palmer, 1981)

(from Palmer, 1981)

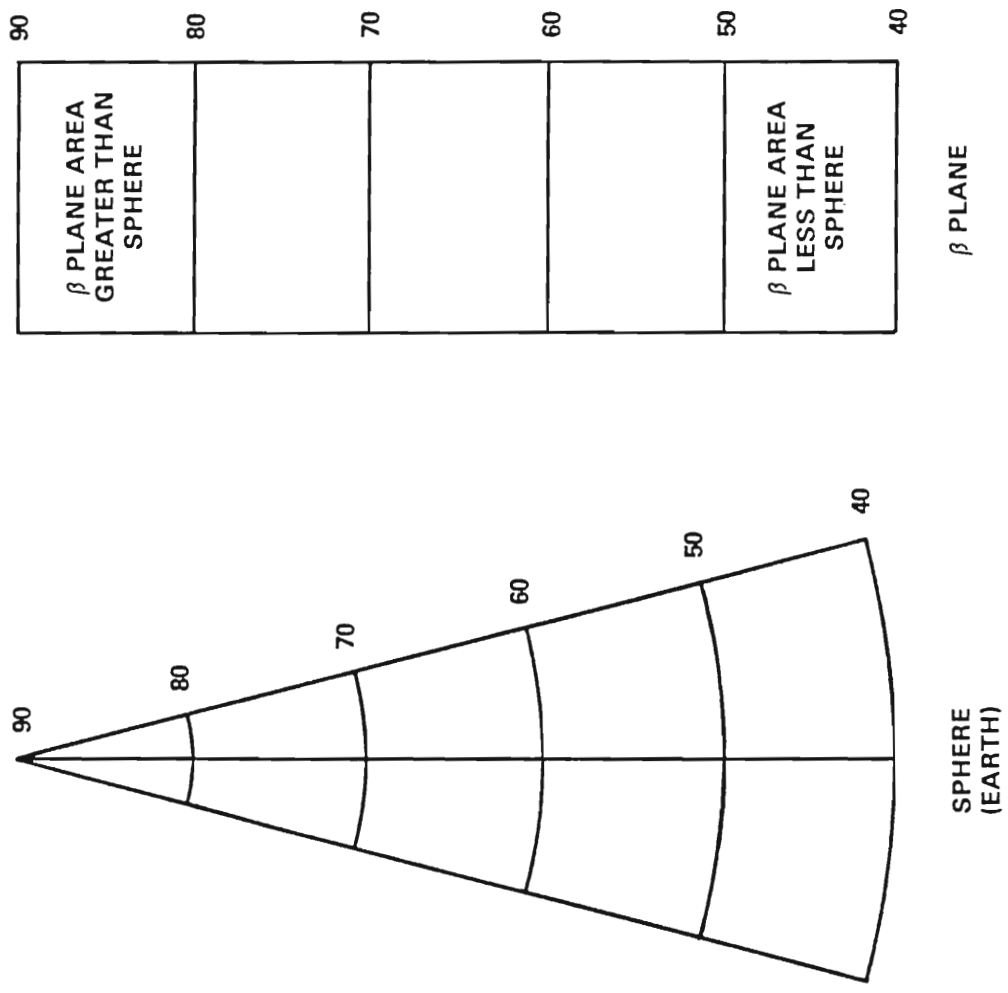


Figure 5.1

STATIONARY WAVE I PHASE ANALYSIS

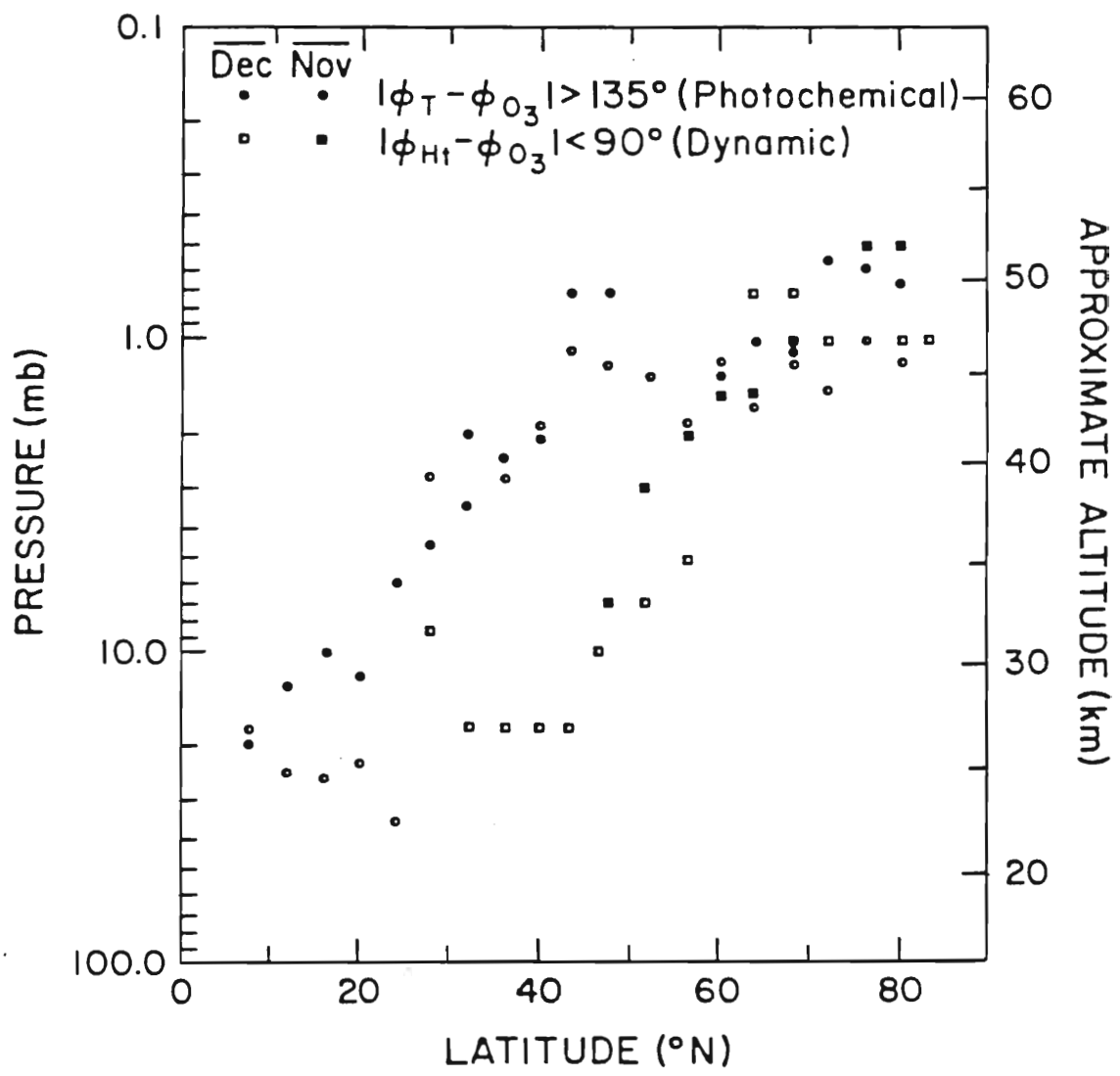


Figure 5.2

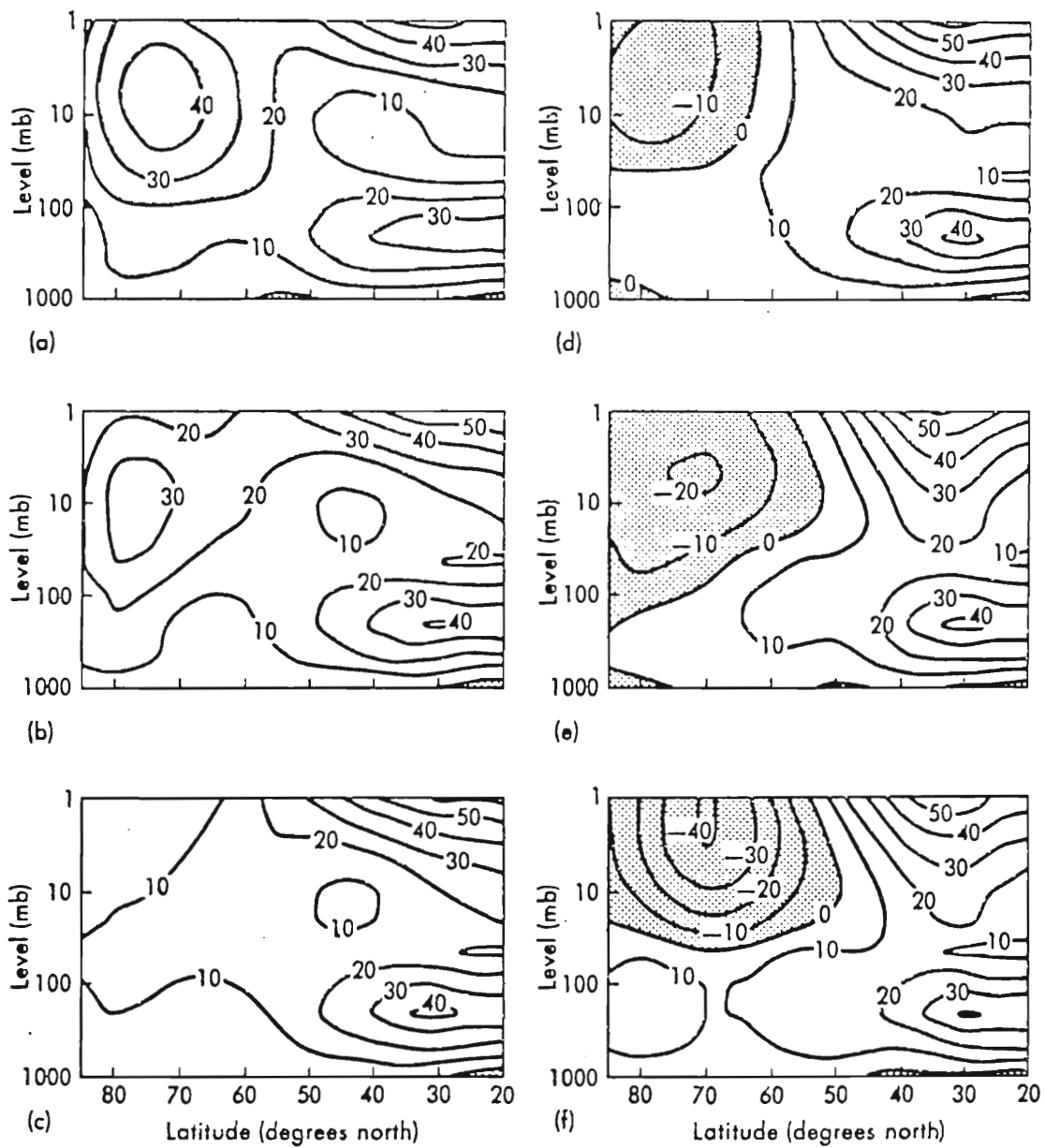


Figure 5.3

d. Planetary waves

The excessive transport out of the southern regions of the model during sudden warmings is influenced by all of the processes discussed above; however, the problem is exaggerated by the simplicity of the planetary wave dynamics. The critical lines in many of the figures in Chapter 4 (Fig 4.23 for instance) are nearly horizontal and extend from the northern boundary to the southern boundary. During stratospheric sudden warmings, the critical line generally does not extend south of 50° , which is close to the center of this model (Fig. 5.3). Furthermore, the critical line is rarely perfectly horizontal and is likely to be in the photochemical region at midlatitudes and in the conservative region at high latitudes. Therefore, much of the excessive transport out of the south exists because the model distorts the horizontal scale of the warming event. More realistic initial wind profiles would help alleviate this problem.

5.3. Vertical structure

a. Small scale dynamics

In Chapter 4 the high latitude total ozone was well estimated, but the polar buildup occurred higher than observed. This was attributed to the lack of subplanetary scale dynamics in the lower stratosphere. Since ozone is nearly conservative in the lower stratosphere, transport here would serve only to redistribute ozone and not change the total amount. Planetary waves which are not capable of propagating to very high altitudes (wavenumber 2-5) are

often present in the lower stratosphere as are the remnants of tropospheric weather systems. Also, it is well known that intense baroclinic zones in the upper troposphere cause excursions of ozone into the troposphere and may be instrumental in the downward transport of ozone (Kida, 1977; Shapiro, 1980). Thus, it appears that a variety of mechanisms exist which can redistribute ozone downward, while maintaining the column density, and that the inability of the current model to properly simulate the vertical distribution does not vitiate the importance of the observed transport mechanisms.

It might be possible to model the subplanetary processes in the lower stratosphere related to the redistribution of ozone by diffusion. However, for chemically active constituents other than ozone, many of the problems that appear when applying diffusion models to ozone might become important. In order to evaluate that effects of pollutants on ozone, the dynamics of the pollutants must be accurately calculated; therefore, any diffusion model must be used judiciously.

b. Photochemistry

Many aspects of the chemistry of ozone as used in this model are inadequate and might contribute to incorrect results. The chemistry was deliberately simplified so that attention could be focused on the transport and interaction of the dynamics and photochemistry. Rather than speculate on the particular effects of the omission of certain chemical species, it is more pertinent to

comment on the spatial variation of the simple chemistry included.

Garcia and Hartmann (1980) found that the latitudinal variation of photochemistry (the effect of the polar night) was important in enhancing the polar buildup of ozone. In Section 4.3 the latitudinal variation of photochemistry was shown to have little effect on transport by the diabatic circulation into the lower stratosphere. When ozone is assumed to be conserved in the polar night, a significant depletion develops over the course of the winter above 40 km. Very weak chemistry, though, will significantly moderate this depletion since the advection time scales are so long.

As the planetary wave transport is modeled here for time dependent waves, the latitudinal variation of photochemistry would have relatively little effect at high latitudes. Most of the transport occurs below the transition layer where ozone is nearly conservative at all times. The reduction of chemistry would have a more noticeable effect on transport during minor warmings when the critical line does not descend very low.

5.4 Unstable waves

During the transient transport an unstable wave exists within the critical level which causes the layered transport phenomenon discussed in Section 4.6. For ozone this layering had little effect, because it occurred in the photochemical region. For a conservative tracer or a compound with its transition region located correct, because it occurred in the photochemical region. For a conservative tracer or a compound with its transition region located in the unstable region, the unstable wave may have considerable transport consequences.

5.5 Summary and discussion

Despite the simplifications discussed above, the transport as calculated in this model reproduces many of the features of the wintertime ozone distribution. Furthermore, due to the simplicity of the model, specific mechanisms which are responsible for transport can be identified.

a. Steady state waves

In Chapter 3, transport by steady state dissipative planetary waves was examined from both an Eulerian and Lagrangian-mean viewpoint. In the lower stratosphere these waves were found to cause ozone depletion at low latitudes and an ozone enhancement toward the pole. The increase in ozone in the northern region is consistent with the observations; however, there is not an observed decrease at low latitudes as is calculated here. The ozone transport in the lower stratosphere was due to advection by the Lagrangian-mean velocity associated with the planetary waves.

In the lower part of the transition region there is an increase of mean ozone at high latitudes and a decrease at low latitudes (see Figures 3.7 and 3.14). This behavior in the transition region was shown to be due to the strong photochemical gradients in the region (Sec. 3.3d). The particle trajectories associated with the planetary waves are such that parcels move through a region of widely varying photochemistry. As a result the parcels experience a planetary waves are such that parcels move through a region of widely varying photochemistry. As a result the parcels experience a photochemical forcing different from the mean field chemistry at the parcel's equilibrium position. Thus the perturbation chemistry

cannot be balanced by the mean field chemistry, and changes in the mean ozone mixing ratio occur.

Where the photochemical gradients are small there is little or no effect of the planetary waves on the mean field. The steady state model indicates that transport by steady planetary waves might be adequately represented by advection by the Lagrangian-mean velocity in the lower stratosphere, and some scheme which includes the parcels orbiting through regions of strong photochemical gradients. Indeed, a model based on observed trajectories has been recently proposed by Garcia and Solomon (1982).

An accurate estimate of the Lagrangian-mean velocity for a realistic model of the stratosphere is difficult to calculate since the Lagrangian-mean velocity is the residual between two large terms. In atmospheric data since there are large uncertainties in the estimates of the quantities needed to produce the Lagrangian-mean displacement fields, it would be even more difficult to form meaningful estimates of the Lagrangian-mean velocity from observations.

In Section 3.3c the steady state ozone transport using the Eulerian residual circulation was calculated. The results were similar to those found using the Lagrangian-mean velocity, but the advection was consistently overestimated. The greatest differences between the residual velocity and the Lagrangian-mean velocity occur in the photochemical region so that the chemistry obscures the differences between the residual velocity and the Lagrangian-mean velocity in the photochemical region so that the chemistry obscures the errors in transport. For a constituent, with a different photochemistry from ozone, there might be significant differences

between the Lagrangian-mean and residual transport. It appears that the Eulerian formulation is best for carrying out transport calculations in realistic models, and the other formulations are useful for interpreting the results.

Over the course of the winter, the computed ozone increases in the lower stratosphere at high latitudes show reasonable agreement with observation. Using the "realistic" zonal wind profile of Schoeberl (1981a) too much ozone was transported into the northern region. The depletion of ozone in the southern lower stratosphere, could be partially alleviated with the inclusion of the diabatic circulation. The diabatic circulation would serve to transport ozone into the lower stratosphere and help replenish the depleted areas. However, even with the inclusion of the diabatic circulation the steady state ozone model would not describe the winter ozone transport and would exhibit many of the failures of the total ozone field calculated with the diabatic circulation alone (Sec. 4.3). The north-south transport associated with the planetary waves is larger than that associated with the diabatic circulation but is still not adequate to supply the required northward transport observed in the winter.

Figure 5.4. Simulated zonal mean total ozone (DU)
(from Mahlman et al., 1980).

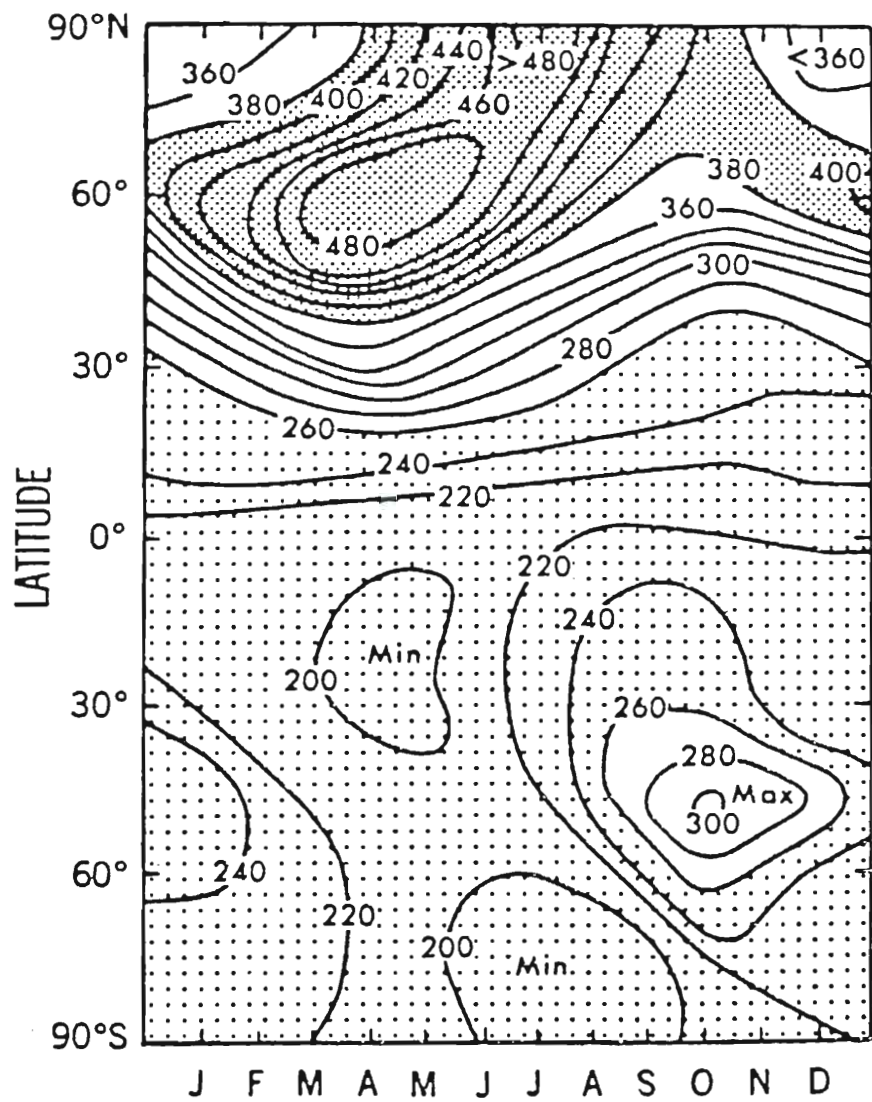


Figure 5.4

It is interesting to consider the results of Mahlman et al. (1980) within the context of the simple transport models used here. Figure 5.4 taken from Mahlman et al. shows their predicted total ozone field. Comparison with Fig. 2.8 shows that they predict a spring ozone maximum which occurs too far south, too late in the year, and that is too large. There is an intrusion of ozone into the polar region during the springtime reversal of the mean circulation. These errors are consistent with the errors associated with transport by the diabatic circulation alone or the diabatic circulation with steady state planetary waves. The results from this study suggest that it is the inability of the Mahlman et al. model to simulate stratospheric warmings which is responsible for much of the error in their total ozone field.

b. Time dependent waves

The transport by transient planetary waves (Chapter 4) was found to be much different from steady state transport, but it is conceptually quite simple. Intense poleward transport is associated with the deceleration and reversal of the zonal mean flow during warmings, and equatorward transport is associated with the reacceleration of the flow after the warming. The transport by highly transient planetary waves is largely confined to the horizontal plane with only a small vertical component. More realistic zonal wind profiles might generate critical lines which horizontal plane with only a small vertical component. More realistic zonal wind profiles might generate critical lines which have a larger vertical transport associated with them (Schoeberl 1981a, 1981b).

With the transport being so much different for transient and steady state waves, the question arises as to the consistency between the two models. To compare the two models an experiment was run in which the time dependent model was forced with a 200 m mountain. Such forcing causes large wave-mean flow interaction initially but there is never a reversal in the zonal mean wind field, and an equilibrium state is reached with westerlies present in the entire domain. At an altitude of 40 km the wave amplitude assumes a near steady value of approximately 350 gpm.

The anomaly field is shown at 74° in Fig. 5.5. There is a positive change in the lower part of the transition region and a negative change just below the transition region which is in qualitative agreement with the steady state model (Fig 3.14). The buildup found in the lower stratosphere at high latitudes is not reproduced in this experiment. The changes in the mean field for the 200 m waves are an order of magnitude or more smaller than those calculated with the 600 and 900 m waves and are also much smaller than those calculated with the steady state model.

The difference in the lower stratosphere between the steady state and time dependent models is due to wave-mean flow interaction in the upper stratosphere. In the time dependent model the wave induced mean velocity fields are strongest in the region of large wave-mean flow interaction. These fields are active at a significantly higher altitude than in the steady state model so that wave-mean flow interaction. These fields are active at a significantly higher altitude than in the steady state model so that the largest advection by the planetary waves does not occur in the lower stratosphere. This implies that the assumption in the steady

state model (Section 2.3a) that the changes in the mean field are small may significantly affect the results.

It is interesting to compare the eddy flux field from the 200 m experiment with those actually observed by Gille et al. (1980) (Fig 5.6). The model results agree well with the observations suggesting that the 200 m experiment might be appropriate for the early winter.

The steady state model may be useful for modeling transport in the late fall and early winter; however, the time dependent model more accurately represents the atmospheric transport in late winter and spring. Figure 5.7 schematically summarizes the different transport mechanisms studied here. Both planetary wave models deplete ozone in the south and enhance it in the north. The effects of the transition layer are not obvious for transport during stratospheric warmings as is expected because the transport at the critical line is so strong that it obscures this relatively weak effect.

The different topographies used to generate the time dependent dynamics in Chapter 4 allow for the study of transport during all types of warming events: major (900 m), minor (600 m), and final. The critical line remains above 32 km in the 600 m experiment and is analogous to a minor warming while the 900 m critical line extends below 32 km as it does during a major warming. The persistence of the critical line for such a long period of time after the 900 m warming allows for the study of transport during a final warming. The critical line for such a long period of time after the 900 m warming allows for the study of transport during a final warming.

Figure 5.5. Change in ozone at 74° for 200 m topography (ppm).

Figure 5.6. Horizontal eddy flux of ozone (ppm m sec^{-1}).

a. measured by Gille et al. (1980)

b. for 200 m topography

Figure 5.7. Schematic summary of transport mechanisms.

a. steady state planetary waves

b. diabatic circulation and transient waves

CHANGE IN $\bar{\mu}$ (ppm)

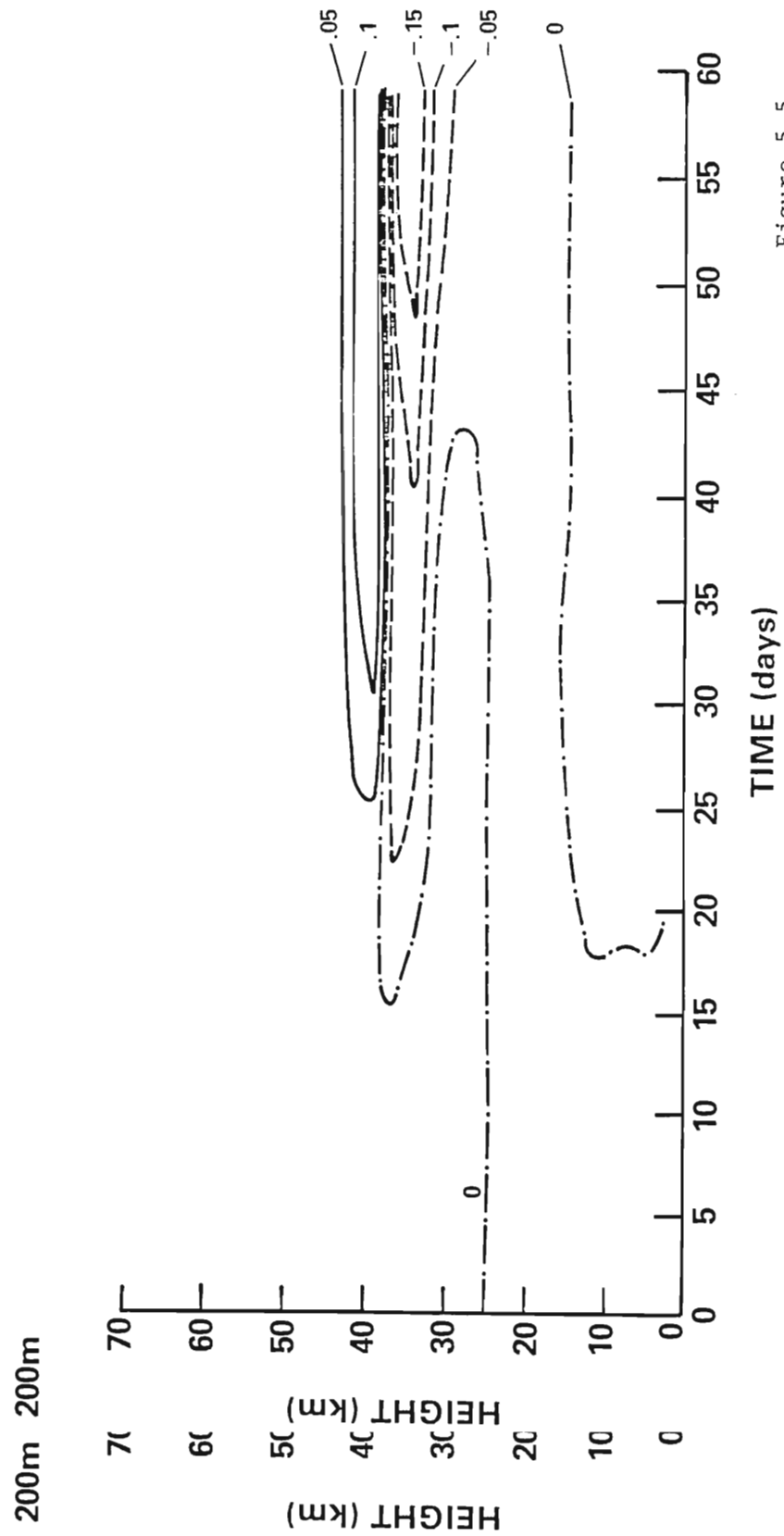


Figure 5.5

STATIONARY WAVE I OZONE TRANSPORT
(ppmV-m/sec)

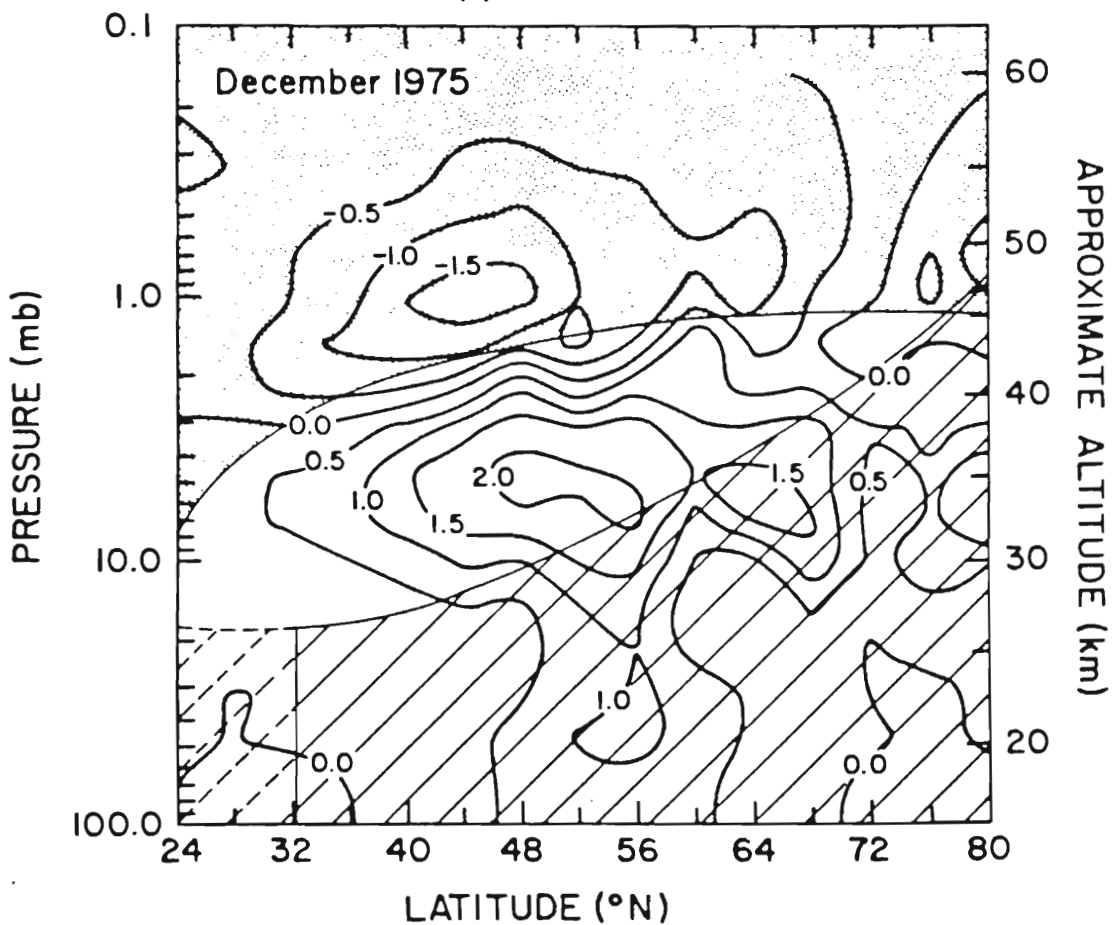


Figure 5.6a

$\overline{v' \mu'}$
(ppm m sec⁻¹)

D, DAY 40, 200 m, CHEMISTRY

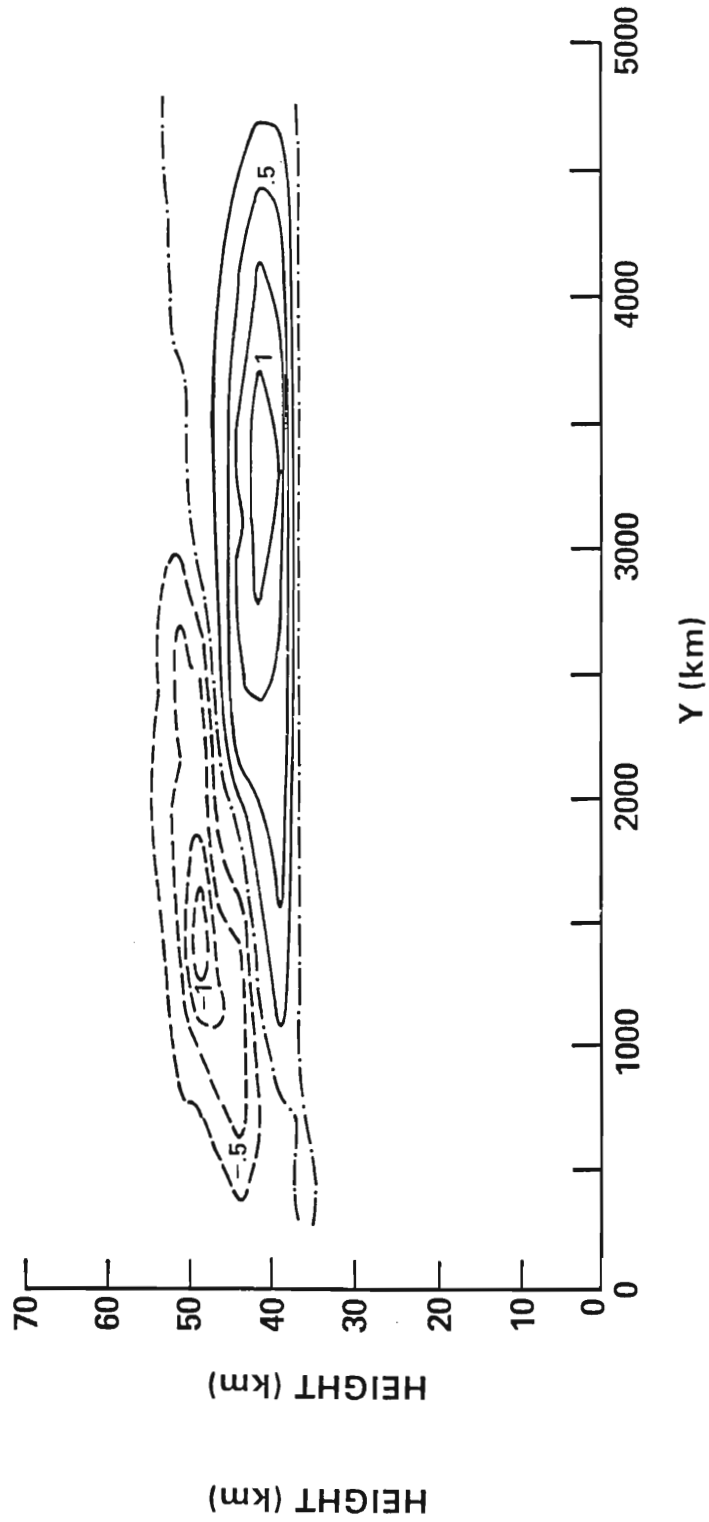
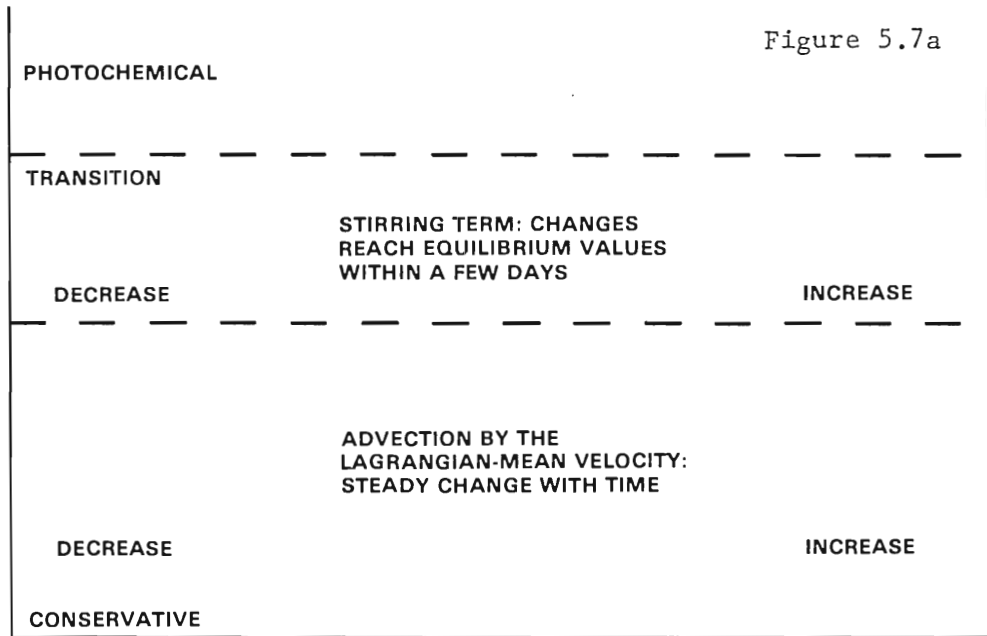
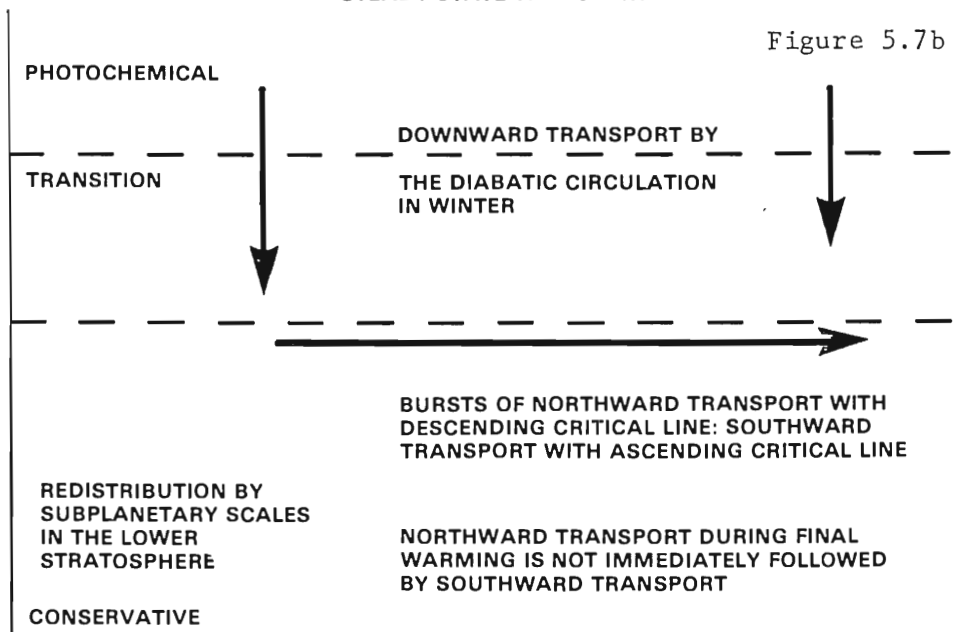


Figure 5.6b



STEADY STATE TRANSPORT



DIABATIC - CRITICAL LINE TRANSPORT

DIABATIC - CRITICAL LINE TRANSPORT

The transport for the 900 m topography is a factor of 3 or more greater than that for the 600 m topography. The increased transport associated with the 900 m topography arises because the critical line descends through the transition region into the conservative region where the transport is not countered by the chemistry. This suggests that transport during major warmings should be more pronounced than during minor warmings. This behavior is consistent with the observations in Fig. 2.10 where in the two years that major warmings occur the ozone maximum at high latitudes is 6% greater than the year in which no major warming occurs.

After both major and minor warmings there is a tendency for westerlies to develop and the stratosphere to return to its climatological state. In this event the critical line rises and much of the ozone transported into the north is transferred back to the south. This is clearly seen by the slight rise in the critical line that occurs in the 900 m experiment on day 47 (Fig. 4.3). Such behavior might be responsible for the oscillatory structure seen in Fig. 2.10.

The rise in the 900 m critical line (Fig 4.3) followed by the descent and persistence of the critical line is representative of what happens in a winter when there is a major warming followed by a final warming. The descent of the critical line after Feb. 1 is instrumental in the formation of the sharp high latitude total ozone maximum calculated with the combined circulation (Fig 4.9).

maximum calculated with the combined circulation (Fig 4.9).

The suggestion is made from this model that transport during major sudden warmings is large and may have significant effect on

the zonal mean ozone distribution, but that the high latitude spring maximum is due largely to transport during the spring reversal. Following the spring reversal the stratosphere remains in an easterly state so that there is not a strong reverse flow. It might also be suggested that the fall minimum is associated with the reformation of westerlies in the stratosphere.

c. A possible transport scenario

Using the transport mechanisms described in this dissertation, and the observed behavior of ozone in both the stratosphere and general circulation models; it is possible to derive a possible scenario for large scale ozone transport in the stratosphere. First it is necessary to form an analogue of the dynamics in the different models used here to the atmosphere.

Diabatic forcing determines the direction of the mean zonal wind, which in turn controls the propagation of waves into the stratosphere; therefore, the planetary wave transport and the diabatic transport are not completely independent as modeled here. The changeover from winter westerlies to summer easterlies after the final stratospheric warming is related the insolation at high latitudes forcing the zonal mean wind in a easterly direction. It is possible that major and minor warmings in the winter cause the springtime reversal to occur somewhat earlier than if diabatic forcing alone were responsible for the reversal. This possibility
springtime reversal to occur somewhat earlier than if diabatic
forcing alone were responsible for the reversal. This possibility
is supported by the reversal of the zonal westerlies in the Southern Hemisphere which occur somewhat later in the winter than in the

Northern Hemisphere. Stratospheric warmings are not as a predominate feature of the Southern Hemisphere circulation as of the Northern Hemisphere circulation. Furthermore, the model of Mahlman et al. (1980) shows the intrusion of ozone into high latitudes coincident with the spring reversal. This intrusion occurs later than is actually observed. Since this general circulation model does not simulate stratospheric warmings, the idea that planetary wave activity is important in the formation of the summertime easterlies is further supported.

During summer, with continual diabatic forcing at the pole, easterlies dominant the stratospheric circulation and planetary waves become unimportant. In the fall as the insolation decreases at high latitudes westerlies reform and planetary wave activity once again increases.

In Figure 4.8 the diabatic circulation produced a fall minimum in October in good agreement with observation. The minimum occurs at the time that diabatic circulation is changing over from upward motion at high latitudes during the summer to the downward motion present in the winter. This minimum is also coincident with the change over from zonal mean easterlies to zonal mean westerlies in the stratosphere.

After the ozone minimum in October, downward advection by the diabatic circulation tends to build up ozone in the lower stratosphere. As ozone is increasing, planetary wave activity is ~~diabatic circulation~~ tends to build up ozone in the lower stratosphere. As ozone is increasing, planetary wave activity is becoming more vigorous and warming events begin to occur. "Steady" waves constantly transport ozone poleward, but during major

stratospheric warmings large amounts of ozone are transported northward. Due to small scale "diffusive" processes, some of the ozone transported to high latitudes during warmings remains there leading to the enhanced extratropical total ozone evidenced in Fig. 2.10. Also, as ozone is being advected into the conservative region, small scale dynamics conservatively redistribute it into the lower stratosphere and troposphere. All of these features are evident in Fig. 2.6 where there is first an increase of ozone at 30 mb and then downward propagation from mid-January through March.

At the time of the final warming, which is determined not only by planetary wave forcing but also by insolation at high latitudes, there is strong northward transport. The total ozone maximum is coincident with the breakdown of the polar vortex; this maximum occurs somewhat earlier than the maximum calculated using the diabatic circulation in Fig. 4.9. The transport during the final warming is strong because of the interaction of the well developed winter planetary waves with the critical line. During fall when the westerlies reappear, such dramatic transport does not occur because the wave-mean flow interaction is much smaller. After the spring maximum, during summer, the diabatic circulation slowly reduces the total ozone as it transports it upward into the photochemical region where the ozone then assumes its equilibrium value.

In the Southern Hemisphere the intrusion of ozone into polar latitudes occurs during the reversal of the mean circulation
in the southern hemisphere the intrusion of ozone into polar latitudes occurs during the reversal of the mean circulation associated with the diabatic forcing. This indicates the reduced

importance of major stratospheric warmings in Southern Hemisphere dynamics.

Transport as described by this scenario suggests that the diabatic circulation (Brewer-Dobson circulation) is responsible for many of the large scale features of the observed ozone distribution. However, the diabatic circulation cannot effectively transport ozone into polar regions, and transport to very high latitudes is accomplished by planetary waves during sudden and final warmings. Subplanetary scale and evanescent planetary scales redistribute ozone in the lower stratosphere and transport ozone into the troposphere.

Finally, some comment must be made about the implications of the modeled transport on diffusion models. The transport by the diabatic circulation is advective and simple to model. The advective transport by steady planetary waves does not seem to be adequate to model the northward transport of ozone during winter. The transport during sudden warmings is large, coherent, rapid, and not diffusive.

The model results indicate that the large scale ozone transport is dominated by vertical diabatic transport and rapid pulses of horizontal transport during warmings. The planetary waves are not responsible for much vertical transport; though, subplanetary waves in the lower stratosphere might cause significant vertical transport.

in the lower stratosphere might cause significant vertical transport.

The diffusion coefficients as calculated by Strobel (1981) clearly indicate the complexities involved in accurately calculating

diffusion coefficients. They are a strong function of source terms, mean field gradients, and wave transience. The type of transport calculated here is highly transient and indicates that rapidly varying diffusion coefficients are required to properly simulate transport processes. If these coefficients are to be calculated from dynamic and chemical quantities then the entire purpose of diffusion parameterizations, computational simplicity, is defeated.

Appendix A

NOMENCLATURE AND CONVENTIONS

- a Newtonian cooling and Rayleigh friction coefficients
- f Coriolis parameter ($1 \times 10^{-4} \text{sec}^{-1}$)
- H scale height (7 km)
- k zonal wave number ($6.28 \times 10^{-9} \text{cm}^{-1}$)
- N^2 Brunt-Väisälä frequency squared ($4 \times 10^{-4} \text{sec}^{-2}$)
- p pressure; p_0 reference pressure
- \bar{q}_y horizontal derivative of the mean potential vorticity
- Q photochemical source term
- $(u, v, w) = (u_1, u_2, u_3) = (\text{zonal, meridional, vertical})$
velocity
- $(u, v, w) = (u_1, u_2, u_3) = (\text{zonal, meridional, vertical})$
velocity

$(v^*, w^*) = (\text{meridional, vertical})$ residual velocity

(Andrews and McIntyre, 1976)

t time

$(x, y, z) = (x_1, x_2, x_3) = (\text{east-west, north-south,}$

$z = -H \ln \frac{p}{p_0})$ coordinates

β meridional variation of Coriolis parameter, f

λ photochemical time constant

μ ozone mixing ratio

$(\xi, \eta, \zeta) = (\xi_1, \xi_2, \xi_3) = (\text{longitudinal, meridional,}$
vertical)

displacement fields

ϕ geopotential

CONVENTIONS:

For a given T

$\bar{T} \equiv$ zonal average (Eulerian)

$T' = T - \bar{T} \equiv$ zonal deviation

$\bar{T} \equiv$ zonal average (Eulerian)

$T' = T - \bar{T} \equiv$ zonal deviation

$T^L \equiv$ Lagrangian-mean (Andrews and McIntyre, 1978)

$T^S = T^L - \bar{T} \equiv$ Stokes correction (see Eq. (3.5))

Appendix B

NUMERICAL PROPERTIES OF THE ADVECTION-DIFFUSION EQUATION

The one dimensional advection-diffusion equation is

$$\frac{\partial S}{\partial t} + u \frac{\partial S}{\partial x} = D \frac{\partial^2 S}{\partial x^2} \quad (\text{B.1})$$

Using second order, centered time differences and generalized spatial differences (B.1) can be written in discrete form as

$$S_i^{n+1} = S_i^{n-1} - \frac{2u \Delta t}{\Delta x} \{ A_1 (S_{i+1}^n - S_{i-1}^n) + B_1 (S_{i+2}^n - S_{i-2}^n) \} \\ + \frac{2D \Delta t}{\Delta x^2} \{ A_2 (S_{i+1}^n - 2S_i^n + S_{i-1}^n) + B_2 (S_{i+2}^n - 2S_i^n + S_{i-2}^n) \} \quad (\text{B.2})$$

where Δx is the spatial grid increment and Δt is the time step. The superscripts are time indices and the subscripts are space indices. Both second order and fourth order differences will be considered, and the values of the A and B coefficients in (B.2) are given in table B.1.

Table B.1
Coefficients for Spatial Difference Scheme

	2 nd order	4 th order
A ₁	1/2	2/3
B ₁	0	-1/12
A ₂	1	4/3
B ₂	0	-1/12

Assuming the solution can be written as

$$S = B e^{n\Delta t} e^{imk\Delta x} \quad (\text{B.3})$$

where m is the spatial index, then (B.2) can be written following Haltiner and Williams (1980, Chapter 5) as

Haltiner and Williams (1980, Chapter 5) as

$$\begin{aligned}
 B^{\Delta t} = & B^{-\Delta t} - i \frac{4u \Delta t}{\Delta x} \{A_1 \sin(k\Delta x) + B_1 \cos(2k\Delta x)\} \\
 & + \frac{4D \Delta t}{\Delta x^2} \{A_2 (\cos(k\Delta x) - 1) + B_2 (\cos(2k\Delta x) - 1)\}
 \end{aligned}
 \tag{B.4}$$

In the transport model there is no diffusion so first consider (B.4) with $D = 0$. It can then be shown that for second order differences

$$\frac{u \Delta t}{\Delta x} < 1 \quad \text{for stability, and for fourth order differences}$$

$$\frac{u \Delta t}{\Delta x} < .73 \quad \text{for stability.}$$

Thus, for a given Δx , the fourth order scheme requires a smaller time step than the second order scheme to assure numerical stability. However, as demonstrated in Fig. 2.1, the phase error for the fourth order differences is considerably reduced (see Haltiner and Williams, 1980, Table 5.1). Haltiner and Williams (1980) discuss in detail the numerical properties of the second order and fourth order advection equation. Kreiss and Olinger (1972) argue that, by comparing the error in the phase speed with the number of computations, the fourth order scheme is "optimal."

Clancy (1981) suggests using forward time differences and second order spatial differences to integrate the advection-diffusion equation. Clancy derives a new stability criterion, second order spatial differences to integrate the advection-diffusion equation. Clancy derives a new stability criterion,

$$\Gamma R_c \leq 1$$

where

$$\Gamma = \frac{u \Delta x}{\Delta t} \quad \text{and} \quad R_c = \frac{u \Delta x}{D} \tag{B.5}$$

Using this stability criterion R_c can be infinitely large if Γ is small enough to keep the inequality (B.5) true. It had been shown previously that R_c must be less than or equal to 2, if this scheme is to be numerically stable. In the derivation of the stability criterion (B.5), however, Clancy effectively divided by zero in the formation of his equation (15), and the usefulness of (B.5) is questionable.

If the first term on the right hand side of (B.4) is replaced by 1 and the second and third terms are divided by 2, then (B.4) is the appropriate equation for forward time differences instead of centered time differences. If $D = 0$, this finite difference scheme becomes the Euler scheme, and it can be shown that the Euler scheme is unstable for almost all wavelengths (Haltiner and Williams, 1980, p.130). The addition of diffusion to this method serves to stabilize an otherwise unstable numerical scheme.

This stabilizing effect is illustrated in Fig. B.1 where the growth rate, G , is plotted against the diffusion parameter, D . If G is greater than 1 then numerical instability exists. As D increases from 0, G decreases until it is less than 1 and the scheme is stable. As D gets very large G once again increases and the method becomes unstable. So while it is possible to make the Euler scheme

stable by adding diffusion, the physical meaning of the diffusion is obscure; because the diffusion coefficient must not only represent physical processes, but must also counteract the inherent numerical instability.

While it is possible to produce a finite difference formulation that appears to be stable using Clancy's criterion 3.5, this is done at great computational expense. For Clancy's ocean case (the case presented in Fig. 2.1) $R_c = 60$ and $\Gamma = .022$. With Γ of this magnitude it takes almost 50 time steps for a parcel to propagate through one grid increment. Using centered spatial differences the time step can be increased by more than an order of magnitude and better results are obtained than using the Clancy algorithm. Using fourth order spatial differences, with a 10 times larger time step, the numerical results and the analytic results are very nearly equal (Fig. B.2). Any additional computations required by the fourth order scheme are more than compensated for by the increased accuracy and the larger time step.

Figure B.1. Growth rate of the numerical solution for forward time differences as a function of diffusion.

For $G > 0$, the solution is unstable.

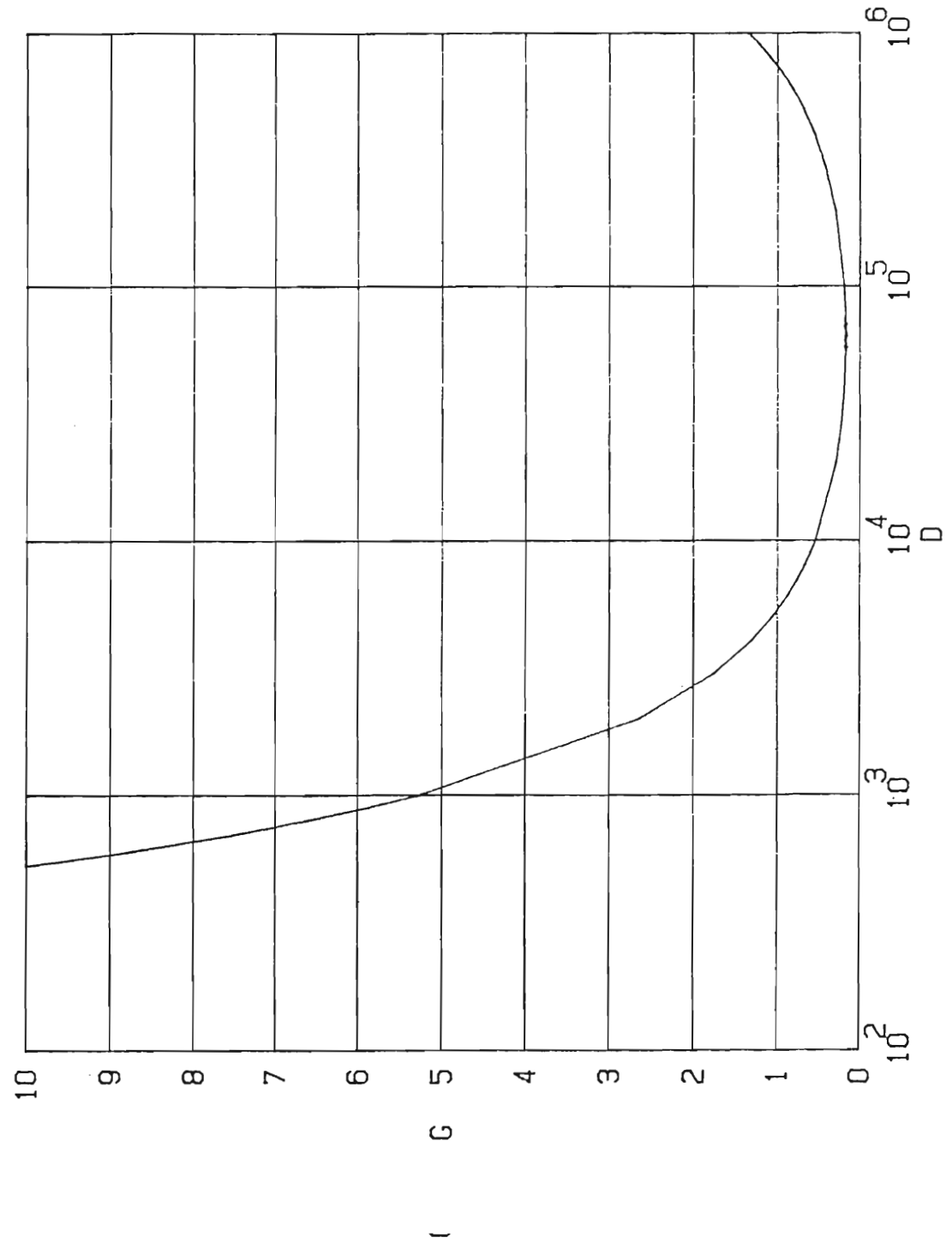
($\Delta x = 100$ km, $\Delta t = 10$ hours, $u = .6$ m sec⁻¹)

Figure B.2. Integration of Clancy's (1981) oceanic case with $\Delta t = 10$ hours. Same as Figure 2.1c but with the time step increased an order of magnitude.

The numerical solution (+) is virtually indistinguishable from the analytic solution

Figure B.1

GROWTH VERSUS DIFFUSION



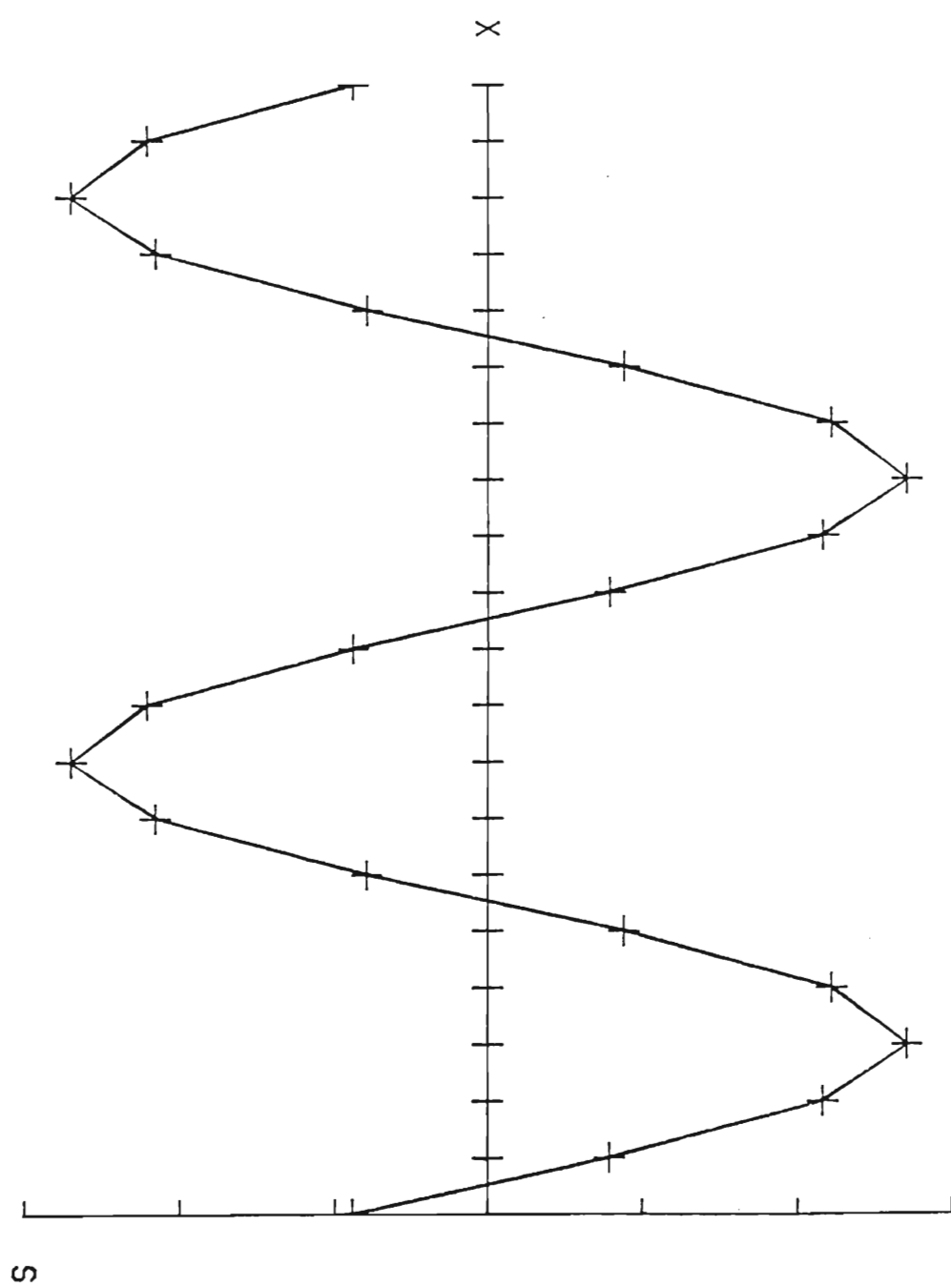


Figure B.2

References

- Ames, W.F., Numerical Methods for Partial Differential Equations,
2nd Ed., Academic Press, New York, pp.365, 1977.
- Andrews, D.G. and M.E. McIntyre, Planetary waves in horizontal and
vertical shear: The generalized Eliassen-Palm relation and the
mean zonal acceleration, J. Atmos. Sci., 33, 2031-2048, 1976.
- Andrews, D.G. and M.E. McIntyre, An exact theory of nonlinear waves
on a Lagrangian-mean flow, J. Fluid Mech., 89, 609-646, 1978.
- Apruzese, J.P., M.R. Schoeberl, and D.F. Strobel, Parameterization
of IR cooling in a middle atmosphere dynamics model, J. Geophys.
Res., in press, 1982.
- Berkofsky, L. and E.A. Bertoni, Mean topographic charts for the
entire earth, Bull. Amer. Meteor. Soc., 36, 350-354, 1955.
- Benson, S.W. and A.E. Axworthy, Jr., Mechanism of the gas phase,
thermal decomposition of ozone, J. Chem. Phys., 26, 1718-1726,
1957.
- Boyd, J.P., The noninteraction of waves with the zonally averaged
flow on a spherical earth and the interrelationships of eddy
fluxes of energy, heat, and momentum, J. Atmos. Sci., 33, 2285-
2291, 1976.
- 4471, 1970.

- Brewer, A.W., Evidence for a world circulation provided by the measurements of helium and water vapour distribution in the stratosphere, Quart. J. Roy. Meteor. Soc. 75, 351-363, 1949.
- Chapman, S., A theory of upper-atmospheric ozone, Mem. Roy. Meteor. Soc., 3, 103-125, 1930.
- Charney, J.G. and P.G. Drazin, Propagation of planetary-scale disturbances from the lower into the upper stratosphere, J. Geophys. Res., 66, 83-109, 1961.
- Charney, J.G. and M.E. Stern, On the stability of internal baroclinic jets in a rotating atmosphere, J. Atmos. Sci., 19, 159-172, 1962.
- Clancy, R.M., A note on finite differencing of the advection-diffusion equation, Mon. Wea. Rev., 109, 1807-1809, 1981.
- Clark, J.H.E., A quasi-geostrophic model of the winter stratospheric circulation, Mon. Wea. Rev., 98, 443-461, 1970.
- Clark, J.H.E. and T.G. Rogers, The transport of conservative trace gases by planetary waves, J. Atmos. Sci., 35, 2232-2235, 1978.
- Craig, R.A., The observations and photochemistry of atmospheric ozone and their meteorological significance, Meteor. Mongr., 1, No. 2, 1-50, 1950.
- Craig R.A., The Upper Atmosphere: Meteorology and Physics, Academic Press, New York, pp. 509, 1965.
- Cunnold, D., F. Alyea, N. Phillips, and R. Prinn, A three-dimensional dynamical-chemical model of atmospheric ozone, J. Atmos. Sci., 32, 170-194, 1975.
- Cunnold, D., F. Alyea, N. Phillips, and R. Prinn, A three-dimensional dynamical-chemical model of atmospheric ozone, J. Atmos. Sci., 32, 170-194, 1975.

- Danielsen, E.F., An objective method for determining the generalized transport tensor for two-dimensional Eulerian models, J. Atmos. Sci., 38, 1319-1339, 1981.
- Dickinson, R.E., Method of parameterization for infrared cooling between altitudes of 30 and 70 kilometers, J. Geophys. Res., 78, 4451-4457, 1973.
- Dobson, G.M.B., Observations of the amount of ozone in the earth's atmosphere and its relation to other geophysical conditions, part IV, Proc. Roy. Soc. London, A129, 411-433, 1930.
- Dobson, G.M.B., Origin and distribution of polyatomic molecules in the atmosphere, Proc. Roy. Soc. London, A236, 187-193, 1956.
- Dunkerton, T., On the mean meridional mass motions of the stratosphere and mesosphere, J. Atmos. Sci., 35, 2325-2333, 1978.
- Dunkerton, T., A Lagrangian-mean theory of wave, mean-flow interaction with applications to nonacceleration and its breakdown. Rev. Geophys. Space Phys., 18, 387-400, 1980.
- Dunkerton, T., C.-P.F. Hsu, and M.E. McIntyre, Some Eulerian and Lagrangian diagnostics for a model stratospheric warming, J. Atmos. Sci., 38, 819-843, 1981.
- Dütsch, H.U., Atmospheric ozone and ultraviolet radiation, World Survey of Climatology, Vol. 4, D.F. Rex, Ed., Elsevier, 383-432, 1969.
- Dütsch, H.U., The ozone distribution in the atmosphere, Can. J. Chem., 52, 1491-1504, 1974.
- Dütsch, H.U., The ozone distribution in the atmosphere, Can. J. Chem., 52, 1491-1504, 1974.

- Fels, S.B., J.D. Mahlman, M.D. Schwarzkopf, and R.W. Sinclair, Stratospheric sensitivity to perturbations in ozone and carbon dioxide: Radiative and dynamic response, J. Atmos. Sci., 37, 2265-2297, 1980.
- Garcia, R.R. and D.L. Hartmann, The role of planetary waves in the maintenance of the zonally averaged ozone distribution of the upper atmosphere, J. Atmos. Sci., 37, 2248-2264, 1980.
- Garcia, R.R. and S. Solomon, A numerical model of the zonally-averaged dynamical and chemical structure of the middle atmosphere, submitted to J. Geophys. Res., 1982.
- Gille, J.C., G.P. Anderson, W.J. Kohri, and P.L. Bailey, Observation of the interaction of ozone and dynamics, Proceedings of the Quadrennial International Ozone Symposium, J. London, Ed., 1007-1011, 1980.
- Götz, F.W.P., Ozone in the atmosphere, in Compendium of Meteorology, American Meteorology Society, Boston, 275-291, 1951.
- Haltiner, G.J. and R.T. Williams, Numerical Prediction and Dynamic Meteorology, 2nd Ed., John Wiley and Sons, Inc., New York, pp. 477, 1980.
- Hartmann, D.L., Some aspects of the coupling between radiation, chemistry, and dynamics in the stratosphere, J. Geophys. Res., 86, 9631-9640, 1981.
- Hartmann, D.L. and R. Garcia, A mechanistic model of ozone 86, 9631-9640, 1981.
- Hartmann, D.L. and R. Garcia, A mechanistic model of ozone transport by planetary waves in the stratosphere, J. Atmos. Sci., 36, 350-364, 1979.

- Harwood, R.S. and J.A. Pyle, Studies of the ozone budget using a zonal mean circulation model and linearized photochemistry, Quart. J. Roy. Meteor. Soc., 103, 319-343, 1977.
- Hidalgo, H. and P.J. Crutzen, The tropospheric and stratospheric composition perturbed by NO_x emissions of high altitude aircraft, J. Geophys. Res., 82, 5833-5866, 1977.
- Hilsenrath E., D.F. Heath, B.M. Schlesinger, Seasonal and interannual variations in total ozone revealed by the Nimbus 4 backscattered ultraviolet experiment, J. Geophys. Res., 84, 6969-6979, 1979.
- Holton, J.R., The Dynamic Meteorology of the Stratosphere and Mesosphere, Meteor. Monographs, Vol. 15, #37, pp. 218, 1975.
- Holton, J.R., An advective model for two dimensional transport of stratospheric trace species, J. Geophys. Res., 86, 11989-11994, 1981.
- Hsu, C.-P.,F., Air parcel motions during a numerically simulated sudden stratospheric warming, J. Atmos. Sci., 37, 2768-2792, 1980.
- Hunt, B.G., Photochemistry of ozone in a moist atmosphere, J. Geophys. Res., 71, 1385-1398, 1966.
- Hunten, D.M., Vertical transport in atmospheres, in Atmospheres of Earth and the Planets, B.M. McCormac, Dordrecht, Holland, 59-72, 1975.
- Johnston, H.S. and J. Podolske, Interpretations of stratospheric
1975.
- Johnston, H.S. and J. Podolske, Interpretations of stratospheric photochemistry, Rev. Geophys. Space Phys., 16, 491-520, 1978.

- Kida, H., A numerical investigation of the stratospheric general circulation and stratospheric tropospheric mass exchange. II. Lagrangian motion of the atmosphere, J. Meteor. Soc. Japan, 55, 71-88, 1977.
- Kreiss, H.O. and J. Oliger, Comparison of accurate methods for the integration of hyperbolic equations, Tellus, 24, 199-215, 1972.
- Kreuger, A.J. and R.A. Minzner, A mid-latitude ozone model for the 1975 U.S. Standard Atmosphere, J. Geophys. Res., 81, 4477-4481, 1976.
- Labitzke, K. and B. Goretzki, A catalogue of dynamic parameters describing the variability of the middle stratosphere during the northern winters, in Handbook for MAP, 5, Middle Atmosphere Program, C.F. Sechrist, Ed., 1982.
- Lindzen, R.S., B. Farrel, and K.K. Tung The concept of wave overreflection and its application to baroclinic instability, J. Atmos. Sci., 37, 44-63, 1980.
- London, J., R. Bojkov, S. Oltmans, and J. Kelley, Atlas of the Global Distribution of Total Ozone July 1957-June 1967, NCAR Technical Note, TN113, Boulder, pp. 276, 1976.
- Luther, F.M., Large scale eddy transport, in Second Annual Report, UCRL-51336-74, pp. 66-73, Lawrence Livermore Lab., Calif., 1974.
- Mahlman, J.D., Heat balance and mean meridional circulations in the polar stratosphere during the sudden warming of January 1958, Mon. Wea. Rev., 97, 534-540, 1969.
- polar stratosphere during the sudden warming of January 1958, Mon. Wea. Rev., 97, 534-540, 1969.

- Mahlman, J.D., Some fundamental limitations of simplified transport models as implied by results from a three-dimensional general circulation/tracer model, Proc. Fourth Conference Climatic Impact Assessment Program, T.M. Hard and A.J. Broderick, ed. DOT-TSC-OST-75-38, U.S. Dept. of Trans., Washington, D.C., 132-146, 1975.
- Mahlman, J.D. and W.M. Moxim, Tracer simulation using a global general circulation model: Results from a midlatitude instantaneous source experiment, J. Atmos. Sci., 35, 1340-1374, 1978.
- Mahlman, J.D. and R.W. Sinclair, Tests of various numerical algorithms applied to a simple trace constituent air transport problem, Fate of Pollutants in the Air and Water Environments, Part 1, 8, I.H. Suffet, ed., John Wiley and Sons, Inc., 1977.
- Mahlman, J.D., H. Levy II, and W.J. Moxim, Three-dimensional tracer structure and behavior as simulated in two ozone precursor experiments, J. Atmos. Sci., 37, 655-685, 1980.
- Matsuno, T., Lagrangian motion of air parcels in the stratosphere in the presence of planetary waves, Pure Appl. Geophys., 118, 189-216, 1980.
- Matsuno, T. and K. Nakamura, The Eulerian- and Lagrangian-mean meridional circulations in the stratosphere at the time of a sudden warming, J. Atmos. Sci., 36, 640-654, 1979.
- McConnell, J.C. and M.B. McElroy, Odd nitrogen in the atmosphere. Sudden warming, J. Atmos. Sci., 30, 1465-1477, 1973.
- McConnell, J.C. and M.B. McElroy, Odd nitrogen in the atmosphere. J. Atmos. Sci., 30, 1465-1477, 1973.

- McIntyre, M.E., Towards a Lagrangian-mean description of stratospheric circulations and chemical transports, Phil. Trans. Roy. Soc. Lond., A296, 129-148, 1980.
- Miller, C., D.L. Filkin, A.J. Owens, M.J. Steed, and J.P. Jesson, A two dimensional model of stratospheric chemistry and transport, J. Geophys. Res., 86, 12039-12065, 1981.
- Murgatroyd, R.J. and F. Singleton, Possible meridional circulation in the stratosphere and mesosphere, Quart. J. Roy. Meteor. Soc., 87, 125-135, 1961.
- Newell, R.E., The transport of trace substances in the atmosphere and their implications for the general circulation of the stratosphere, Geofis. Pura Appl., 49, 137-158, 1961.
- Newell, R.E., Transfer through the tropopause and within the stratosphere, Quart. J. Roy. Meteor. Soc., 89, 167-204, 1963.
- Palmer, T.N., Diagnostic study of a wavenumber-2 stratospheric sudden warming in a transformed Eulerian-mean formalism, J. Atmos. Sci., 38, 844-855, 1981.
- Plumb, R.A., Eddy fluxes of conserved quantities by small-amplitude waves, J. Atmos. Sci., 36, 1699-1704, 1979.
- Pyle, J.A. and C.F. Rogers, Stratospheric transport by stationary planetary waves- The importance of chemical processes, Quart. J. Roy. Meteor. Soc., 106, 421-446, 1980a.
- Pyle, J.A. and C.F. Rogers, A modified diabatic circulation model for stratospheric tracer transport, Nature, 287, 711-714, 1980b.
- for stratospheric tracer transport, Nature, 287, 711-714, 1980b.

- Reed, R.J. and K.E. German, A contribution to the problem of stratospheric diffusion by large-scale mixing, Mon. Wea. Rev., 93, 313-321, 1965.
- Schlesinger, M.E. and Y. Mintz, Numerical simulation of ozone production, transport and distribution with a global atmospheric general circulation model, J. Atmos. Sci., 36, 1325-1361, 1979.
- Schoeberl, M.R., The secondary circulation associated with a vertically aligned planetary wave critical line, Geophys. Res. Lett., 7, 153-156, 1980.
- Schoeberl, M.R., A simple model of the Lagrangian-mean flow produced by dissipating planetary waves, J. Atmos. Sci., 38, 1841-1855, 1981a.
- Schoeberl, M.R., The secondary flow near a baroclinic planetary wave critical line, J. Atmos. Sci., 38, 630-638, 1981b.
- Schoeberl, M.R., Vacillation, sudden warmings and potential enstrophy balance in the stratosphere, to appear in J. Atmos. Sci., 1982a.
- Schoeberl, M.R., A study of stratospheric vacillations and sudden warmings on a β -plane Part I: Single wave-mean flow interaction, submitted to J. Atmos. Sci., 1982b.
- Schoeberl, M.R. and D.F. Strobel, The zonally averaged circulation of the middle atmosphere, J. Atmos. Sci., 35, 577-591, 1978.
- Shapiro, M.A., Turbulent mixing within tropospheric folds as a mechanism for the exchange of chemical constituents between the
- Shapiro, M.A., Turbulent mixing within tropospheric folds as a mechanism for the exchange of chemical constituents between the stratosphere and troposphere, J. Atmos. Sci., 37, 994-1004, 1980.

- Strobel, D.F., Parameterization of linear wave chemical transport in planetary atmospheres by eddy diffusion, J. Geophys. Res., 86, 9806-9810, 1981.
- Tuck, A.F., A comparison of one- two- three- dimensional model representations of stratospheric gases, Phil. Trans. Roy. Soc. Lon., A290, 477-495, 1979.
- Van Loon, H., R.L. Jenne and K. Labitzke, Zonal harmonic standing waves, J. Geophys. Res., 78, 4463-4471, 1973.
- WMO, The Stratosphere 1981: Theory and Measurements, WMO Global Ozone Research and Monitoring Project Report No.11, 1981.
- Zullig, W., Relation between the intensity of the stratospheric circumpolar vortex and the accumulation of ozone in the winter hemisphere, Pure Appl. Geophys., 106-108, 1544-1552, 1973.

Vita

Richard B. Rood was born November 23, 1954 in Raleigh, North Carolina, and lived happily in Cary, North Carolina, through the completion of high school. After spending the summer in Cambridge, England, he entered the University of North Carolina at Chapel Hill in 1972 and managed to graduate with a Bachelor of Science in Physics in 1976.

In 1976 he began graduate work at Florida State University under the direction of Professor Richard A. Craig and received a Master of Science degree in Meteorology in 1979. After the death of Professor Craig he went to work on his doctoral research with Dr. Mark Schoeberl at the Naval Research Laboratory. Hopefully he will graduate in 1982 and be able to accept his postdoctoral fellowship at the NASA Goddard Space Flight Center.

In 1977 Richard Rood married Janna Broili and has been studying various obscure subjects ever since.